University of Alberta

REGULATING PEROXISOME MOTILITY IN THE YEAST *SACCHAROMYCES CEREVISIAE*

by

ANDREI DRAGOS FAGARASANU, M.D. ©

A thesis submitted to the Faculty of Graduate Studies and Research in partial fulfillment
of the requirements for the degree of *Doctor of Philosophy*

Department of Cell Biology

Edmonton, Alberta

Fall 2008

Library and
Archives Canada

Published Heritage
Branch

395 Wellington Street
Ottawa ON K1A 0N4
Canada

Bibliothèque et
Archives Canada

Direction du
Patrimoine de l'édition

395, rue Wellington
Ottawa ON K1A 0N4
Canada

Your file Votre référence
ISBN: 978-0-494-46314-7
Our file Notre référence
ISBN: 978-0-494-46314-7

NOTICE:
The author has granted a non-exclusive license allowing Library and Archives Canada to reproduce, publish, archive, preserve, conserve, communicate to the public by telecommunication or on the Internet, loan, distribute and sell theses worldwide, for commercial or non-commercial purposes, in microform, paper, electronic and/or any other formats.

The author retains copyright ownership and moral rights in this thesis. Neither the thesis nor substantial extracts from it may be printed or otherwise reproduced without the author's permission.

AVIS:
L'auteur a accordé une licence non exclusive permettant à la Bibliothèque et Archives Canada de reproduire, publier, archiver, sauvegarder, conserver, transmettre au public par télécommunication ou par l'Internet, prêter, distribuer et vendre des thèses partout dans le monde, à des fins commerciales ou autres, sur support microforme, papier, électronique et/ou autres formats.

L'auteur conserve la propriété du droit d'auteur et des droits moraux qui protège cette thèse. Ni la thèse ni des extraits substantiels de celle-ci ne doivent être imprimés ou autrement reproduits sans son autorisation.

In compliance with the Canadian Privacy Act some supporting forms may have been removed from this thesis.

While these forms may be included in the document page count, their removal does not represent any loss of content from the thesis.

Conformément à la loi canadienne sur la protection de la vie privée, quelques formulaires secondaires ont été enlevés de cette thèse.

Bien que ces formulaires aient inclus dans la pagination, il n'y aura aucun contenu manquant.

Canada

ABSTRACT

Eukaryotic cells divide their metabolic labor among functionally distinct, membrane-enveloped organelles, each precisely tailored for a specific set of biochemical reactions. Peroxisomes are ubiquitous organelles intimately connected to lipid metabolism. Upon cell division, cells must strictly control peroxisome division and inheritance to maintain an appropriate number of peroxisomes in each cell.

We studied the inheritance of peroxisomes using the budding yeast *Saccharomyces cerevisiae* as a model eukaryotic organism. In contrast to cells that divide by fission, *S. cerevisiae* must actively and vectorially deliver half of its organelles to the growing bud. To achieve this, proteins called formins are strategically localized to the bud, where they assemble an array of actin cables that radiate deep into the mother cell. The class V myosin motors, Myo2p and Myo4p, use these cables as tracks to transport various organelles, including peroxisomes, a portion of the vacuole, mitochondria and elements of the endoplasmic reticulum and Golgi complex. Bud-directed transport of peroxisomes is driven by Myo2p along actin cables. How Myo2p attaches to peroxisomes was unknown.

We identified Inp2p as the peroxisome-specific receptor for Myo2p. Cells lacking Inp2p fail to partition peroxisomes to the bud but are unaffected in the inheritance of other organelles. Inp2p is a peroxisomal membrane protein, preferentially enriched in peroxisomes delivered to the bud. Inp2p interacts directly with the globular tail of Myo2p. Cells overproducing Inp2p often transfer their entire populations of peroxisomes to buds. The levels of Inp2p oscillate with the cell cycle. Organelle-specific receptors like

Inp2p explain how a single motor can move different organelles in distinct and specific patterns. Inp2p is the first peroxisomal protein implicated in the vectorial movement of peroxisomes.

To gain further insight into the Inp2p-Myo2p interaction, we made various point mutations in the surface residues in the Myo2p tail to map its peroxisome-binding region. We determined that the region resides in subdomain II of the Myo2 globular tail and partially overlaps the region that binds secretory vesicles. Our discovery of Inp2p and investigation of its interaction with Myo2p have provided a better understanding of how cells dynamically control the intracellular motility of their peroxisomes.

TABLE OF CONTENTS

CHAPTER ONE: INTRODUCTION 1
  1.1 Introduction to Peroxisomes 2
  1.2 The Strategies Used by Eukaryotic Cells to Maintain their Peroxisomes 3
  1.3 Peroxisome Division 8
    1.3.1 Introduction to Peroxisome Division 8
    1.3.2 Elongation of Peroxisomes: The Role of Pex11 Proteins 9
    1.3.3 Constriction of the Peroxisomal Membrane 11
    1.3.4 Fission of Peroxisomes: Involvement of Dynamin-Related Proteins 12
    1.3.5 Other Proteins that Regulate the Size and Number of Peroxisomes 16
  1.4 Peroxisome Inheritance 17
    1.4.1 Introduction to Organelle Inheritance in Yeast 17
    1.4.2 Peroxisome Inheritance in *S. cerevisiae* 20
  1.5 Strategies Used by *S. cerevisiae* to Segregate Other Membrane-Bounded Organelles 26
    1.5.1 Vacuoles 26
    1.5.2 Mitochondria 32
    1.5.3 The Golgi Complex 38
    1.5.4 Endoplasmic Reticulum 41
  1.6 Focus of this thesis 44
CHAPTER TWO: MATERIALS AND METHODS 45
  2.1 Materials 46
    2.1.1 Chemicals and Reagents Used in This Study 46
    2.1.2 Enzymes 48
    2.1.3 Molecular Size Standards 48
    2.1.4 Multicomponent Systems 48
    2.1.5 Plasmids 48
    2.1.6 Antibodies 49
    2.1.7 Oligonucleotides 50
    2.1.8 Standard Buffers and Solutions 53
  2.2 Microorganisms and Culture Conditions 54
    2.2.1 Bacterial Strains and Culture Conditions 54
    2.2.2 Yeast Strains and Culture Conditions 55
    2.2.3 Mating, Sporulation and Tetrad Dissection of *S. cerevisiae* 57
  2.3 Introduction of DNA into Microorganisms 58
    2.3.1 Chemical Transformation of *E. coli* 58
    2.3.2 Electroporation of *E. coli* 59
    2.3.3 Chemical Transformation of Yeast 60
    2.3.4 Electroporation of Yeast 60
  2.4 Isolation of DNA from Microorganisms 61
    2.4.1 Isolation of Plasmid DNA from Bacteria 61
    2.4.2 Isolation of Chromosomal DNA from Yeast 62

2.5 DNA Manipulation and Analysis 62
  2.5.1 Amplification of DNA by the Polymerase Chain Reaction (PCR) 63
  2.5.2 Digestion of DNA by Restriction Endonucleases 63
  2.5.3 Dephosphorylation of 5'-ends 63
  2.5.4 Separation of DNA Fragments by Agarose Gel Electrophoresis 64
  2.5.5 Purification of DNA Fragments from Agarose Gel 64
  2.5.6 Purification of DNA from Solution 64
  2.5.7 Ligation of DNA Fragments 65
  2.5.8 DNA Sequencing 65
  2.5.9 Construction of Strains Carrying Plasmid-encoded *myo2* Point Mutants as Sole Copies of *MYO2* 66
2.6 Protein Manipulation and Analysis 68
  2.6.1 Preparation of Yeast Whole Cell Lysates 68
  2.6.2 Precipitation of Proteins 69
  2.6.3 Determination of Protein Concentration 69
  2.6.4 Separation of Proteins by Electrophoresis 70
  2.6.5 Detection of Proteins by Gel Staining 70
  2.6.6 Detection of Proteins by Immunoblotting 70
2.7 Subcellular Fractionation of S. *cerevisiae* Cells 71
  2.7.1 Peroxisome Isolation from *S. cerevisiae* 71
  2.7.2 Extraction and Subfractionation of Peroxisomes 73
2.8 Microscopy 73
  2.8.1 Confocal 4D Video Microscopy 73
  2.8.2 Quantification of Rates of Peroxisome Inheritance 75
  2.8.3 Immunofluorescence Microscopy 76
2.9 Yeast Two-hybrid Analysis 77
  2.9.1 Construction of Chimeric Genes 77
  2.9.2 Assays for Two-hybrid Interactions 78
2.10 Assay for Direct Protein Interaction 78
2.11 Cell Cycle Arrest 79
CHAPTER THREE: INP2P IS THE PEROXISOME-SPECIFIC RECEPTOR FOR THE MYOSIN V MOTOR MYO2P OF *SACCHAROMYCES CEREVISIAE* 80
Overview 81
3.1 The Identification of Inp2p 84
3.2 Cells Lacking Inp2p Exhibit a Specific Impairment in Peroxisome Inheritance 85
3.3 Inp2p Is a Peroxisomal Integral Membrane Protein Whose Levels Vary with the Cell Cycle 88
3.4 Inp2p Interacts Directly with the Globular Tail of Myo2p 92
3.5 Peroxisome Inheritance Is Abolished or Delayed in Cells Lacking Inp2p 95
3.6 Peroxisome Movements within Buds of *inp2Δ* Cells Are Not Dependent on the Actomyosin System 98
3.7 Overexpression of *INP2* Leads to the Depletion of Peroxisomes from Mother Cells100
3.8 The Interplay between Inp2p and Inp1p 104
3.9 Discussion 107
  3.9.1 Inp2p is the Peroxisome-specific Receptor for Myo2p 107
  3.9.2 Inp2p Dynamics during the Cell Cycle 109

3.9.3 Coordination between Peroxisome Retention and Transport: Interplay between Inp1p and Inp2p 111
CHAPTER FOUR: IDENTIFICATION OF THE SURFACE AREA OF THE PEROXISOME-BINDING REGION OF MYO2P 114
4.1 Overview 115
4.2 Isolation of Mutants of the Myo2p Globular Tail Defective in Peroxisome Distribution 118
4.3 Mutants of Myo2p Defective in Peroxisome Inheritance Display Decreased Affinity for Inp2p 122
4.4 Myo2p Point Mutants Defective in Peroxisome Inheritance Are Not Defective in Vacuolar or Mitochondrial Inheritance 124
CHAPTER FIVE: PERSPECTIVES 128
5.1 Synopsis 129
5.2 Future directions for studies on Inp2p 129
5.3 Future directions for studies on peroxisome inheritance in general 131
5.4 Future directions for the field of organelle inheritance 132
5.5 Concluding remarks 135
CHAPTER SIX: REFERENCES 137

LIST OF TABLES

Table 2-1. Primary antibodies 49

Table 2-2. Secondary antibodies 50

Table 2-3. Oligonucleotides 50

Table 2-4. Common solutions 53

Table 2-5. *E. coli* strains 55

Table 2-6. Bacterial culture media 55

Table 2-7. *S. cerevisiae* strains 56

Table 2-8. Yeast culture media 57

Table 2.9 *myo2* point mutants used in this study 67

LIST OF FIGURES

Figure 1-1. A model for peroxisome biogenesis and division 6

Figure 1-2. A model for Inp1p function in peroxisome retention.................................... 24

Figure 1-3. Bud-directed transport of organelles in *S. cerevisiae* cells 28

Figure 3-1. Peroxisome dynamics in wild-type *S. cerevisiae* cells.................................. 82

Figure 3-2. Deletion of the *INP2* gene affects specifically peroxisome inheritance 86

Figure 3-3. Inp2p is a peroxisomal integral membrane protein whose levels vary with the cell cycle 89

Figure 3-4. Inp2p interacts directly with the globular tail of Myo2p 93

Figure 3-5. Peroxisome dynamics in *inp2Δ*, *bni1Δ*, and *myo2-66* cells 96

Figure 3-6. Peroxisome velocity in wild-type and *inp2Δ* cells....................................... 99

Figure 3-7. Overproduction of Inp2p alters the partitioning of peroxisomes without affecting the segregation of other organelles 102

Figure 3-8. Interplay between Inp1p and Inp2p.. 105

Figure 4-1. Surface representation of the Myo2p globular tail indicating the initial point mutants tested for defects in peroxisome inheritance... 117

Figure 4-2. Screening of point mutations in subdomain II of Myo2p for defects in peroxisome inheritace 119

Figure 4-3. Mutants of Myo2p defective in peroxisome inheritance display decreased affinity for Inp2.. 123

Figure 4-4. Myo2p point mutants defective in peroxisome inheritance are not defective in vacuolar or mitochondrial inheritance 125

Figure 4-5. Surface representation of the Myo2p globular tail indicating the regions that bind peroxisomes and secretory vesicles 126

LIST OF SYMBOLS AND ABBREVIATIONS

20KgP	pellet obtained from centrifugation at 20,000x *g*
20KgS	20KgS supernatant obtained from centrifugation at 20,000x *g*
4D	four dimensional
bp	base pair
BSA	bovine serum albumin
Da	dalton
DRP	dynamin related protein
DMF	N, N-Dimethylformamide
dNTP	Deoxyribonucleoside triphosphate
ECL	Enhanced Chemiluminescence
ER	Endoplasmic reticulum
F-actin	filamentous actin
g	gram
g	gravitational force
G1	stage G1 of the cell cycle
G6PDH	glucose-6-phosphate dehydrogenase
GFP	green fluorescent protein
GST	glutathione S-transferase
h	hour
HRP	horseradish peroxidase
IgG	immunoglobulin G
IPTG	isopropyl β-D-thiogalactoside
PTS	peroxisomal targeting signal
M	stage M of the cell cycle
mRFP	monomeric red fluorescence protein
OD	optical density
pA	protein A
PAGE	polyacrylamide gel electrophoresis
PBD	peroxisome biogenesis disorder

PCR	polymerase chain reaction
PEX#	wild-type gene encoding *Pex#*p
pex#	mutant *PEX#* gene
PI-(3,4)/P2	phosphatidylinositol 3,4,5-trisphosphate
Pot1	thiolase
PNS	post-nuclear supernatant
S	stage S of the cell cycle
S. cerevisiae	*Saccharomyces cerevisiae*
Sdh2	succinate dehydrogenase
SDS	sodium dodecyl sulphate
TAP	tandem affinity purification
TCA	trichloroacetic
U	unit of enzyme activity
v	volume
w	weight
X-gal	5-bromo-4-chloro-3-indolyl-β-D-galactopyranoside
Y. lipolytica	*Yarrowia lipolytica*

CHAPTER ONE: INTRODUCTION

A version of this chapter has been published.
Fagarasanu, A., M. Fagarasanu and R. A. Rachubinski. 2007. Maintaining Peroxisome Populations: A Story of Division and Inheritance. *Annu. Rev. Cell Dev. Biol.* 23:321-344.
Fagarasanu, A., and R. A. Rachubinski. 2007. Orchestrating organelle inheritance in *Saccharomyces cerevisiae*. *Curr. Opin. Microbiol.* 10:528-538.

1.1 Introduction to Peroxisomes

Compartmentalization of different metabolic pathways into discrete membrane-bounded compartments, called organelles, is a defining feature of eukaryotic cells. By virtue of this spatial compartmentalization, eukaryotic cells are able to create interdependent, yet diverse, microenvironments that separate potentially competing biochemical reactions. Organelles constantly communicate with one another, which leads to the establishment of an effective and cooperative division of metabolic labor (Fagarasanu et al., 2007).

Peroxisomes, originally called microbodies, are single-membrane-bounded organelles, first described by the Swedish graduate student Johannes Rhodin in 1954 as "spherical or oval bodies in mouse proximal kidney tubules". However, the functions of these organelles started to be unraveled by the pioneering work of Christian de Duve and coworkers (de Duve, 1965; de Duve and Baudhuin, 1966), who first isolated peroxisomes using density gradient centrifugation. They defined peroxisomes as organelles containing at least one flavin oxidase, which produces hydrogen peroxide (H_2O_2), and catalase, which degrades it. The introduction of techniques for the detection of intracellular localization of catalase (Fahimi, 1968; Hirai, 1969; Novikoff and Goldfischer, 1969) revealed the widespread occurrence of peroxisomes in virtually all eukaryotic cells. Also belonging to the peroxisome family are glyoxysomes of plant seeds, Woronin bodies of some fungi, and glycosomes from tripanosomatids (Cajaraville et al., 2003).

Peroxisomes harbor a wide spectrum of metabolic activities that vary among different species, developmental stages, and cell types (Purdue and Lazarow, 2001; Schrader and Fahimi, 2006; Fagarasanu et al., 2007). As new roles for peroxisomes were discovered, it became clear that heterogeneity in morphology and metabolic plasticity are distinguishing features of peroxisomes. Two widely distributed and conserved functions of peroxisomes are fatty acid β-oxidation and hydrogen peroxide (H_2O_2) metabolism. Other metabolic pathways in peroxisomes function in the α-oxidation of specific fatty acids; the catabolism of purines, polyamines, prostaglandins, and eicosanoids; and the biosynthesis of plasmalogens and sterols. Peroxisomes have also been implicated in the metabolism of oxygen free radicals and nitric oxide. They are also involved in intra- and intercellular signaling (Masters, 1996; Titorenko and Rachubinski, 2004).

Given this array of peroxisomal functions, it is not at all surprising that peroxisomes are, under certain conditions, indispensable organelles. Peroxisome-defective yeast mutants fail to grow on various nutrients that require peroxisomal enzymes for their metabolism. These nutrients are diverse and vary with yeast species, further underscoring the versatility of peroxisomal functions among different organisms. Peroxisomes are also essential for normal human development and physiology, as demonstrated by the lethality of the peroxisome biogenesis disorders, in which peroxisomes fail to assemble correctly (Purdue and Lazarow, 2001).

1.2 The Strategies Used by Eukaryotic Cells to Maintain their Peroxisomes

To preserve the advantages of having peroxisomes, eukaryotic cells have evolved molecular mechanisms that ensure the maintenance of the peroxisome population during cell proliferation. These mechanisms essentially regulate the placement and number of peroxisomes. Upon cell division, peroxisomes must be segregated equally between the two resulting cells, thus ensuring their inheritance by the future generations. Secondly, the number of peroxisomes has to increase during the cell cycle to prevent the dilution of these organelles with each round of cell division. Analyzing the mechanisms used by cells to control peroxisome number during the cell cycle requires a brief discussion of peroxisome formation.

For the past two decades, the prevailing view has been that peroxisomes form by the growth and division of preexisting peroxisomes; i.e., they seed their own growth (Lazarow and Fujiki, 1985; Purdue and Lazarow, 2001). This model placed peroxisomes, like mitochondria and chloroplasts, into the category of autonomous organelles, which cannot be made de novo. The propagation of an autonomous organelle entails a constant import of both lipids and proteins to enable it to sustain membrane growth while preventing dilution of its protein constituents. According to the "growth-and-division model", all peroxisomal proteins were posttranslationally acquired, whereas the endoplasmic reticulum (ER) was viewed only as a possible source of membrane lipids.

However, this longstanding paradigm for peroxisome biogenesis has recently been challenged by multiple observations that have compellingly showed that peroxisomes can also form de novo from the ER (Titorenko et al., 1997; Titorenko and Rachubinski, 1998a; Mullen et al., 1999; Geuze et al., 2003; Hoepfner et al., 2005; Tam et al., 2005; Kim et al., 2006). It is now well established that several peroxisomal membrane proteins (PMPs) are initially sorted to the ER. Once in the ER, these PMPs are sequestered into discrete specialized regions of the ER membrane and then incorporated into expanding vesicles (for a review, see Titorenko and Mullen, 2006). These vesicles eventually bud from the ER, generating peroxisomal precursor vesicles. In most cells, these preperoxisomes are deemed to be small vesicles that mature into peroxisomes through a sequence of steps that probably requires homotypic membrane fusion as well as protein import (Figure 1-1). Fusion of ER-derived preperoxisomal vesicles has already been shown to occur in the yeasts *Yarrowia lipolytica* (Titorenko et al., 2000) and *Pichia pastoris* (Faber et al., 1998).

Collectively, these observations indicate that peroxisomes represent an outgrowth of the ER and thus constitute another branch of the secretory pathway (Titorenko and Rachubinski, 1998b; Schekman, 2005). Therefore, we posited that the biogenesis of peroxisomes obeys the same principles that govern vesicular transport in the classical ER secretory system (Fagarasanu et al., 2007). To maintain organelle homeostasis, the forward movement of cargo from the ER to the peroxisomal endomembrane system must be accompanied by a retrograde, vesicle-mediated transport for the retrieval of escaped ER-resident proteins (Bonifacino and Glick, 2004) (Figure 1-1). Moreover, such an ER-destined retrograde vesicular flow may also be required for the recycling of those PMPs that orchestrate the first stages of peroxisome membrane assembly at the ER (Mullen and Trelease, 2006; Titorenko and Mullen, 2006). To date, such peroxisome-to-ER vesicular transport has been observed only in infected plant cells (McCartney et al., 2005). It remains to be established whether this type of reverse protein sorting pathway also exists in uninfected plant cells and in the cells of other organisms.

As already mentioned, upon cell division, cells need to double the number of their peroxisomes and distribute them equitably between the two resulting cells. Considering the current view of peroxisomes as organelles that can arise from the ER, but also possess

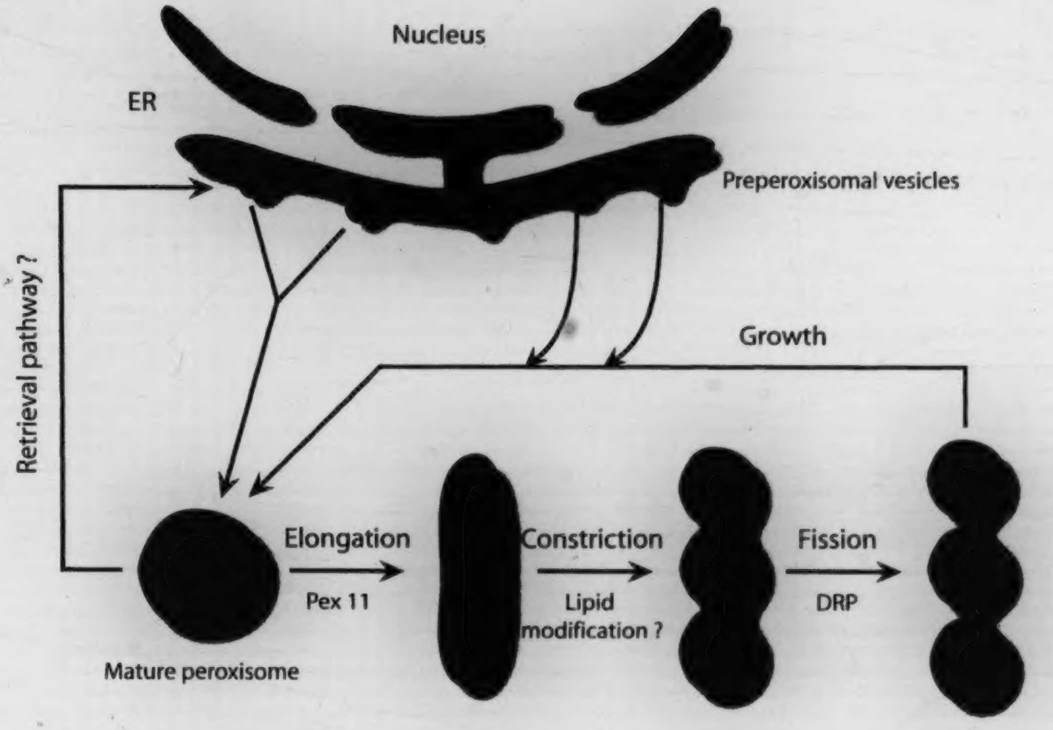

Figure 1-1. A model for peroxisome biogenesis and division. Preperoxisomal vesicles originate in specialized compartments of the endoplasmic reticulum (ER). Fusion of these preperoxisomes is probably required to form a mature, metabolically active peroxisome. A retrograde pathway can be envisioned for the retrieval of escaped ER proteins and recycling of the preperoxisome assembly machinery. The division of peroxisomes proceeds through three distinct steps: elongation of peroxisomes, membrane constriction, and final fission of peroxisomal tubules. Pex11 proteins are implicated in the elongation step of peroxisome division, whereas dynamin-related proteins (DRPs) catalyze the fission event. A modification in membrane lipid composition probably underlies the membrane curvature necessary for membrane constriction (see the text for details). Peroxisomes grow by fusion with preperoxisomal vesicles and through the direct import of matrix and membrane proteins.

the ability to grow and divide, an important question is whether the doubling of peroxisome number during cell division is due solely to the fission of preexisting peroxisomes or is also the result of the synthesis of new peroxisomes from the ER. A recent study (Kim et al., 2006) showed that, in mammals, both processes, the division of peroxisomes and the production of new ones, account for the formation of peroxisomes in constitutively dividing cells. However, Motley and Hettema (2007) recently provided evidence that in wild-type yeast cells, peroxisomes multiply by growth and division and do not form de novo. Only yeast cells lacking peroxisomes as a result of a segregation defect were observed to form peroxisomes de novo from the ER. Therefore, at least in yeast cells, de novo formation may therefore represent a rescue mechanism that becomes functional only in case peroxisomes are lost (Schrader and Fahimi, 2008). The ER-to-peroxisome pathway would normally function to supply existing peroxisomes with essential membrane constituents so that they sustain their growth and division. Thus, the physiological significance of the mechanism of de novo formation in comparison to the classical pathway of growth and division for controlling peroxisome number in yeast has again been challenged (Shrader and Fahimi, 2008). It is tempting to speculate that during their growth, mature peroxisomes acquire their membrane constituents by fusion with the same ER-derived preperoxisomal vesicles that could otherwise homotypically fuse to form a "new" peroxisome (Fagarasanu et al., 2007). Such a scenario would also provide a way for those PMPs that constitutively pass through the ER to be incorporated into a growing peroxisome so that their concentrations within the peroxisomal membrane are maintained during multiple rounds of peroxisomal growth and division. For example, the integral PMP Pex3p of the yeast *Saccharomyces cerevisiae* reaches preexisting, mature peroxisomes after initially sampling the ER membrane (Hoepfner et al., 2005; Motley and Hettema, 2007).

I will now review the mechanisms regulating the division and inheritance of peroxisomes, with particular attention given to these processes in our chosen eukaryotic model organism, the yeast *S. cerevisiae*.

1.3 Peroxisome Division

1.3.1 Introduction to Peroxisome Division

Peroxisome division must be coordinated with the cell cycle to maintain the number of peroxisomes in each cell. However, peroxisomes have the ability to proliferate, i.e., to increase in number and/or size, in response to external stimuli that induce peroxisome-housed enzymes. Probably the same set of proteins choreographs peroxisome division, regardless of whether it is cell-cycle-dependent or linked to peroxisome proliferation (Yan et al., 2005). As mentioned earlier, the exact contribution of the ER to the cell-cycle-related duplication of peroxisomes and peroxisome proliferation remains to be established.

Multiple observations point to the existence of a tight coordination between peroxisome maturation and division. In *Y. lipolytica* and *Hansenula polymorpha*, peroxisomal vesicles can undergo division only after they have matured through the import of matrix proteins, whereas in *Candida boidinii*, peroxisome division precedes growth. However, in mammalian cells, both mature and immature peroxisomes have the ability to divide (Thoms and Erdmann, 2005).

Morphological observation shows that peroxisome division proceeds through at least three partially overlapping steps: the elongation of peroxisomes, the constriction of the peroxisomal membrane, and the fission of peroxisomes. Pex11 proteins are implicated in the elongation step of peroxisome division, whereas dynamin-related proteins (DRPs) catalyze the final fission event. Little is known about how the various components of the peroxisome division machinery coordinate their activities with events of the cell cycle.

1.3.2 Elongation of Peroxisomes: The Role of Pex11 Proteins

Pex11p was the first protein to be implicated in peroxisome division (Erdmann and Blobel, 1995; Marshall et al., 1995). In *S. cerevisiae*, Pex11p-deficient cells exhibit fewer, but considerably larger, peroxisomes as compared to the peroxisomes of wild-type cells (Erdmann and Blobel, 1995). Conversely, overexpression of the *PEX11* gene leads to an increase in the number of peroxisomes. A striking feature of cells overproducing Pex11p is the appearance of elongated peroxisomal structures. This distinctive phenotype implicated Pex11p in the tubulation step of peroxisome division (Marshall et al., 1995; Yan et al., 2005) (Figure 1-1). Two additional *S. cerevisiae* proteins, Pex25p (Smith et al., 2002) and Pex27p (Rottensteiner et al., 2003; Tam et al., 2003), that share weak amino acid sequence similarity to Pex11p, have recently been identified. Pex25p and Pex27p are involved in peroxisome division and appear to have functions partially redundant to that of Pex11p. Pex11p, Pex25p, and Pex27p thus form a protein family of low homology, the Pex11 protein family, involved in the division of peroxisomes.

Pex11p, Pex25p, and Pex27p are all peripheral PMPs, even though some controversy still exists in the case of Pex11p. Individual or pairwise deletions of proteins belonging to the Pex11 protein family result in fewer and larger peroxisomes. Pex11 proteins, in addition to promoting peroxisome division, are required for the efficiency of transport processes across the peroxisomal membrane. A lack of Pex11p impairs the metabolic exchange of intermediates of fatty acid metabolism across the peroxisomal membrane (van Roermund et al., 2000), whereas the *pex11Δ/pex25Δ/pex27Δ* triple deletion strain of *S. cerevisiae* displays a severe defect in the import of peroxisomal matrix proteins (Rottensteiner et al., 2003).

In mammals, three Pex11 isoforms, designated Pex11α, Pex11β and Pex11γ, have been identified. They are all integral PMPs and have both their amino and carboxyl termini exposed to the cytosol. Some important observations are worth mentioning. The overproduction of Pex11β results in peroxisome tubulation, followed by an increase in peroxisome number (Schrader et al., 1998). However, in the absence of a functional DRP, overproduction of Pex11β results in peroxisome hypertubulation alone, without an increase in peroxisome number. This suggests that Pex11 proteins cannot constrict or divide peroxisomes themselves and most likely function upstream of DRPs by promoting peroxisomal membrane tubulation (Koch et al., 2003, 2004; Schrader, 2006). Other eukaryotic cells also contain multiple Pex11 isoforms. Cells of the plant *Arabidopsis thaliana* contain five Pex11 isoforms (Lingard and Trelease, 2006), whereas filamentous fungi have three Pex11 isoforms (Kiel et al., 2006).

Pex11 proteins interact with themselves, suggesting that they may form homodimers or homooligomers (Marshall et al., 1996; Li and Gould, 2003; Rottensteiner et al., 2003; Tam et al., 2003). In *S. cerevisiae*, homooligomerization of Pex11p correlates with loss of function, whereas a mutation that prevents the self-association of Pex11p causes an increase in peroxisome number (Marshall et al., 1996).

How do Pex11 proteins function? Some hints about their mechanism of action have come from analysis of the structures of Pex11 proteins from yeast. A region shared by Pex11p family members shows extensive amino acid sequence similarity to the ligand-binding domains of nuclear hormone receptors (Barnett et al., 2000), especially with the ligand-binding domains of the peroxisome proliferator-activated receptors, which bind fatty acids. This observation may point to a role for Pex11 proteins in phospholipid binding and probably in peroxisome membrane modification and may explain the multiple roles of Pex11 proteins in peroxisome biology. It is tempting to speculate that the membrane-modifying activity of Pex11 proteins is responsible for the tubulation of peroxisomes. The same membrane-modifying properties may also underlie the role of Pex11 proteins in different transport processes across the peroxisomal membrane.

1.3.3 Constriction of the Peroxisomal Membrane

The molecular mechanisms mediating the constriction of the peroxisomal membrane are largely unknown.

Studies of *Y. lipolytica* have revealed an interesting mechanism that controls membrane constriction from inside peroxisomes. *Yl*Pex16p is an intraperoxisomal peripheral PMP that negatively regulates peroxisome division (Eitzen et al., 1997; Guo et al., 2003). *Yl*Pex16p functions by inhibiting a lipid biosynthetic pathway that leads to the formation of diacylglycerol, a potent inducer of membrane curvature. The import of various matrix proteins during the maturation process of peroxisomes gradually displaces the peroxisomal enzyme acyl-CoA oxidase from the matrix to the membrane, where this enzyme interacts with and inhibits *Yl*Pex16p (Guo et al., 2007). As a result, the negative influence of *Yl*Pex16p on peroxisome division is released by its interaction with acyl-CoA oxidase only in mature peroxisomes (Guo et al., 2003). This results in the local accumulation of the cone-shaped diacylglycerol in the outer leaflet of the lipid bilayer, causing membrane curvature and constriction. *Yl*Vps1p, a DRP, is then recruited to the cytosolic face of the membrane to execute the final fission of the peroxisomal membrane (Guo et al., 2007). This mechanism explains why only mature peroxisomes undergo division in *Y. lipolytica*. It remains to be established whether the constriction of peroxisomal membranes in other yeast species and mammalian cells is also regulated by components acting from the lumenal side of peroxisomes. However, the molecular players involved are expected to be different. *S. cerevisiae* does not have a Pex16p homolog, whereas the mammalian Pex16 protein has a role in peroxisome biogenesis at the level of the ER rather than in peroxisome division (Honsho et al., 1998).

1.3.4 Fission of Peroxisomes: Involvement of Dynamin-Related Proteins

Dynamins constitute a superfamily of large GTPases that carry out a broad range of functions within the cell and are implicated mainly in vesicle scission reactions. On the basis of the presence of specific domains within their protein structure, dynamins have been subdivided into classical dynamins and DRPs (Praefcke and McMahon, 2004). Dynamins and DRPs probably function as mechanochemical enzymes that use GTPase-dependent conformational changes to drive fission directly rather than through the recruitment of downstream effectors (Praefcke and McMahon, 2004). Dynamin and DRPs are known for their ability to induce membrane curvature, which results in both the constriction and scission of membranes (Praefcke and McMahon, 2004; McMahon and Gallop, 2005). However, many times, membranes are constricted by other factors first, and then dynamins are recruited to execute the final fission reaction. For example, in endocytosis, dynamin promotes membrane scission only after clathrin and other coat proteins have constricted the neck of an endocytic vesicle (Osteryoung and Nunnari, 2003).

Mammalian or yeast cells deficient in peroxisomal DRPs display elongated peroxisomes with segmented morphology, resembling beads on a string (Hoepfner et al., 2001; Koch et al., 2003) (Figure 1-1). Therefore, without DRPs, peroxisomes are able to constrict but are unable to divide. This suggests that DRPs act late in the process of peroxisome division, after the peroxisomal membrane has been constricted through still poorly understood mechanisms (Yan et al., 2005). Thus, peroxisome constriction and peroxisome scission are distinct processes that require distinct sets of molecular components (Schrader, 2006). Thinning of the peroxisomal tubule is probably required for the DRP ring to be efficiently assembled around the tubule and promote the scission of the peroxisome. Growing evidence supports the view that DRPs are essential for the fission of peroxisomes in all cell types.

Involvement of a DRP in peroxisome fission was first observed in *S. cerevisiae* (Hoepfner et al., 2001). The *S. cerevisiae* genome encodes three DRPs (Dnm1p, Mgm1p and Vps1p) but no classical dynamin. Initially, of these DRPs, only Vps1p was found to be required for peroxisome division. The number of peroxisomes in cells lacking Vps1p is drastically reduced. Most cells lacking Vps1p contain only one or two giant peroxisomes, which often appear as elongated tubular structures. Ultrastructural analysis revealed that these peroxisomes display constrictions and appear like beads on a string (Hoepfner et al., 2001), showing that, in the absence of Vps1p, peroxisomes still retain the ability to constrict their membranes. A partial colocalization of Vps1p with peroxisomes was detected. Vps1p is required for peroxisome fission under both peroxisome-inducing and -noninducing conditions (Hoepfner et al., 2001; Li and Gould, 2003). Interestingly, Dnm1p, which normally mediates mitochondrial fission, is also required for peroxisome fission, especially under peroxisome-inducing conditions (Kuravi et al., 2006). Evidence for this conclusion comes from the observation that deletion of the *DNM1* gene in cells already lacking Vps1p further decreases the number of peroxisomes and causes virtually all cells to contain a single, enlarged peroxisome. Interestingly, the giant peroxisomes observed in *vps1Δ* and *vps1Δ/dnm1Δ* mutants undergo constitutive division and then are correctly apportioned between mother and daughter cells (Hoepfner et al., 2001; Kuravi et al., 2006). This observation suggests that neither Vps1p nor Dnm1p plays a direct role in peroxisome distribution and inheritance. Furthermore, this finding points to the existence of a dynamin-independent mode of peroxisome division. Pulling forces exerted by the Myo2p motor on the one hand, and retention mechanisms on the other hand, may act on the same giant peroxisome, eventually tearing it apart (Kuravi et al., 2006; van der Zand et al., 2006). It remains to be established if such a dynamin-independent peroxisome fission also occurs in wild-type cells (see Section 1.4 Peroxisome Inheritance).

Recently, investigators discovered the DRP DLP1/Drp1 to be essential for peroxisome division in mammalian cells (Koch et al., 2003, 2004; Li and Gould, 2003; Tanaka et al., 2006). Knockdown of DLP1/Drp1 by siRNA-mediated silencing led to a reduction in peroxisome number and an accumulation of elongated peroxisomes. As already described for yeast *vps1Δ* cells, these tubular peroxisomes have a beads-on-a-string segmented appearance (Koch et al., 2004; Schrader, 2006). Furthermore, overexpression of dominant-negative mutants of DLP1/Drp1 exerted similar effects on peroxisome morphology (Koch et al. 2003, 2004; Li and Gould, 2003). Interestingly, DLP1/Drp1 is involved in both peroxisome and mitochondrial fission in mammalian cells (Schrader, 2006).

DLP1/Drp1 physically associates with peroxisomes. DLP1/Drp1 aligns in spots along elongated peroxisomes (Koch et al., 2003). The peroxisomal localization of DLP1/Drp1 is more readily detected upon overexpression of Pex11β (Koch et al., 2003, Li and Gould, 2003) or when peroxisome proliferation is induced by treatment with bezafibrate (Koch et al., 2003). How are DRPs recruited to the peroxisomal membrane? Classical dynamins associate with membranes, using their pleckstrin homology (PH) domains, which bind membrane lipids. However, because DRPs lack PH domains, other factors must recruit DRPs to the membrane of their target organelles. Moreover, these factors must be limiting, because overexpression of wild-type DRPs does not result in peroxisome (or mitochondrial) proliferation (Koch et al., 2004). A candidate for such an adaptor for DRPs in mammalian cells is Fis1. Fis1, a DLP1-interacting protein previously implicated in the process of mitochondrial fission, was recently shown to function in peroxisome fission as well. Fis1 is an integral membrane protein of both peroxisomes and mitochondria. Intriguingly, unlike DLP1/Drp1, which concentrates at discrete sites of constriction on mitochondria and peroxisomes, Fis1 is uniformly distributed along the membranes of these organelles. Knockdown of Fis1 protein levels by siRNA results in the formation of elongated peroxisomes and mitochondria, a phenotype resembling the one observed in DLP1/Drp1-deficient cells. It is noteworthy that the oversynthesis of Fis1 causes an accumulation of numerous minute peroxisomes and promotes mitochondrial fragmentation. These effects, which require a functional DLP1/Drp1 to occur (Koch et al., 2005), show that Fis1 is a limiting factor in the process of peroxisome and mitochondrial division. *S. cerevisiae* Fis1p interacts with Dnm1p to promote mitochondrial division. However, like Dnm1p, Fis1p also plays a role in peroxisome division, especially under conditions of peroxisome induction (Kuravi et al., 2006). It remains to be established what proteins underlie the association of Vps1p with peroxisomes in *S. cerevisiae*.

The requirement for DRPs in peroxisome fission has also been demonstrated in plants. Mano et al. (2004) showed that DRP3A promotes both peroxisome and mitochondrial fission in *A. thaliana*. Collectively, the aforementioned findings suggest that DRPs in various organisms catalyze the last stage of peroxisome division by pinching off small peroxisomes from already constricted tubules.

1.3.5 Other Proteins that Regulate the Size and Number of Peroxisomes

In addition to proteins belonging to the Pex11 family and DRPs, several other peroxisomal proteins that affect the size and number of peroxisomes have been discovered in the yeast *S. cerevisiae*. Pex28p and Pex29p are two highly homologous

PMPs with redundant functions (Vizeacoumar et al., 2003). Single or double deletions of *PEX28*/*PEX29* genes result in clusters of peroxisomes that often exhibit thickened membranes between adjacent peroxisomes. This finding suggests that Pex28p and Pex29p may be involved in the separation of peroxisomes after peroxisome division (Vizeacoumar et al., 2003). Thus, these two peroxins play a role in distributing peroxisomes within cells. However, lack of either Pex28p or Pex29p does not disrupt the distribution of peroxisomes at cell division, and therefore neither peroxin is required for peroxisome inheritance.

The PMPs Pex30p, Pex31p, and Pex32p form another family of homologous peroxins implicated in the regulation of peroxisome size and number in *S. cerevisiae* (Vizeacoumar et al., 2004). Lack of Pex30p leads to an increase in the number of peroxisomes, whereas loss of either Pex31p or Pex32p results in enlarged peroxisomes. The *pex30Δ*/*pex31Δ*/*pex32Δ* triple deletion mutant strain exhibits a pronounced increase in the number of peroxisomes per cell. The molecular mechanisms by which these proteins influence peroxisome size and number have yet to be elucidated.

1.4 Peroxisome Inheritance

1.4.1 Introduction to Organelle Inheritance in Yeast

The past twenty years.have witnessed a tremendous increase in our understanding of the different strategies used by cells to partition their organelles. *S. cerevisiae* has been used extensively to study the mechanisms of organelle inheritance. Since a *S. cerevisiae* cell divides asymmetrically by budding, correct organelle partitioning is achieved by the active and directional delivery of half of its organelles to the attached bud concomitant with the retention of the remaining organelles in the mother cell. This feature makes the detection and isolation of organelle inheritance mutants in *S. cerevisiae* easier than in cells that divide by median fission (Fagarasanu and Rachubinski, 2007).

Because some organelles like the ER, mitochondria and chloroplasts cannot be made de novo, they must be inherited from mother cell to daughter cell upon cell division. The requirement for controlling the inheritance of other cytoplasmic organelles, such as the Golgi complex, lysosomes and peroxisomes, is less apparent because they can be made de novo from the ER (Weisman, 2003; Losev et al., 2006; Fagarasanu et al., 2007). However, multiple studies have shown that cells have evolved partitioning mechanisms for all their organelles, irrespectively of whether they can be made de novo or not. This finding is testament to an acute selection pressure for accurate organelle inheritance that is probably the result of the high energy cost of manufacturing organelles anew.

S. cerevisiae cells undergo a stereotypical pattern of growth and division called budding (Bretscher, 2003; Pruyne et al., 2004a; Fagarasanu and Rachubinski, 2007). After bud emergence in late G1, cell growth is restricted to the bud tip. This focused, apical growth pattern changes to isotropic growth in G2, in which the bud expands evenly over its entire surface. As the bud approaches the size of its mother, growth is directed to the bud neck for assembly of a septum that will separate mother and daughter cells (Bretscher, 2003; Pruyne et al., 2004a). To achieve this pattern of polarized growth, the secretory pathway must deliver material to discrete sites at the cell surface that are distinct for each stage of the cell cycle.

Actin cables form the tracks that direct polarized secretion in budding yeast. Actin cables represent bundles of actin filaments that are assembled by a conserved class of proteins called formins. These specialized proteins associate with the barbed, or plus, end of the actin filament, where polymerization occurs, and remain attached to this site as the filament grows (Pruyne et al., 2004a). Since formins are strategically localized to the bud, actin cables will radiate from the bud deep into the mother cell (Yang and Pon, 2002). In mother cells, class V myosins, which are specialized molecular motors, capture various cargoes, including secretory vesicles, and use the actin cables as tracks toward the formin-rich regions, which thus become sites of active membrane expansion or growth. Changes in the localization of formins during the cell cycle result in the targeting of secretory vesicles to varying locations in the bud (Pruyne et al., 2004b).

Class V myosins function as homodimers whose amino-terminal heads associate with actin and couple ATP hydrolysis to conformational changes that ultimately drive their movement along actin filaments. Class V myosins migrate along actin filaments, using a hand-over-hand walking movement in which the two heads alternate in the lead with each step (Yildiz et al., 2003). Their carboxyl-terminal tail is represented by a globular domain specialized for binding to cargo via adaptor "receptor" protein complexes (Provance et al., 2002; Wu et al., 2002; Ishikawa et al., 2003; Fagarasanu et al., 2006a). Class V myosins move processively along actin tracks and are able to take hundreds of steps before dissociating from the underlying actin filament. This feature ensures the efficient transport of their cargoes over micrometer distances (Sellers and Veigel, 2006). Interestingly, these molecular motors advance 37 nm with each step, which corresponds exactly to the helical periodicity of the actin filament (Mehta et al., 1999; Seabra and Coudrier, 2004). This imposes a rectilinear trajectory of cargoes along the actin filament axis, rather than a spiral one that would lead to increased viscous drag (Sellers and Veigel, 2006). Collectively, these characteristics of class V myosin motors make them ideally suited for intracellular organelle trafficking and explain why they are found ubiquitously in eukaryotic cells. Myo2p and Myo4p are the two class V myosins found in *S. cerevisiae* (Bretscher, 2003; Pruyne et al., 2004a).

Myo2p is an essential protein because of its role in polarizing secretory vesicles for growth (Govindan et al., 1995; Schott et al., 2002). In addition, Myo2p carries other organelles for their proper inheritance, including late compartments of the Golgi (Rossanese et al., 2001), a portion of the vacuole (Ishikawa et al., 2003; Tang et al., 2003), peroxisomes (Hoepfner et al., 2001; Fagarasanu et al., 2006a) and mitochondria (Itoh et al., 2002, 2004; Boldogh et al., 2004; Altmann et al., 2008). Myo2p has also been implicated in orienting the intranuclear mitotic spindle (Beach et al., 2000; Yin et al., 2000). In contrast, Myo4p is not an essential protein and is involved in the inheritance of cortical ER (Estrada et al., 2003) and in the bud-directed transport of at least 24 mRNAs (Shepard et al., 2003).

1.4.2 Peroxisome Inheritance in *S. cerevisiae*

Each *S. cerevisiae* cell contains on average about nine peroxisomes (Hoepfner et al., 2001) that are localized peripherally at the cell cortex (Hoepfner et al., 2001; Fagarasanu et al., 2005, 2006a). Peroxisomes display cell-cycle-coordinated movements that result in their correct distribution upon cell division (Hoepfner et al., 2001; Fagarasanu et al., 2005, 2006a, 2006b). As soon as the bud emerges from the mother cell, peroxisomes detach one by one from their static cortical positions and travel toward the nascent bud. Recruitment of peroxisomes from the mother cell cortex to the bud continues until about half of the initial peroxisomal population is transferred to the daughter cell. The directional migration of peroxisomes is Myo2p-driven and actin-based, since a point mutation that affects Myo2p processivity compromises bud-directed peroxisome motility (Hoepfner et al., 2001; Fagarasanu et al., 2006b). Inside the bud, peroxisomes polarize toward sites of growth, being initially clustered at the growing bud tip. Later, upon isotropic shift, peroxisomes start to distribute over the entire bud cortex. Before cytokinesis, a few peroxisomes in the bud and mother cell relocate to the mother-bud neck region, while the rest remain anchored at the bud and mother cell cortices. All these observations point to a tightly regulated interplay between retention and mobility of peroxisomes that ultimately results in an equitable distribution of peroxisomes during cell division (Fagarasanu et al., 2006b, 2007). Two peroxisomal proteins, called Inp1p and Inp2p, have been identified as playing a role in the retention and motility of peroxisomes, respectively (Fagarasanu et al., 2005, 2006a).

1.4.2.1 Retention of Peroxisomes: The Role of Inp1p

An essential feature of the process of organelle inheritance in *S. cerevisiae* is the retention of a subset of organelles in the mother cell. Moreover, the bud must have a retention mechanism to prevent the diffusion of transferred organelles back to the mother cell. Although it has long been postulated that cells possess mechanisms for the site-specific immobilization or anchoring of their organelles, components specifically involved in this process have not been identified.

1.4.2.1.1 Active retention of peroxisomes in mother cells

As already mentioned, most peroxisomes in the mother cell are static and localized to the cell periphery. During bud growth, half of these immobile peroxisomes are dislodged one by one from their positions and carried to the bud. Interestingly, when the cell cycle of *S. cerevisiae* was artificially prolonged, resulting in a protracted opening of the bud neck, peroxisome distribution at cytokinesis was unperturbed, and approximately half of the peroxisomes were still immobilized in the mother cell (Fagarasanu et al., 2005). This finding clearly indicated that the partitioning of peroxisomes between mother cell and bud is not a time-dependent process indirectly controlled by cytokinesis and that, apart from a regulated transportation system for peroxisomes needed for their delivery to the bud, faithful segregation of peroxisomes upon cell division requires the presence of anchoring structures that actively retain a specific subset of peroxisomes in the mother cell. Peroxisomes retained in the mother cell do not display any preference for a specific location but rather are scattered over the entire cell periphery. In contrast, mitochondria are actively anchored at a specific area in the mother cell situated at the yeast cell pole distal to the bud site, which has been designated the "retention zone" (Yang et al., 1999).

1.4.2.1.2 Inp1p links peroxisomes to cortical structures

The PMP Inp1p was found to be crucial for the retention of peroxisomes in *S. cerevisiae* cells (Fagarasanu et al., 2005). A significant proportion of *inp1Δ* budded cells has their entire peroxisome population concentrated in the buds. The proportion of cells displaying this phenotype increases with bud size. An analysis of peroxisome dynamics in *inp1Δ* cells during the cell cycle provides important insight into the role of Inp1p. All peroxisomes, while still in the mother cell, displayed chaotic movements instead of being static and cortically localized, and no peroxisome maintained a fixed cortical position for a prolonged period of time. Eventually, all peroxisomes were transported to the daughter cell. These observations strongly suggest a role for Inp1p in the retention of peroxisomes at the cell periphery. Moreover, the complete transfer of all peroxisomes to the bud as a result of their lack of attachment to cortical structures further underscores the importance of active retention in attaining an equitable distribution of peroxisomes upon cell division. Consistent with a role for Inp1p in anchoring peroxisomes, the overproduction of Inp1p caused all peroxisomes in the mother cell to maintain static positions at the cell cortex, which prevented their normal delivery to daughter cells. Interestingly, when Inp1p was overproduced, it localized to the cell cortex in addition to, as usual, peroxisomes. This indicates that Inp1p has an intrinsic affinity for structures lining the cell periphery and probably represents the link between peroxisomes and an as-yet-unidentified cortical anchor (Fagarasanu et al., 2005) (Figure 1-2). In addition to its role in anchoring peroxisomes in mother cells, Inp1p is probably also involved in the retention of transferred peroxisomes within buds. Cells lacking Inp1p display a high frequency of peroxisomes that aberrantly return to the mother cell (Fagarasanu et al., 2005). Inp1p most likely functions in attaching peroxisomes to cortical structures in the bud that are the same as those in the mother cell. In wild-type cells, peroxisomes transferred to the bud assume static cortical positions after performing characteristic movements dependent on the actomyosin system. This process is probably

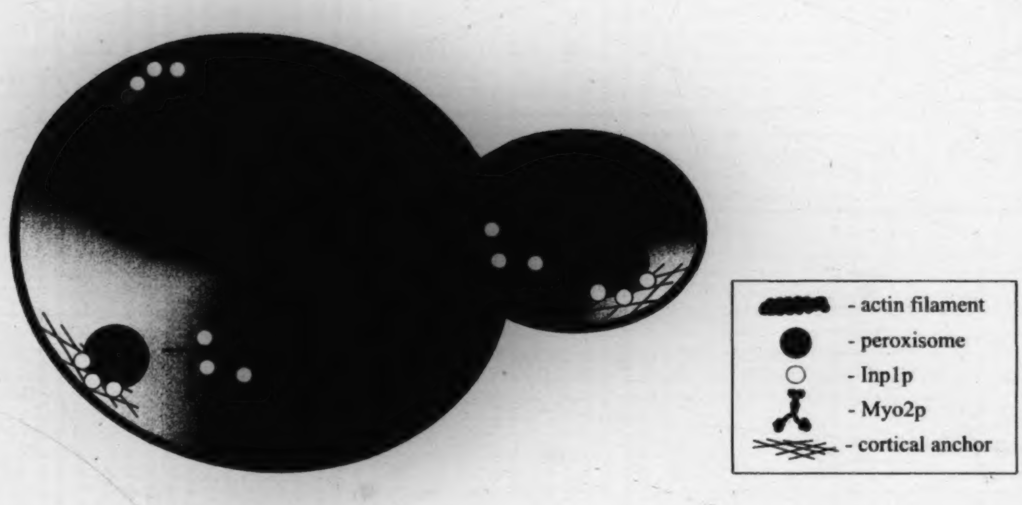

Figure 1-2. A model for Inp1p function in peroxisome retention. Peroxisomes move along polarized actin cables in a Myo2p-dependent manner from mother cell to bud. Concomitantly, a subset of peroxisomes is retained within the mother cell. Inp1p acts to link peroxisomes to a cortical anchor and retain peroxisomes in the mother cell and bud.

important for preparing the bud for the next cell cycle, when, as a mother cell, it will need to retain some of its peroxisomes (Fagarasanu et al., 2005, 2006b) (Figure 1-2).

1.4.2.1.3 Inp1p levels vary during the cell cycle

Inp1p levels fluctuate during the cell cycle, peaking at the G2-M transition. This probably reflects different requirements for peroxisome retention during different stages of the cell cycle. However, a significant amount of Inp1p can be detected throughout the cell cycle, indicative of a constant need for Inp1p in the cell. This observation is consistent with the need to immobilize peroxisomes at the mother cell and bud cortices during all stages of the cell cycle, as observed in wild-type cells. Importantly, Inp1p may contain a PEST sequence that may be involved in its cell-cycle-dependent degradation (Fagarasanu et al., 2005).

1.4.2.1.4 A role for Inp1p in coordinating peroxisome inheritance and division

In addition to having an abnormal distribution of peroxisomes along the mother-bud axis, cells lacking Inp1p also display fewer and larger peroxisomes as compared to wild-type cells. This observation indicates an additional role for Inp1p in regulating the size and number of peroxisomes, possibly through its involvement in peroxisome division. In support of this conclusion, Inp1p interacts with Vps1p, Pex25p, and Pex30p (Fagarasanu et al., 2005), proteins previously implicated in peroxisome division (see Section 1.3 Peroxisome Division). However, the two processes, peroxisome retention and division, may be intrinsically linked. The peroxisome division machinery may function more effectively on an anchored, immobilized peroxisome than on a mobile one. It is also possible that retention mechanisms work with the Myo2p motor together on a subset of peroxisomes and are responsible for their division, as has been suggested in the context of *vps1Δ* cells that contain usually one or two highly enlarged peroxisomes (see Section 1.3 Peroxisome Division). It is well established that cytoskeletal tracks and motor proteins exert tensions on organelle membranes, thus assisting in organelle fission (Schrader and Fahimi, 2006). To determine if the retention and division of peroxisomes are inherently linked or represent two different functions of Inp1p, it will be important to determine if these two processes are genetically dissectible in the Inp1p molecule.

This thesis reports the identification and molecular characterization of Inp2p, a novel protein that functions as the peroxisome-specific receptor for Myo2p (see Chapters Three and Four). To better understand the importance of our findings in peroxisome inheritance and the way in which they integrate with the field of organelle inheritance in general, I will provide a brief review of what is currently known about the mechanisms used by *S. cerevisiae* cells to partition its other membrane-bounded organelles.

1.5 Strategies Used by *S. cerevisiae* to Segregate Other Membrane-Bounded Organelles

1.5.1 Vacuoles

The yeast vacuole is an essential organelle that functionally is the equivalent of the mammalian lysosome and the plant cell vacuole (Weisman, 2003). As such, the yeast vacuole mediates many diverse processes including the turnover and recycling of proteins, the storage of metabolites, osmoregulation, and cytosolic ion and pH homeostasis (Weisman, 2003). *S. cerevisiae* cells ensure the accurate inheritance of their vacuoles at cell division by segregating a portion of this organelle to the daughter cell. Late in G1, before bud emergence, the vacuole aligns along the already polarized actin cytoskeleton, with a portion of the vacuole present at the presumptive bud site (Hill et al., 1996; Catlett and Weisman, 2000). The onset of S phase, when the bud becomes visible, is marked by the formation of one or more vesicular-tubular projections, also known as the vacuolar 'segregation structure' (Raymond et al., 1990; Weisman, 2006). This membrane-bound projection emanates from the region in the parental vacuole that is closest to the bud and, shortly after its appearance, extends from the mother cell into the bud (Hill et al., 1996; Catlett and Weisman, 2000; Weisman, 2003) (Figure 1-3).

The segregation structure is dynamic, continuously being remodeled by fission and fusion (Weisman, 2003) and often appearing as a cluster of aligned vesicles rather than as an extended tubule (Raymond et al., 1990, 1992). The transfer of vacuolar material continues throughout S and G2 and results in the accumulation of numerous vesicles in the bud (Weisman and Wickner, 1988; Raymond et al., 1990; Gomes de Mesquita, 1991). Vacuole inheritance is terminated through dissolution of the segregation structure (Gomes de Mesquita, 1991). Fusion of the maternally derived vacuolar vesicles in the bud results in the formation of a new daughter cell vacuole (Conradt et al., 1992; Wickner and Haas, 2000).

vac mutants are defective in vacuole inheritance and are subdivided into several classes. Class I *vac* mutants are the best candidates for specific impairment in the motility of the segregation structure toward the bud because they display defects in the inheritance, but not the morphology, of vacuoles. Analysis of class I mutants led to the

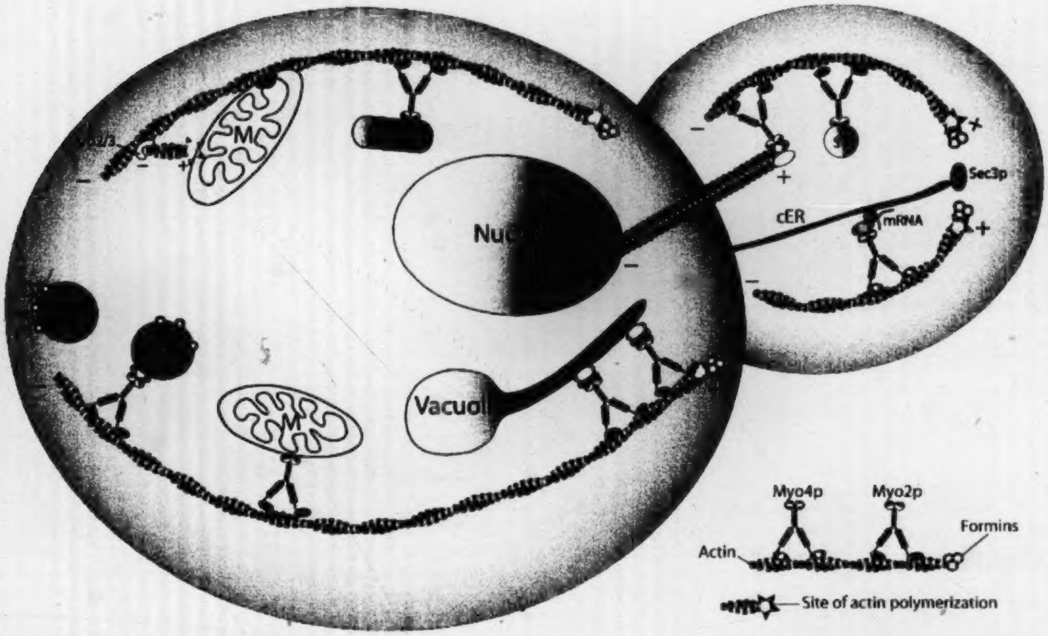

Figure 1-3. Bud-directed transport of organelles in *S. cerevisiae* cells. Formins are anchored at the bud tip and mother-bud neck, where they drive the assembly of polarized actin cables. For simplicity, each actin cable is represented as a single actin filament instead of a bundle of filaments. The class V myosins Myo2p and Myo4p are actin-based, barbed (plus)-end-directed molecular motors that drive most of the intracellular organelle trafficking. Myo2p carries secretory vesicles (SV), late Golgi elements (LG), the vacuolar segregating structure and peroxisomes (P) to sites of active growth. Myo2p also assists in the initial orientation of the nucleus by transporting astral microtubule plus ends into the bud. Myo4p transports precursors of the cortical endoplasmic reticulum (cER) toward Sec3p-containing anchorage sites located at the bud tip. Specific mRNA molecules comigrate with ER tubules into the bud. Two models for mitochondrial (M) movement are presented. In the first, Myo2p underlies mitochondrial motility, while in the second, mitochondria associate with actin cables and use the propulsion generated by Arp2/3-driven actin polymerization to advance toward the bud. Stars represent sites at which new actin monomers are incorporated into growing actin filaments during actin polymerization.

identification of the translocation machinery that propels and directs the movement of vacuolar membranes. Several class I mutations affect the actin cytoskeleton and Myo2p, clearly suggesting that the directed movement of vacuolar material is driven by the Myo2p motor along polarized actin cables (Hill et al., 1996). *VAC8* and *VAC17* were also isolated as class I genes. Vac17p is a peripheral membrane protein that interacts directly with Myo2p (Ishikawa et al., 2003; Tang et al., 2003). Deletion of Vac17p results in a specific defect in vacuole inheritance without affecting all other Myo2p-related processes (Ishikawa et al., 2003). The association of Myo2p with vacuoles is dependent on Vac17p, and an increase in Vac17p levels results in enhanced recruitment of Myo2p to vacuoles (Ishikawa et al., 2003). These and other observations suggest that Vac17p is the vacuole-specific receptor for Myo2p (Ishikawa et al., 2003; Tang et al., 2003). Vac8p interacts directly with Vac17p and is associated with the vacuolar membrane through myristoylation and reversible palmitoylation (Wang et al., 1998; Tang et al., 2003). Vac8p is most probably the docking site for Vac17p on the vacuolar membrane, since the localization of Vac17p to vacuoles is dependent on the presence of Vac8p. Moreover, Vac8p interacts with the Myo2p tail only in the presence of Vac17p (Tang et al., 2003), providing evidence for the existence of Myo2p-Vac17p-Vac8p transport complexes on the vacuolar membrane.

The position of Vac17p as the mediator between vacuolar membranes and the molecular engine driving their movement makes it ideally suited as a regulatory target for vacuole motility. Indeed, Vac17p levels exhibit cell-cycle-dependent oscillations that result in assembly and then disassembly of the Myo2p-Vac17p-Vac8p transport complexes (Tang et al., 2003; Weisman, 2003). Fluctuations in Vac17p availability throughout the cell cycle will thus determine the degree of association of vacuolar membranes with sites of polarized cell growth, where Myo2p concentrates. The levels of Vac17p on the vacuole start to increase before bud emergence, driving vacuolar material to the presumptive bud site and later to the bud tip (Tang et al., 2003). The transit of vacuolar membranes via segregation structures continues as long as Vac17p levels remain high. Later in the cell cycle, Vac17p is degraded, resulting in detachment of Myo2p from the already transferred vacuolar membranes. Consequently, before cytokinesis, the daughter vacuole is located near the bud center and does not accompany Myo2p to the bud neck region, where Myo2p accumulates to deliver material for septum deposition. Removal of the Vac17p PEST sequence (a potential signal for rapid protein turnover) stabilizes Vac17p levels (Tang et al., 2003). This causes the daughter cell vacuole to move backward to the mother-bud neck region, indicative of persistent Myo2p association with vacuolar membranes (Tang et al., 2003). Therefore, the regulated synthesis and turnover of Vac17p determine the timing and final destination of vacuolar movement, respectively (Tang et al., 2003; Weisman, 2006).

Interestingly, mutants defective in the bud-directed movement of vacuoles but that still express *VAC17*, such as cells lacking Vac8p or carrying specific mutations in the Myo2p tail, exhibit greatly enhanced levels of Vac17p on the mother cell vacuole (Tang et al., 2003). This suggests that Vac17p is normally exposed to the degradation machinery only upon its delivery to the bud. The site-specific turnover of Vac17p could indicate that the Vac17p degradation machinery is confined to the bud. Alternatively, the degradation complex may be present throughout the cytoplasm, or even on the vacuolar membrane, but its activity could be manifested only once Vac17p is delivered to the bud

(Tang et al., 2003). This could be achieved either by posttranslational modification of Vac17p, for example, phosphorylation by bud-localized kinases, that makes Vac17p susceptible for degradation or/and by activation of the degradation machinery through a signal transduction pathway triggered by the arrival of vacuolar material into the bud. It would be interesting to determine if the degradation machinery that is responsible for the turnover of Vac17p is coordinated with and/or controlled by other cell cycle events.

Apart from the bud-directed movement of the segregation structure, other important aspects of vacuole inheritance include the initial tubulation required for formation of the segregation structure and the final fission of the segregation structure that leads to the separation of the mother and daughter cell vacuoles (Weisman, 2003, 2006). These two events, which define the beginning and end of vacuole inheritance, respectively (Weisman, 2006), have been found to be defective in various mutants. For example, class III *vac* mutants are defective in both the formation and disintegration of the segregation structure (Bonangelino et al., 1997; Catlett and Weisman, 2000; Weisman, 2006). These mutants are characterized by abnormally low levels of the signaling lipid, phosphatidylinositol-3,5-bisphosphate (PtdIns(3,5)P_2). It is therefore likely that PtdIns(3,5)P_2 mediates the initiation and termination of vacuole inheritance through the recruitment of as yet poorly defined effector proteins (Weisman, 2006; Efe et al., 2007).

To ensure the faithful segregation of vacuoles, it is important that only a part of the mother cell vacuole, and not the entire vacuole, exhibits Myo2p-driven movement. It has been suggested (Catlett and Weisman, 2000; Weisman, 2003, 2006) that the segregation structure might not originate from the vacuole membrane itself but from a prevacuole compartment adjacent to the vacuole. The preferential loading of Myo2p onto the prevacuole membranes would provide a mechanism to designate a specific portion of the vacuole to form the segregation structure (Catlett and Weisman, 2000). It has also been shown that palmitoylation of Vac8p is essential for vacuole inheritance (Wang et al., 1998). Since palmitoylation usually targets proteins to cholesterol-rich membrane domains (Resh, 1999; Catlett and Weisman, 2000), it probably regulates the localization of Vac8p by driving it to a specific region in the vacuole membrane that will become the segregation structure (Catlett and Weisman, 2000). Whereas the molecular components responsible for moving vacuolar membranes toward the bud have been identified, an anchoring system required to immobilize the rest of the vacuole in the mother cell has not been demonstrated.

1.5.2 Mitochondria

Since mitochondria are essential organelles that cannot be synthesized de novo, their inheritance is an essential part of the cell cycle (Boldogh et al., 2005). Mitochondria do not represent discrete, independent entities but rather are remarkably dynamic organelles that frequently fuse and divide (Hoppins et al., 2007). The balance between mitochondrial fusion and fission ultimately determines overall mitochondrial morphology (Hoppins et al., 2007). *S. cerevisiae* mitochondria form a branched tubular reticulum that lies just under the plasma membrane (Warren and Wickner, 1996). Like other organelles, the mitochondrial network displays cell-cycle-coordinated motility that results in the equal distribution of this organelle at cell division (Boldogh et al., 2005; Boldogh and Pon, 2006). The cortical mitochondrial reticulum orients along the mother-bud axis and invades the bud as soon as it appears. During bud growth, extension of a portion of the mitochondrial network into the bud is accompanied by retraction of the remaining portion toward the yeast cell pole distal to the bud (Fehrenbacher et al., 2004; Boldogh et al., 2005; Boldogh and Pon, 2006). Therefore, mitochondria display both anterograde and retrograde movements that result in the accumulation of mitochondria at the bud tip and mother tip, respectively. Once mitochondria reach opposite poles, they are immobilized until the beginning of the next cell cycle (Boldogh and Pon, 2006). This "poleward" movement followed by anchorage at the poles resembles the behavior of chromosomes during cell division (Fehrenbacher et al., 2004; Boldogh and Pon, 2006).

Multiple lines of evidence clearly show that actin cables mediate mitochondrial motility in budding yeast (Boldogh et al., 2005; Boldogh and Pon, 2006). Mitochondria colocalize with actin cables (Drubin et al., 1993), and various mutations and drugs that destabilize the actin cytoskeleton result in defects in mitochondrial distribution and motility, both anterograde and retrograde (Drubin et al., 1993; Fehrenbacher et al., 2004; Boldogh et al., 2005; Boldogh and Pon, 2006). Interestingly, isolated yeast mitochondria exhibit reversible, ATP-sensitive actin-binding activity (Lazzarino et al., 1994).

The retrograde mitochondrial transport towards the base of the mother cell is driven by the retrograde translocation of actin cables (Fehrenbacher et al., 2004; Boldogh et al., 2005; Boldogh and Pon, 2006). As mentioned previously, formins drive the assembly of actin cables by incorporating new actin monomers at the bud-localized barbed end of existing actin filaments. As a result, growing actin cables slowly translocate toward the distal tip of the mother cell. Time-lapse imaging studies have shown that mitochondria assume static positions on a moving actin cable as they undergo retrograde movements so that there is no net displacement of mitochondria relative to the underlying actin cable (Fehrenbacher et al., 2004). Thus, mitochondria passively move in the retrograde direction by attaching to elongating actin cables, using them as "conveyor belts" (Fehrenbacher et al., 2004; Boldogh et al., 2005; Boldogh and Pon, 2006).

On the other hand, anterograde movement toward the bud requires force generation mechanisms to overcome the aforementioned inherent retrograde flow (Fehrenbacher et al., 2004; Valiathan and Weisman, 2008). Some controversy exists as regards the nature of the force generator for anterograde mitochondrial movement. Two potential mechanisms for mitochondrial movement have been suggested.

The first proposed mechanism is similar to the one underlying the movement of other membrane-bounded organelles in yeast, i.e. dependence on association with a myosin motor. The first evidence for the involvement of myosin motors in mitochondrial dynamics came from the observation that several yeast actin point mutants that destabilize the actin filament under or near the myosin footprint display defects in mitochondrial organization (Drubin et al., 1993). Subsequently, several Myo2p mutant alleles were identified that specifically impair mitochondrial inheritance, further underscoring the importance of myosins in mitochondrial transport (Itoh et al., 2002, 2004; Boldogh et al., 2004). Moreover, two Myo2p-interacting proteins, Ypt11p and Mmr1p, were found to be essential for the correct partitioning of mitochondria during the cell cycle (Itoh et al., 2002, 2004) (Figure 1-3).

However, other observations were not concordant with a major role of myosin motors in the bud-directed movement of mitochondria. For example, reduction of the length of the Myo2p lever arm or deletion of the *MYO4* gene had no effect on the velocity of mitochondrial movement (Boldogh et al., 2004). Further doubt for the direct involvement of Myo2p in mitochondrial movement was raised by the observation that Ypt11p resides in the ER rather than mitochondria (Buvelot Frei et al., 2006; Valiathan and Weisman, 2008). Moreover, a more detailed analysis (Boldogh et al., 2004) showed the Ypt11p-Myo2p complex to be involved in the retention of inherited mitochondria in the bud rather than for movement of mitochondria toward the bud.

The second proposed mechanism for anterograde mitochondrial movement is motor-independent and implicates the Arp2/3 complex as the main force generator. This mechanism is very similar to that used by some bacterial and viral pathogens to circulate through the cytoplasm of infected host cells (Boldogh and Pon, 2006). Proteins at the surface of these pathogens activate the Arp2/3 complex, the best characterized stimulator of actin nucleation (for a review, see Fehrenbacher et al., 2003). The activated Arp2/3 complex binds to the side of a preexisting actin filament, where it serves to nucleate assembly of a new filament that grows at an acute angle relative to the original filament. Repeated rounds of branching nucleation result in a tree-like meshwork of actin filaments that grow at their barbed ends, while Arp2/3 complexes stabilize their pointed ends (Kaksonen et al., 2006). Since barbed ends are associated with the surface of the pathogens, continuous actin polymerization "rockets" them forward (Boldogh and Pon, 2006; Fehrenbacher et al., 2003) (Figure 1-3). Multiple lines of evidence show that Arp2/3-complex-mediated actin polymerization also drives mitochondrial anterograde movements in *S. cerevisiae* (Boldogh et al., 2001). The Arp2/3 complex is associated with the mitochondrial surface, and mutations in Arp2/3 complex subunits inhibit anterograde mitochondrial movements (Boldogh et al., 2001; Fehrenbacher et al., 2005). These observations support a model in which the Arp2/3 complex stimulates the formation and growth of actin filament meshworks at the interface between actin cables and mitochondria that ultimately propel these organelles (Boldogh and Pon, 2006).

While pushed by newly formed Arp2/3-assembled actin filaments, mitochondria remain in contact with actin cables. The association of mitochondria with actin was found to be dependent on three proteins, Mmm1p, Mdm10p and Mdm12p, that constitute a mitochondrial membrane protein complex (Sogo and Yaffe, 1994; Burgess et al., 1994; Berger et al., 1997; Kondo-Okamoto et al, 2003). Loss of any of these proteins decreases the reversible, cyclic association of mitochondria with actin filaments in vitro. Interestingly, the Mmm1p/Mdm10p/Mdm12p complex has been shown to physically interact with mitochondrial DNA nucleoids (Berger et al., 1997; Hobbs et al., 2001; Boldogh et al., 2003; Boldogh and Pon, 2006). Since the complex connects mitochondrial DNA to the cytoskeletal system that drives its poleward movement and segregation during cell division, it could functionally be considered the mitochondrial counterpart of the kinetochore, a so-called “mitochore” (Boldogh and Pon, 2006). Since the mitochore continuously mediates the reversible, cyclic binding of mitochondria to actin cables, mitochondria will use actin cables as tracks for their anterograde movement (Figure 1-3).

In the middle of the ongoing controversy about the mechanisms of mitochondrial movement in yeast, Altmann et al. (2008) very recently provided the most compelling evidence to date for a direct role for Myo2p in both mitochondria-actin interaction and anterograde mitochondrial movement. They showed that depletion of Myo2p results in a drastically reduced interaction between mitochondria and actin filaments. Furthermore, this interaction is abolished by prior incubation of purified mitochondria with Myo2p-specific antibodies. This study also identified specific surface residues in the cargo-binding domain of Myo2p that bind mitochondria. Mutation of these residues causes both impairment in the anterograde transport of mitochondria as well as decreased binding of mitochondria to the actin cytoskeleton (Altmann et al., 2008; Valiathan and Weisman, 2008). However, a mitochondria-specific receptor for Myo2p has yet to be identified.

In an attempt to reconcile these two completely different models of mitochondrial motility, we have to accept the coexistence of multiple pathways that contribute to mitochondrial movement (Figure 1-3). Probably, different mechanisms cooperate and act either simultaneously or in different conditions to ensure the delivery of mitochondria to daughter cells. For retrograde movement, the mitochore attaches mitochondria to polymerizing actin cables. For anterograde movement, the mitochore-mediated transient interactions between mitochondria and actin cables guide mitochondria in the presence of an applied force, generated by either Myo2p or the Arp2/3 complex (Fehrenbacher et al., 2004; Boldogh et al., 2005; Boldogh and Pon, 2006, 2007; Fagarasanu and Rachubinski, 2007; Altmann et al., 2008). However, some observations still remain difficult to explain. For example, if Myo2p is the main transporter of mitochondria in yeast, one would expect a reduction in the length of the Myo2p lever arm to result in decreased velocity of mitochondria. A possible explanation for the observed unchanged velocity of mitochondria upon change in the lever arm length (Boldogh et al., 2004) is that since a large organelle is carried by multiple motor molecules, the resultant velocity would not be expected to be limited by the speed of a single motor molecule (Altmann et al., 2008). It remains to be established if other organelles are also endowed with multiple mechanisms of transport that ultimately result in increased efficiency of partitioning upon cell division.

In addition to mitochondrial movement, anchoring of mitochondria at the distal tip of the mother cell and the bud tip contributes to the increased efficiency of mitochondrial inheritance (Fehrenbacher et al., 2004; Boldogh et al., 2005). Retention of mitochondria at the bud tip requires Myo2p and the Rab-GTPase, Ypt11p (Boldogh et al., 2004). However, destabilization of actin cables and the resulting displacement of Myo2p from the bud tip have no significant effect on the immobilization of mitochondria at the bud tip (Boldogh et al., 2004). This suggests that Myo2p does not function by capturing transferred mitochondria at the bud tip but probably mediates the transport of other retention factors to this site (Boldogh et al., 2004, 2005). In contrast, mitochondrial retention in the mother cell was shown to be dependent on the actin cytoskeleton (Yang et al., 1999). Recently, Num1p has been implicated in the retention of mitochondria in the mother cell, but its exact role in this process remains to be established (Cerveny et al., 2007).

1.5.3 The Golgi Complex

The Golgi complex in *S. cerevisiae* cells is not arranged in coherent stacks, as is the case in most cell types, including mammalian cells. Instead, the *S. cerevisiae* Golgi is represented by a collection of single, isolated cisternae scattered throughout the cytoplasm (Preuss et al., 1992; Rossanese et al., 2001; Rossanese and Glick, 2001). Interestingly, early and late Golgi elements are inherited by two distinct pathways. Late

Golgi elements follow the rearrangements of the actin cytoskeleton, being strongly polarized to sites of active growth, i.e., the presumptive bud site, the bud tip in small budded cells and the mother-bud neck at cytokinesis (Rossanese et al., 2001). The localization of late Golgi cisternae to these sites requires both an intact actin cytoskeleton and a functional Myo2p motor, implicating Myo2p in the transport of these Golgi structures (Rossanese et al., 2001). Moreover, as is the case for vacuoles and peroxisomes, late compartments of the Golgi remain associated with the Myo2p motor at sites of active growth. Evidence for this conclusion has come from the observation that a mutation in the motor domain of Myo2p causes the delocalization of already polarized late Golgi elements (Rossanese et al., 2001) (Figure 1-3).

By contrast, early Golgi elements do not show any preference for sites of growth but, nevertheless, are detected in buds very early in the cell cycle (Rossanese et al., 2001). One proposed explanation for this apparent paradox is that the early Golgi elements found in incipient buds are not inherited from the mother cell but are synthesized de novo within buds (Rossanese et al., 2001; Rossanese and Glick, 2001). A logical extension of the "cisternal maturation" model, which predicts that each Golgi cisterna is a transient entity that matures through the retrieval of specific Golgi-resident proteins from later Golgi compartments (Allan and Balch, 1999), is that ER-derived membranes nucleate new early Golgi cisternae (Reinke et al., 2004; Losev et al., 2006). Since cisternal maturation has been directly observed in *S. cerevisiae* (Losev et al., 2006), bud-localized ER membranes could represent the source of early Golgi compartments. In line with this scenario, mutants defective in ER inheritance also lack early Golgi elements in newly formed buds (Reinke et al., 2004). Together, these findings (Losev et al., 2006) support a model in which inherited ER membranes would give rise to early Golgi cisternae, which would in turn mature into late Golgi cisternae. Late Golgi cisternae are then carried to and retained at sites of growth by Myo2p. Therefore, the endowment of buds with late Golgi elements is achieved through a combination of bud-directed transport and de novo formation of these Golgi compartments. The former process seems to be the slower of the two, since the small buds of mutants affected in ER inheritance exhibit a delay in the appearance of both early and late Golgi elements as compared with the buds of wild-type cells (Reinke et al., 2004). If the de novo production of late Golgi elements is so efficient, why does *S. cerevisiae* ensure that these compartments recruit Myo2p to be carried to sites of polarized growth? One possible explanation is that the polarization of late Golgi elements enables secretory vesicles to reach their destinations more rapidly (Preuss et al., 1992; Rossanese et al., 2001). Also, polarized growth is probably more efficient if an entire set of secretory organelles is delivered to sites of growth (Rossanese et al., 2001).

The protein complex that recruits Myo2p to the membranes of late Golgi compartments has not been identified. The long-proposed but only recently visualized (Losev et al., 2006) cisternal maturation model also predicts that secretory vesicles are actually late Golgi elements that have matured through their retrieval of recycling components from preexisting secretory vesicles. Therefore, it is likely that late Golgi elements and post-Golgi secretory vesicles share the same receptor for Myo2p.

1.5.4 Endoplasmic Reticulum

The ER of *S. cerevisiae* consists of membrane sheets that enclose the nucleus, the so-called perinuclear ER or nuclear envelope, and a highly dynamic network of interconnected tubules that lines the cell periphery, termed the peripheral or cortical ER (Preuss et al., 1991; Fehrenbacher et al., 2002; Du et al., 2004; Estrada et al., 2005). Continuity between the perinuclear and cortical ERs is maintained through the presence of finger-like cytoplasmic tubules that connect the two ER subdomains (Koning et al., 1993).

During cell division, the fate of the cortical ER is radically different from that of the perinuclear ER (Lowe and Barr, 2007). Since *S. cerevisiae* undergoes a closed mitosis, the nuclear envelope remains intact throughout the cell cycle (Salina et al., 2001). Therefore, the perinuclear ER is partitioned together with the nucleus through a microtubule-based mechanism (a process not detailed here) (Fehrenbacher et al., 2002; Estrada et al., 2005; Lowe and Barr, 2007). On the contrary, the inheritance of cortical ER is actin-based and powered by myosin motors.

The cortical ER is inherited in an ordered, cell-cycle-coordinated, multistep process. Very early in the cell cycle, ER cytoplasmic tubules, termed "ER segregation structures" align along the mother-bud axis. Subsequently, they extend into the newly developed bud, where they become anchored at the bud tip (Preuss et al., 1991; Du et al., 2001, 2004). Following anchorage at the apex, the ER tubules extend from the bud tip into a polygonal cortical ER network that lines the entire bud cortex (Du et al., 2004; Estrada et al., 2005). Intriguingly, the ER tubules that are segregated to the bud to form the cortical ER of the daughter cell emanate from a perinuclear region of the mother cell cytoplasm (Estrada et al., 2003).

The alignment and directed movement of ER segregation structures suggest that cytoskeletal elements underlie the partitioning of cortical ER. Actin and Myo4p were recently shown to be required for both the orientation of cortical ER tubules along the mother-bud axis and their extension into the daughter cell (Estrada et al. 2003, 2005). The ER is the only organelle whose partitioning is dependent on Myo4p. The only previously known function of Myo4p was in the bud-directed transport of specific mRNA molecules (Long et al. 1997; Takizawa et al. 2000). Myo4p associates with mRNAs via the Myo4p-tail-binding protein She3p and the mRNA-associated protein She2p, resulting in the formation of trimeric Myo4p-She3p-She2p transport complexes (Takizawa et al. 2000). Myo4p requires its adaptor She3p, but not She2p, to transport ER tubules to the bud. Moreover, ER inheritance and the asymmetrical distribution of mRNA molecules were believed to represent two independent functions of Myo4p (Estrada et al., 2003). However, this view has been challenged by the recent observation that mRNA molecules associate with segregating ER membranes during their bud-directed transport (Schmid et al., 2006). In addition, biochemical experiments clearly showed that She2p, but not Myo4p or She3p, is required for the association of mRNAs with ER tubules that grow toward the bud. Therefore, the tripartite Myo4p-She3p-She2p complex, which has been proposed as the basic machinery for mRNA transport, is only part of a still more complex machinery that underlies the comigration of ER membranes and specific mRNAs (Schmid et al., 2006) (Figure 1-3). However, the protein that recruits the Myo4p-She3p-She2p complex to the ER membrane has not been identified.

The anchoring of segregating ER tubules to the bud tip has been shown to require Sec3p (Estrada et al., 2005; Wiederkehr et al., 2003). Sec3p is a component of the exocyst, a multiprotein complex implicated in tethering secretory vesicles to the plasma membrane (Finger et al., 1998). In *sec3* mutants, ER tubules display normal bud-directed motility, but they fail to dock at the apex of the daughter cell. Conversely, overproduction of Sec3p results in abnormal accumulation of ER membranes at the bud tip (Wiederkehr et al., 2003). Therefore, Sec3p is likely to be a key component of the structure that anchors ER tubules at the tips of newly developed buds. Interestingly, given the tubular rather than particulate morphology of this organelle, the capture of ER structures at the bud tip early in the cell cycle might enable entire ER networks to be pulled into the bud as it enlarges (Fehrenbacher et al., 2002). Therefore, the segregation of cortical ER to the daughter cell might be achieved by a combination of active Myo4p-driven transport and anchorage-dependent extraction of ER membranes from the mother cell.

A number of other proteins required for cortical ER inheritance have been identified. Aux1p/Swa2p, a protein previously implicated in clathrin-mediated membrane trafficking, was recently found to be required for cortical ER inheritance (Du et al., 2001). Disruption of *AUX1/SWA2* causes a specific delay in the transport of cortical ER elements into the daughter cell, whereas the inheritance of perinuclear ER and the general morphology of the ER are unaffected. The exact role of Aux1p/Swa2p in cortical ER inheritance remains to be determined. In addition, the serine/threonine phosphatase Ptc1p has recently been implicated in a later step of cortical ER inheritance, being involved in the delivery of ER tubules from the bud tip to the bud periphery (Du et al., 2006).

1.6 Focus of this thesis

The aim of this thesis is to study the regulation of peroxisome motility in the budding yeast *Saccharomyces cerevisiae*. This thesis uses different approaches from classical biochemical experiments to modern *in vivo* confocal video microscopy to elucidate the strategies used by cells to partition their peroxisomes upon cell division. The work presented herein describes the identification and characterization of Inp2p as the peroxisome-specific receptor of the class V myosin Myo2p. Furthermore, we will present structural details of the Inp2p-Myo2p interaction, which provide a better understanding of how cells dynamically control the intracellular motility and inheritance of their peroxisomes.

CHAPTER TWO: MATERIALS AND METHODS

2.1 Materials

2.1.1 Chemicals and Reagents Used in This Study

2-(*N*-Morpholino)ethanesulfonic acid (MES)	Sigma-Aldrich
5-bromo-4-chloro-3-indolyl-β-D-galactoside (X-gal)	Rose Scientific
acetone	Fisher
acrylamide	Roche
agar	Difco
agarose, UltraPure	Invitrogen
albumin, bovine serum (BSA)	Roche
α-factor	Sigma-Aldrich
ammonium bicarbonate (NH_4HCO_3)	Sigma-Aldrich
ammonium chloride (NH_4Cl)	EM Science
ammonium persulfate	BDH
ammonium sulfate ($((NH4)_2SO_4)$)	BDH
ampicillin	Sigma-Aldrich
anhydrous ethyl alcohol	Commercial Alcohols
antipain	Roche
aprotinin	Roche
benzamidine hydrochloride	Sigma-Aldrich
boric acid	EM Science
Brij 35	EM Science
bromophenol blue	BDH
calcium pantothenate	Sigma-Aldrich
chloroform	Fisher
Complete Protease Inhibitor Cocktail	Roche
complete supplement mixture (CSM)	BIO 101
Coomassie Brilliant Blue R-250	ICN
cytochrome *c*, horse heart	Sigma-Aldrich
D-(+)-glucose	EM Science
dithiothreitol (DTT)	Fisher
ethylenedinitrilo-tetraacetic acid (EDTA)	EM Science
formaldehyde, 37% (v/v)	Biochemicals
Geneticin	Invitrogen
glass beads	Sigma-Aldrich
glycerol	EM Science
glycine	Roche
isoamyl alcohol	Fisher
isopropyl β-D-thiogalactopyranoside (IPTG)	Roche
lanolin	Alfa Aesar
leupeptin	Roche
L-histidine	Sigma-Aldrich
lithium acetate	Sigma-Aldrich

L-leucine	Sigma-Aldrich
L-lysine	Sigma-Aldrich
magnesium sulfate ($MgSO_4$)	Sigma-Aldrich
maltose	Sigma-Aldrich
MitoTracker CMXRos	Molecular Probes
N,N,N',N'-tetramethylethylenediamine (TEMED)	EM Science
N,N'-dimethyl formamide (DMF)	BDH
N,N'-methylene bisacrylamide	Sigma-Aldrich
N-propyl gallate	Sigma-Aldrich
Nycodenz	BioLynx
oleic acid	Fisher
paraffin	Fisher
Pefabloc SC	Roche
pepstatin A	Sigma-Aldrich
Peptone	Difco
phenanthroline	Roche
phenol, buffer saturated	Invitrogen
phenylmethylsulphonylfluoride (PMSF)	Roche
poly *L*-lysine	Sigma-Aldrich
polyethylene glycol, M.W. 3350 (PEG)	Sigma-Aldrich
Ponseau S	Sigma-Aldrich
potassium acetate	BDH
potassium chloride	BDH
potassium permanganate ($KMnO_4$)	BDH
potassium phosphate, dibasic (K_2HPO_4)	EM Science
potassium phosphate, monobasic (KH_2PO_4)	EM Science
salmon sperm DNA, sonicated	Sigma-Aldrich
Sephadex G25	Amersham
skim milk	Carnation
sodium acetate	EM Science
sodium cacodylate	Fisher
sodium carbonate (Na_2CO_3)	BDH
sodium chloride	EM Science
sodium dithionite ($Na_2S_2O_4$)	BDH
sodium dodecyl sulfate (SDS)	Bio-Rad
sodium fluoride (NaF)	Sigma-Aldrich
sodium phosphate, dibasic (Na_2HPO_4)	BDH
sodium sulphite (Na_2SO_3)	Sigma-Aldrich
sorbitol	EM Science
sucrose	EM Science
thiamine-HCl	Sigma-Aldrich
trichloroacetic acid (TCA)	EM Science
tris(hydroxymethyl)aminomethane (Tris)	Roche
Triton X-100	VWR
tryptone	Difco
Tween 20	Sigma-Aldrich

Tween 40	Sigma-Aldrich
uracil	Sigma-Aldrich
vaseline	Vaseline
xylene cyanol FF	Sigma-Aldrich
yeast extract	Difco
yeast nitrogen base without amino acids (YNB)	Difco
2-mercaptoethanol	BioShop

2.1.2 Enzymes

CIP (calf intestinal alkaline phosphatase)	NEB
Easy-A high-fidelity polymerase	Stratagene
restriction endonucleases	NEB
Quick T4 DNA ligase	NEB
RNase A (ribonuclease A), bovine pancreas	Sigma-Aldrich
T4 DNA ligase	NEB
Zymolyase 20T	ICN
Zymolyase 100T	ICN

2.1.3 Molecular Size Standards

1 kb DNA ladder (500-10,000 bp)	NEB
prestained protein marker, broad range (6-175 kDa)	NEB

2.1.4 Multicomponent Systems

BigDye Terminator Cycle Sequencing Ready Reaction Kit	Applied Biosystems
Matchmaker Two-Hybrid System	Clontech
pGEM-T Vector System	Promega
pMAL Protein Fusion and Purification System	NEB
QIAprep Spin Miniprep Kit	Qiagen
QIAquick Gel Extraction Kit	Qiagen
QIAquick PCR Purification Kit	Qiagen
Ready-To-Go PCR Beads	Amersham Biosciences

2.1.5 Plasmids

pBluescript II SK(-)	Stratagene

pGEM-7Zf	Promega
pGEM-T	Promega
pGEX4T1	Amersham Biosciences
pMAL-c2	NEB
pRS413	ATCC
pRS416	ATCC
YEp13	Broach et al.,1979

2.1.6 Antibodies

The antibodies used in this study are described in Tables 2-1 and 2-2.

Table 2-1. Primary antibodies

Specificity	Type	Name	Dilution[a]	Reference
S. cerevisiae Myo2p	guinea pig	Q27-final	1:10,000	This study
S. cerevisiae Pex3p	rabbit	P84-final	1:4000	This study
S. cerevisiae Pex27p	guinea pig	Q10-final	1:4000	This study
TAP	rabbit	CAB 1001	1:5000	Open Biosystems
MBP[b]	rabbit	E8030S	1:10,000	NEB
GST	mouse	GST-2	1:10,000	Sigma-Aldrich
S.cerevisiae Clb2p	rabbit	Y-180	1:1000	Santa Cruz
S.cerevisiae Gsp1p[c]	rabbit	4G9	1:10,000	Makhnevych et al., 2003
S. cerevisiae Sdh2p[d]	rabbit	Sdh2	1:5000	Dibrov et al., 1998
Y. lipolytica thiolase	guinea pig	N-3*	1:10,000	Eitzen et al., 1996

[a] Dilutions are for use in immnunoblotting. Dilutions used in microscopy were ten-fold less.
[b] A gift from Dr. Gary Eitzen (University of Alberta, Edmonton, Canada).
[c] A gift from Dr. Rick Wozniak (University of Alberta, Edmonton, Canada).
[d] A gift from Dr. Bernard Lemire (University of Alberta, Edmonton, Canada).

Table 2-2. Secondary antibodies

Specificity	Type	Dilution	Source
horseradish peroxidase (HRP)-conjugated anti-rabbit IgG	donkey	1:30,000	Amersham Biosciences
HRP-conjugated anti-guinea pig IgG	goat	1:30,000	Sigma-Aldrich
rhodamine-conjugated anti-guinea pig IgG	donkey	1:250	Jackson Immunoresearch Laboratories
AlexaFluor 680-conjugated anti-mouse IgG	goat	1:10,000	Invitrogen
AlexaFluor 750-conjugated anti-rabbit IgG	goat	1:10,000	Invitrogen

2.1.7 Oligonucleotides

The oligonucleotides used in this study were synthesized by Sigma-Genosys (Oakville, Ontario) and are listed in Table 2-3.

Table 2-3. Oligonucleotides

Name	Sequence[a,b,c]	Application
0319-myo2-2HyR	ATTCTGCAGTTAGTGGCCGTCTTGAACGAC	pGAD424-*MYO2,* pGBT9-*MYO2*
0320-myo2t2HyF	ATTCTGCAGAAATGCTTGAGAATTCCGACTTATC	pGAD424-*MYO2,* pGBT9-*MYO2*
0353-myo2tU-NxF	ATTGGATCCATGCTTGAGAATTCCGACTTATC	pGEX4T1-*MYO2*
0354-myo2tU-NxR	ATTGGATCCTTAGTGGCCGTCTTGAACGAC	pGEX4T1-*MYO2*
0423-MF-ymrpMal-Fw	ATTGGATCCATGGTTTTATCAAGGGGAGAAAC	pMAL-*INP1*
0424-MF-ymrpMal-Re	ATTGTCGACTCAAAGGTCGCCAAGACCAGA	pMAL-*INP1*

0543-FwYmr-oexp	ATTGGATCCTCAATTAATGTTAACCCATGTTTTT	pYep13-*INP1*
0544-ReYmr-oexp	ATTGGATCCTGTAACGACTTCTCCCTCCAG	pYep13-*INP1*
0605-pex19twoH-F	ATTCCTGCAGAGATGCCAAACATACAACACGAA	pGAD424-*PEX19*, pGBT9-*PEX19*
0606-pex19twoH-R	ATTCCTGCAGAGTTATTGTTGTTTGCACCGTC	pGAD424-*PEX19*, pGBT9-*PEX19*
0654-MF-Ymr2HyFwd	ATTGGATCCAAATGGTTTTATCAAGGGGAGAAACA	pGAD424-*INP1*, pGBT9-*INP1*
0655-MF-Ymr2HyRev	ATTGTCGACTCAAAGGTCGCCAAGACCAGAT	pGAD424-*INP1*, pGBT9-*INP1*
0910-RP-SDH2 WEB A	*CCAAAGGGCTTGAATCCTGGTTTGGCTATTGCTGAAATTAAGAAATCTTTGGCATTTGCC*GGCGGTGGCGGTGAAGCTCAAAAACTTAAT	*SDH2-GFP+* construction
0911-RP-SDH2 WEB B	*AGATACTAGAACACCTTGTCGCCTATGATGGACATATATACAGACCGGGTCATAGCATTG*GACGGTATCGATAAGCTTT	*SDH2-GFP+* construction
0983-AF-INP2C	TTTCTAGGATACAAAAGGTATCCCC	Checking oligo for *INP2* gene
0984-AF-INP2D	GCACTTGATCTTTTCTCAAGACTTC	Checking oligo for *INP2* gene
0985-AF-INP2oeF	ATTGGATCCAGCGTTCTTGTAACCAAATTTCTAT	pYep13-*INP2*
0986-AF-INP2oeR	ATTGGATCCTTGCTGTATGGAAGCTATGTGTAT	pYep13-*INP2*
0987-AF-INP2iF	*TCTTCGGAAGAAACTATCCCATTTTTGTATGAATTAAAAGGATTACTAGGAAATGATTCA*GGTGAAGCTCAAAAACTTAAT	*INP2-GFP+* construction
0988-AF-INP2iR	*TTCCTGCAATATTGAATTCTTCTTTGTTAAATATTCGCTTACTTAAAGCACTTGACAGAC*GCTGACGGTATCGATAAGCTT	*INP2-GFP+* construction
0989-AF-INP2hyF	ATTGAATTCATGACAACAAACTCACGTCCATCC	pGAD424-*INP2*, pGBT9-*INP2*
0990-AF-INP2hyR	ATTGAATTCTCATGAATCATTTCCTAGTAATCCT	pGAD424-*INP2*, pGBT9-*INP2*
1005-ES-ScYMR163f	GCCGAATTCATTTGCTATAAAACCTTATTAAAGGTA	pMAL-*INP2*
1006-ES-ScYMR163r	GCCGTCGACTCATGAATCATTTCCTAGTAATCC	pMAL-*INP2*

1316-DW-YIL160c-3WebA	*GGGGTTGTTAGTATGTGTATCGGTACTGGTATGGGTGCCGCCGCCATCTTTATTAAAGAA*GGTGAAGCTCAAAAACTTAAT	*POT1-GFP+* construction
1317-DW-YIL160c-3WebB	*AAATATTGAAAATGGAAAATTATAAACAAATTGATAAACTACGTAATAGCTTTTACAAA*GCTGACGGTATCGATAAGCTT	*POT1-GFP+* construction
1775-MF-Inp1koF	*AAGGTCTACATTTTTCGTCTGATAACTCTCAGGAAATTAAACAAAGTGGT*AGATTGTACTGAGAGTGCAC	*INP1* deletion
1776-MF-Inp1koR	*ATTTATATTCACATTGTATACTCCTTCACTTTGGTTTACACCTACATTCA*CTGTGCGGTATTTCACACCG	*INP1* deletion
2532-AF-F1334A	*CCGAATCATTACCAGGTGCCAGCGCGGGAGAAACCA*	pRS413-*myo2-F1334A*
2533-AF-F1334A-as	*TGGTTTCTCCCGCGCTG*GC*ACCTGGTAATGATTCGG*	pRS413-*myo2-F1334A*
2534-AF-K1408A	*GAAACGTAATTTCTTGTCGTGG*GC*AAGGGGTCTTCAATTGAACTAC*	pRS413-*myo2-K1408A*
2535-AF-K1408A-as	*GTAGTTCAATTGAAGACCCCTT*GC*CCACGACAAGAAATTACGTTTC*	pRS413-*myo2-K1408A*
2536-AF-R1449A	*CGCTAAGCTACTGCAAGTCGCTAAGTATACTATCGAAGAC*	pRS413-*myo2-R1449A*
2537-AF-R1449A_as	*GTCTTCGATAGTATACTTA*GC*GACTTGCAGTAGCTTAGCG*	pRS413-*myo2-R1449A*
2538-AF-D1482A	*ACAATACCAGGTGGCAGCCTATGAGTCTCCAATTC*	pRS413-*myo2-D1482A*
2539-AF-D1482A_as	*GAATTGGAGACTCATAG*GC*TGCCACCTGGTATTGT*	pRS413-*myo2-D1482A*
2540-AF-Y1451A	*CTAAGCTACTGCAAGTCCGTAAG*GC*TACTATCGAAGACATTGATATCT*	pRS413-*myo2-Y1451A*
2541-AF-Y1451A_as	*AGATATCAATGTCTTCGATAGTA*GC*CTTACGGACTTGCAGTAGCTTAG*	pRS413-*myo2-Y1451A*
2542-AF-Y1483A	*ACAATACCAGGTGGCAGAC*GC*TGAGTCTCCAATTCCACAG*	pRS413-*myo2-Y1483A*
2543-AF-Y1483A_as	*CTGTGGAATTGGAGACTCA*GC*GTCTGCCACCTGGTATTGT*	pRS413-*myo2-Y1483A*
2544-AF-E1484A	*CAGGTGGCAGACTATGCGTCTCCAATTCCACAG*	pRS413-*myo2-E1484A*

2545-AF-E1484A_as	*CTGTGGAATTGGAGAC*G*CATAGTCTGCCACCTG*	pRS413-*myo2-E1484A*
2546-AF-L1411A	*GTAATTTCTTGTCGTGGAAAAGGGGT*GC*TCAATTGA ACTACAACGTTAC*	pRS413-*myo2-L1411A*
2547-AF-L1411A_as	*GTAACGTTGTAGTTCAATTGA*GC*ACCCCTTTTCCAC GACAAGAAATTAC*	pRS413-*myo2-L1411A*
2548-AF-V1448A	*CGCTAAGCTACTGCAAG*C*CCGTAAGTATACTATCG*	pRS413-*myo2-V1448A*
2549-AF-V1448A_as	*CGATAGTATACTTACGG*G*CTTGCAGTAGCTTAGCG*	pRS413-*myo2-V1448A*
2978-AF-IP2iFmR	*TCTTCGGAAGAAACTATCCCATTTTTGTATGAATTAA AAGGATTACTAGGAAATGATTCA*GGTGGAGGCGGT GGCGGAGTGAGCAAGGGCGAGGAT	*INP2-mRFP* construction
2979-AF-IP2iRmR	*TTCCTGCAATATTGAATTCTTCTTTGTTAAATATTCG CTTACTTAAAGCACTTGACAGAC*GTACTGAGAGTG CACCATAC	*INP2-mRFP* construction

---

[a]Restriction endonuclease recognition sites used in cloning are underlined.
[b]Sequences for homologous recombination are italicized.
[c] Changed bases in mutagenesis primers are shown in red.

2.1.8 Standard Buffers and Solutions

The compositions of routinely used buffered solutions are given in Table 2-4.

Table 2-4. Common solutions

Solution	Composition	Reference
1 × PBS	137mM NaCl, 2.7 mM KCl, 8 mM Na_2HPO_4, 1.5 mM K_2HPO_4, pH 7.3	Pringle et al., 1991
1 × protease inhibitor (PIN) cocktail	1 µg/ml each of antipain, aprotinin, leupeptin, pepstatin, 0.5 mM benzamidine hydrochloride, 5 mM NaF, 1 mM PMSF or 0.5 mg Pefabloc SC/ml	Smith, 2000
1 × TBST	20 mM Tris-HCl, pH 7.5, 150 mM NaCl, 0.05% (w/v) Tween 20	Huynh et al., 1988

1 × Transfer buffer	20 mM Tris-HCl, 150 mM glycine, 20% (v/v) methanol	Towbin et al., 1979; Burnette, 1981
5 × SDS-PAGE running buffer	0.25 M Tris-HCl, pH 8.8, 2 M glycine, 0.5% SDS	Ausubel et al., 1989
10 × TBE	0.89 M Tris-borate, 0.89 M boric acid, 0.02 M EDTA	Maniatis et al., 1982
2× sample buffer	20% (v/v) glycerol, 167 mM Tris-HCl, pH 6.8, 2% SDS, 0.005% bromophenol blue	Ausubel et al., 1989
6 × DNA loading dye	0.25% bromophenol blue, 0.25% xylene cyanol, 30% (v/v) glycerol	Maniatis et al., 1982
Breakage buffer	2% (v/v) Triton X-100, 1% SDS, 100 mM NaCl, 10 mM Tris-HCl, pH 8.0, 1 mM EDTA, pH 8.0	Ausubel et al., 1989
Disruption buffer	20 mM Tris-HCl, pH 7.5, 0.1 mM EDTA, pH 7.5, 100 mM KCl, 10% (w/v) glycerol	Eitzen, 1997
Ponceau stain	0.1% Ponceau S, 1% TCA	Szilard, 2000
Solution B	100 mM KH_2PO_4, 100 mM K_2HPO_4, 1.2 M sorbitol	Pringle et al., 1991
TE	10 mM Tris-HCl, pH 7.0-8.0 (as needed), 1 mM EDTA	Maniatis et al., 1982

2.2 Microorganisms and Culture Conditions

2.2.1 Bacterial Strains and Culture Conditions

The *Escherichia coli* strains and culture media used in this study are described in Tables 2-5 and 2-6, respectively. Bacteria were grown at 37ºC. Cultures of 5 ml or less were grown in culture tubes in a rotary shaker at 200 rpm. Cultures greater than 5 ml were grown in flasks in a rotary shaker at 250 rpm. Culture volumes were approximately 20% of flask volumes.

Table 2-5. ***E. coli*** **strains**

Strain	Genotype	Source
DH5α	F$^-$, Φ80d*lac*ZΔM15, Δ(*lac*ZYA-*arg*F), U169, *rec*A1, *end*A1, *hsd*R17(r_k^-, m_k^+), *pho*A$^-$, *sup*E44, λ$^-$, *thi*-1, *gyr*A96, *rel*A1	Invitrogen
BL21-DE3	F$^-$, *omp*T, *hsd*SB(r_B^- m_B^-) *gal*, *dcm* (DE3)	Novagen

Table 2-6. Bacterial culture media

Medium	Composition	Reference
LB^{a,b}	1% tryptone, 0.5% yeast extract, 1% NaCl	Maniatis et al., 1982
SOB	2% tryptone, 0.5% yeast extract, 10 mM NaCl, 2.5 mM KCl	Maniatis et al., 1982
TYP^a	1.6% tryptone, 1.6% yeast extract, 0.5% NaCl, 0.25% K_2HPO_4	Promega Protocols and Applications Guide, 1989/1990

[a] Ampicillin was added to 100 μg/ml for plasmid selection when necessary.
[b] For solid media, agar was added to 1.5%.

2.2.2 Yeast Strains and Culture Conditions

The *S. cerevisiae* strains used in this study are listed in Table 2-7. Yeast culture media are described in Table 2-8. Yeasts were grown at 30°C, unless otherwise indicated. Cultures of 10 ml or less were grown in 16 × 150-mm glass tubes in a rotating wheel. Cultures greater than 10 ml were grown in flasks in a rotary shaker at 250 rpm. Culture volumes were approximately 20% of flask volumes.

Table 2-7. ***S. cerevisiae*** **strains**

Strain	Genotype	Reference
BY4741	*MATa, his3Δ1, leu2Δ0, met15Δ0, ura3Δ0*	Giaever et al., 2002
BY4742	*MATα, his3Δ1, leu2Δ0, lys2Δ0, ura3Δ0*	Giaever et al., 2002
SFY526	*MATa, ura3-52, his3-200, ade2-101, lys2-801, trp1-901, leu2-3, 112, gal4-542, gal80-538, LYS2::*$GAL1_{UAS}$-$GAL1_{TATA}$*-lacZ, MEL1*	Harper et al., 1993
inp2Δ	*MATα, his3Δ1, leu2Δ0, lys2Δ0, ura3Δ0, inp2::KanMX4*	Giaever et al., 2002
inp1Δ/POT1-GFP	*MATα, his3Δ1, leu2Δ0, lys2Δ0, ura3Δ0, inp1::KanMX4, pot1::POT1-GFP (HIS5)*	Fagarasanu et al., 2005
BY4741/POT1-GFP	*MATa, his3Δ1, leu2Δ0, met15Δ0, ura3Δ0, pot1::POT1-GFP (HIS5)*	This study
inp2Δ/POT1-GFP	*MATα, his3Δ1, leu2Δ0, lys2Δ0, ura3Δ0, inp2::KanMX4, pot1::POT1-GFP (HIS5)*	This study
INP2-TAP	*MATa, his3Δ1, leu2Δ0, met15Δ0, ura3Δ0, inp2::INP2-TAP (HIS3)*	This study
INP2-GFP	*MATa, his3Δ1, leu2Δ0, met15Δ0, ura3Δ0, inp2::INP2-GFP (HIS5)*	This study
BY4741/SDH2-GFP	*MATa, his3Δ1, leu2Δ0, met15Δ0, ura3Δ0, sdh2::SDH2-GFP (HIS5)*	This study
inp2Δ/SDH2-GFP	*MATα, his3Δ1, leu2Δ0, lys2Δ0, ura3Δ0, inp2::KanMX4, sdh2::SDH2-GFP (HIS5)*	This study
BY4741/POT1-mRFP/SDH2-GFP	*MATa, his3Δ1, leu2Δ0, met15Δ0, ura3Δ0, pot1::POT1-mRFP(HIS5), sdh2::SDH2-GFP (natR)*	This study
inp2Δ/GFP-TUB1	*MATα, his3Δ1, leu2Δ0, lys2Δ0, ura3::GFP-TUB1-URA3, inp2::KanMX4*	This study
kar9Δ/GFP-TUB1	*MATα, his3Δ1, leu2Δ0, lys2Δ0, ura3::GFP-TUB1-URA3, kar9::KanMX4*	This study
BY4742/GFP-TUB1	*MATα, his3Δ1, leu2Δ0, lys2Δ0, ura3::GFP-TUB1-URA3*	This study
inp1Δ/ inp2Δ/ POT1-GFP	*MATα, his3Δ1, leu2Δ0, lys2Δ0, ura3Δ0, inp2::KanMX4, inp1::LEU2, pot1::POT1-GFP (HIS5)*	This study
bni1Δ/POT1-GFP	*MATα, his3Δ1, leu2Δ0, lys2Δ0, ura3Δ0, bni1::KanMX4, pot1::POT1-GFP (HIS5)*	This study

myo2-66/POT1-GFP	*MATa, his3Δ1, leu2Δ0, met15Δ0, ura3Δ0, myo2-66, pot1::POT1-GFP (HIS5)*	This study
MYO2/myo2Δ	*MATa/MATα, his3Δ1/his3Δ1, leu2Δ0/leu2Δ0, met15Δ0/+, +/lys2Δ0, ura3Δ0/ura3Δ0, myo2::KanMX4/MYO2*	Giaever et al., 2002
myo2Δ/pRS416-MYO2	*MATa, his3Δ1, leu2Δ0, lys2Δ0, ura3Δ0, myo2::KanMX4, pRS416-MYO2 (URA3)*	This study
myo2Δ /POT1-GFP/pRS416-MYO2	*MATa, his3Δ1, leu2Δ0, lys2Δ0, ura3Δ0, pot1::POT1-GFP (natR), myo2::KanMX4, pRS416-MYO2 (URA3)*	This study

Table 2-8. Yeast culture media

Medium	**Composition**[a,b]	**Reference**
Nonfluorescent medium	6.61 mM KH_2PO_4, 1.32 mM K_2HPO_4, 4.06 mM $MgSO_4\cdot 7H_20$, 26.64 mM $(NH_4)SO_4$, 1 × CSM, 2% glucose, 1% agarose	This study
SCIM	0.67% YNB, 0.5% yeast extract, 0.5% peptone, 0.5% Tween (w/v) 40, 0.3% glucose, 0.3% (v/v) oleic acid, 1 × CSM	This study
Sporulation medium	1% potassium acetate, 0.1% yeast extract, 0.05% glucose	Rose et al., 1988
SM	0.67% YNB, 2% glucose, 1× CSM without leucine, uracil, or tryptophan as required	This study
YEPD	1% yeast extract, 2% peptone, 2% glucose	Rose et al., 1988
YNBD[c]	0.67% YNB, 2% glucose	Rose et al., 1988
YPBO	0.3% yeast extract, 0.5% peptone, 0.5% K_2HPO_4, 0.5% KH_2PO_4, 0.2% (w/v) Tween 40 or 1% (v/v) Brij 35, 1% (v/v) oleic acid	Kamiryo et al., 1982

[a] For solid media, agar was added to 2%.

[b] Glucose and oleic acid were added after autoclaving.

[c] Supplemented with histidine, leucine, lysine or uracil, each at 50 μg/ml, as required.

2.2.3 Mating, Sporulation and Tetrad Dissection of *S. cerevisiae*

S. cerevisiae strains were mated according to the method of Rose et al. (1988). Haploid strains of opposite mating types were streaked in single straight lines on separate YEPD agar plates (Table 2-8) and incubated overnight. They were then replica-plated onto a fresh YEPD agar in such a way that streaks of cells of opposite mating types were perpendicular to each other and incubated overnight. Cells on this plate were then replica-plated onto YNBD agar (Table 2-8) supplemented for the auxotrophic requirements of the diploid strain. Diploid cells appeared after overnight incubation.

Sporulation and tetrad dissection of *S. cerevisiae* strains were performed according to Rose et al. (1988) with modifications. An individual diploid strain was grown overnight in 5 ml of YNBD medium (Table 2-8) supplemented for its auxotrophic requirements. Cells were harvested by centrifugation and washed twice with 10 ml of water. 5 μl of cell pellet was transferred to and incubated in 3 ml of sporulation medium for 3 to 7 days. Formation of tetrads was examined by light microscopy. When approximately 10% or more cells formed tetrads, 1 ml of cells was transferred to a microcentrifuge tube and washed twice with water. The cell pellet was resuspended in 1 ml of water. 10 μl of cells was transferred to 1 ml of water containing 3 to 5 μg of Zymolyase 20T and incubated at 30°C in a rotating wheel for 15 min. 20 μl of spheroplasted cells was spread in a single line near the edge of a thin agar YEPD plate. Tetrads were dissected using a Zeiss Axioskop 40 microscope equipped with a Tetrad Manipulator System (Carl Zeiss). Isolated spores were incubated for 2 days at 30°C.

2.3 Introduction of DNA into Microorganisms

2.3.1 Chemical Transformation of *E. coli*

Plasmid DNA was introduced into Subcloning Efficiency, chemically competent *E. coli* DH5α cells, as recommended by the manufacturer (Invitrogen). Essentially, 1 to 2 μl of ligation reaction (Section 2.5.7) or 0.5 μl (0.25 μg) of plasmid DNA was added to

25 μl of cells. The mixture was incubated on ice for 30 min, subjected to a 20 sec heat shock at 37°C, and chilled on ice for 2 min. 1 ml of LB medium (Table 2-6) was added, and the cells were incubated in a rotary shaker for 45 to 60 min at 37°C. Cells were spread onto LB agar plates (Table 2-6) containing ampicillin and incubated overnight at 37°C. 100 μl of 2% X-gal in DMF and 50 μl of 100 mM IPTG were added to agar plates to allow for blue/white selection of colonies carrying recombinant plasmids, when necessary.

2.3.2 Electroporation of *E. coli*

For high-efficiency transformation of *E. coli* DH5α or BL21-DE3 cells with plasmid DNA, cells were made electrocompetent as recommended by Invitrogen. Cells were grown overnight in 10 ml of SOB medium (Table 2-6). 0.5 ml of this overnight culture was transferred to and incubated in 500 ml of SOB until the culture reached an OD_{600} (optical density at a wavelength of 600 nm) of 0.5. Cells were harvested by centrifugation at 2,600 × *g* for 15 min at 4°C, washed twice with 500 ml of ice-cold 10% (v/v) glycerol, and resuspended in a minimal amount of 10% (v/v) glycerol. Cells were either used immediately or frozen as 100 μl aliquots by immersion in a dry ice/ethanol bath and stored at -80°C. For transformation, 1 μl of ligation reaction or 0.5 μl of plasmid DNA was added to 20 μl of cells. The mixture was placed between the bosses of an ice-cold disposable microelectroporation chamber (width ~0.15 cm) (Whatman Biometra) and submitted to an electrical pulse of 395 V (amplified to ~2.4 kV) at a capacitance of 2 μF and a resistance of 4 kΩ using a Cell-Porator connected to a Voltage Booster (Whatman Biometra). Cells were then immediately transferred to 1ml of LB, incubated in a rotary shaker at 37°C for 45 to 60 min, and spread on LB agar plates containing ampicillin.

2.3.3 Chemical Transformation of Yeast

Plasmid DNA was introduced into yeast according to the procedure of Gietz and Woods (2002). Essentially, 25 µl of cells was scraped with a sterile toothpick from a plate not more than one week old and resuspended in 1 ml of water. Cells were harvested by centrifugation, resuspended in 1 ml of 100 mM lithium acetate, and incubated at 30°C for 5 min. Cells were again harvested by centrifugation, and the following components were added on top of the cell pellet in this order: 240 µl of 50% PEG, 36 µl of 1 mM lithium acetate, 50 µl of 2 mg sheared salmon sperm DNA/ml, 1 µl of plasmid DNA and 20 µl of water. The mixture was vortexed vigorously for 1 min and incubated at 42°C for 20 min. Cells were harvested by centrifugation, resuspended gently in 200 µl of water and plated onto SM agar plates (Table 2-8). Plates were incubated at 30°C for 3 days for colony formation.

2.3.4 Electroporation of Yeast

Yeast cells were made electrocompetent as recommended by Ausubel et al. (1989). Cells were grown overnight in 10 ml of YEPD. 5 ml of overnight culture was transferred to 45 ml of YEPD, and incubated for 4 to 5 h or until the culture reached an OD_{600} of ~1.0. Cells were then harvested by centrifugation at 2,000 × *g*, resuspended in 50 ml TE 7.5 (Table 2-4) containing 100 mM lithium acetate, and incubated for 30 min at room temperature or 30°C with gentle agitation. DTT was added to a final concentration of 20 mM, and the incubation was continued for another 15 min. Cells were harvested by centrifugation at 2,000 × *g*, washed once with 50 ml each of room-temperature water, ice-cold water, and ice-cold 1 M sorbitol. Cells were resuspended in a minimal volume of ice-cold 1 M sorbitol. 20 µl of cells was mixed with 1 µl of plasmid DNA or 100 to 150 ng of purified DNA fragment, placed between the bosses of an ice-cold microelectroporation chamber, submitted to an electrical pulse of 250 V (amplified to ~1.6 kV) at a capacitance of 2 µF and a resistance of 4 kΩ using a Cell-Porator connected to a Voltage Booster. Cells were immediately resuspended in 100 µl of ice-cold 1 M sorbitol and plated onto SM agar plates. Plates were incubated at 30°C for 3 to 5 days for colony formation.

2.4 Isolation of DNA from Microorganisms

2.4.1 Isolation of Plasmid DNA from Bacteria

Single bacterial colonies were inoculated into 2 ml of LB containing ampicillin and incubated overnight at 37°C. Cells were harvested by microcentrifugation, and plasmid DNA was isolated using a QIAprep Spin Miniprep Kit according to the manufacturer's instructions (Qiagen). This method is based on the alkaline lysis of bacterial cells, followed by adsorption of DNA onto silica in the presence of high salt and elution of DNA in low salt buffer. Plasmid DNA was usually eluted in 50 µl of the supplied elution buffer.

2.4.2 Isolation of Chromosomal DNA from Yeast

Yeast genomic DNA was prepared as recommended by Ausubel et al. (1989). Cells were grown overnight in 10 ml of YEPD, harvested by centrifugation for 5 min at 2,000 × *g*, washed twice in 10 ml of water, and transferred to a 2.0 ml microcentrifuge tube. 200 µl each of breakage buffer (Table 2-4), glass beads and phenol/chloroform/isoamyl alcohol (25:24:1) were added to the cells. The mixture was vortexed for 3 to 5 min at 4°C to simultaneously break yeast cells and separate nucleic acids from proteins. 200 µl of TE 8.0 (Table 2-4) was added, and the mixture was vortexed briefly. The organic and aqueous phases were separated by centrifugation at 16,000 × *g* for 5 min at room temperature. The aqueous phase was extracted once against an equal volume of phenol/chloroform/isoamyl alcohol (25:24:1). DNA was precipitated by the addition of 2.5 volumes of absolute ethanol and centrifugation at 16,000 × *g* for 5 min at room temperature. The pellet was washed once with 1 ml 70% (v/v) ethanol, dried in a rotary vacuum desiccator and dissolved in 50 µl of TE 8.0 containing 100 µg RNase A/ml. DNA was incubated at 37°C for 1 to 2 h to allow for digestion of RNA.

2.5 DNA Manipulation and Analysis

Unless otherwise indicated, reactions were carried out in 1.5-ml microcentrifuge tubes, and microcentrifugation was performed in an Eppendorf microcentrifuge at 16,000 × *g*.

2.5.1 Amplification of DNA by the Polymerase Chain Reaction (PCR)

PCR was used to amplify specific DNA sequences or to introduce modifications in the amplified DNA sequence. Primer design, reaction components and cycling conditions were performed following standard protocols (Innis and Gelfand, 1990; Saiki, 1990). A reaction usually contained 0.1 to 0.5 µg of yeast genomic DNA or 0.1 to 0.2 µg of plasmid DNA, 20 pmol of each primer, 0.25 mM of each dNTP, 1 mM Mg_2SO_4, and 1.25 U of Easy-A high-fidelity polymerase in 50 µl of the supplied reaction buffer (Stratagene). Reactions were performed in 0.6-ml microcentrifuge tubes in a Robocycler 40 with a Hot Top attachment (Stratagene). Alternatively, Ready-to-Go PCR Beads were used as recommended by the manufacturer (Amersham Biosciences).

2.5.2 Digestion of DNA by Restriction Endonucleases

In general, 1 to 2 µg of plasmid DNA or purified DNA was digested by restriction endonucleases for 1 to 1.5 h according to the manufacturer's instructions. Digestion was immediately terminated by agarose gel electrophoresis of the DNA fragments, except for plasmid DNA, which required dephosphorylation.

2.5.3 Dephosphorylation of 5'-ends

Plasmid DNA linearized by one restriction endonuclease was subjected to dephosphorylation at its 5'-ends to prevent intramolecular ligations. After digestion of plasmids, reactions were mixed with 10 U of CIP and incubated at 37°C for 30 min. The dephosphorylation reaction was terminated by agarose gel electrophoresis of the DNA fragments.

2.5.4 Separation of DNA Fragments by Agarose Gel Electrophoresis

DNA fragments in solution were mixed with 0.2 volume of 6 × DNA loading dye (Table 2-4) and separated by electrophoresis in 1% agarose gels in 1 × TBE (Table 2-4) containing 0.5 μg of ethidium bromide/ml. Gels were subjected to electrophoresis at 10 V/cm in 1 × TBE, and DNA fragments were subsequently visualized on an ultraviolet transilluminator (Photodyne, Model 3-3006).

2.5.5 Purification of DNA Fragments from Agarose Gel

A DNA fragment of interest was excised from the agarose gel using a razor blade. DNA was extracted from the agarose slice using the QIAquick Gel Extraction Kit according to manufacturer's instructions (Qiagen). This method is based on the dissolution of agarose gel and adsorption of DNA to the silica membrane in the presence of a high concentration of chaotropic salts, followed by washing and elution of DNA in the presence of low salt. DNA was usually eluted in 30 to 50 μl of the supplied elution buffer.

2.5.6 Purification of DNA from Solution

Contaminants (small oligonucleotides, salts, enzymes, etc.) were removed from a DNA solution using the QIAquick PCR Purification Kit as described by the manufacturer (Qiagen). The principle of this method is similar to that of the QIAquick Gel Extraction Kit (Section 2.5.5), except that no dissolution of agarose gel was involved. DNA was usually eluted in 30 to 50 μl of the supplied elution buffer.

2.5.7 Ligation of DNA Fragments

DNA fragments treated with restriction endonucleases and purified as described in Section 2.5.5 were ligated using 1 µl of T4 DNA ligase in the buffer supplied by the manufacturer (NEB). The reaction was typically conducted in a volume of 10 µl, with the molar ratio of plasmid to insert being between 1:3 and 1:10, and incubated overnight at 16°C. Alternatively, 1 µl of Quick T4 DNA ligase (NEB) in 1 × Quick Ligation Buffer was used in a reaction volume of 20 µl. The reaction was incubated at room temperature for 10 min.

Occasionally, PCR products after purification by agarose gel electrophoresis were ligated with the vector pGEM-T using the pGEM-T Vector System according to the manufacturer's instructions (Promega).

2.5.8 DNA Sequencing

DNA sequencing was performed using the BigDye Terminator v1.1/3.1 Cycle Sequencing Ready Reaction Kit as described by the manufacturer (Applied Biosystems). This method is based on the method of Sanger et al. (1977) and involves the random incorporation of fluorescent dideoxy terminators during the elongation of DNA sequences with a modified version of *Taq* DNA polymerase. Essentially, a reaction contained 1 µl of plasmid DNA, 3.2 pmol of primer, 3 µl of Terminator Ready Reaction Mix, and 2.5 µl of the supplied 5 × buffer in a total volume of 20 µl. The reaction was subjected to cycle sequencing using the Robocycler 40 with a Hot Top attachment and the following conditions: 1 cycle at 96°C for 2 min; 25 cycles at 96°C for 46 sec, 50°C for

51 sec and 60°C for 4 min 10 sec; 1 cycle at 6°C to hold until ready to purify. Reaction products were precipitated with 80 µl of 75% (v/v) isopropanol for 20 min at room temperature, subjected to microcentrifugation at 16,000 × *g* for 20 min, washed twice with 250 µl of 75% isopropanol, dried in a rotary vacuum dessicator and resuspended in 15 µl of Template Suppression Reagent. They were then heated at 95°C for 2 min and immediately cooled on ice. Finally, they were separated by capillary electrophoresis, and fluorescence was detected and recorded by an ABI 310 Genetic Analyzer (Applied Biosystems).

2.5.9 Construction of Strains Carrying Plasmid-encoded *myo2* Point Mutants as Sole Copies of *MYO2*

2.5.9.1 Site-directed mutagenesis of *MYO2*

Individual point mutations were made by the QuikChange Site-Directed mutagenesis method (Stratagene) using pRS413-MYO2 (HIS3) as a template. The oligonucleotides used are listed in Table 2.3 (oligonucleotides 2532 to 2549). Each individual mutation was verified by DNA sequencing. The list of all *myo2* mutants used in this study, including the ones previously made by Pashkova et al. using a similar method, is presented in Table 2-9.

2.5.9.2 Construction of strains carrying pRS413-*myo2* point mutants as sole copies of *MYO2*

The heterozygous deletion diploid strain MYO2/*myo2Δ* (Table 2-7) was transformed with pRS416-*MYO2* (URA3). A successful transformant was then sporulated, and tetrads were dissected to select for the haploid *MATa* strain *myo2Δ/pRS416-MYO2* (Table 2-7). To fluorescently label peroxisomes, *POT1* was genomically tagged with the sequence encoding an improved version of GFP (GFP+) from *Aequoria victoria* (Scholz et al., 2000) by homologous recombination with a PCR-based integrative transformation, making the strain *myo2Δ/POT1-GFP/pRS416-MYO2* (Table 2-7).

Cells of the strain *myo2Δ/POT1-GFP/pRS416-MYO2* carrying pRS416-*MYO2* (*URA3*) as the sole copy of *MYO2* were transformed with pRS413 (HIS3) containing either wild-type *MYO2* or *myo2* harboring a point mutation. Transformants were streaked onto SM lacking histidine and uracil (SM-His-Ura) to select for the presence of both plasmids and then onto SM containing 5-fluoroorotic acid (5-FOA) to remove pRS416-MYO2. The resulting strains contained pRS413-*MYO2* or pRS413-*myo2* as sole copies of the *MYO2* gene.

Table 2.9 *myo2* point mutants used in this study

Mutation	Reference
D1297N	Pashkova et al., 2006
D1297G	Pashkova et al., 2006
L1301P	Pashkova et al., 2006
N1304S	Pashkova et al., 2006
N1304D	Pashkova et al., 2006
N1307D	Pashkova et al., 2006
Q1233R	Pashkova et al., 2006
L1331S	Pashkova et al., 2006
L1411S	Pashkova et al., 2006
Y1415E	Pashkova et al., 2006
K1444A	Pashkova et al., 2006
Q1447R	Pashkova et al., 2006
G1461D	Pashkova et al., 2006
D1457N	Pashkova et al., 2006
R1162E	Pashkova et al., 2006
D1357K	Pashkova et al., 2006

E1375V	Pashkova et al., 2006
R1402C	Pashkova et al., 2006
K1450I	Pashkova et al., 2006
W1407F	Pashkova et al., 2006
T1418V	Pashkova et al., 2006
E1422A	Pashkova et al., 2006
K1425A	Pashkova et al., 2006
N1414S	Pashkova et al., 2006
F1334A	This study
K1408A	This study
R1449A	This study
D1482A	This study
Y1451A	This study
Y1483A	This study
E1484A	This study
L1411A	This study
V1448A	This study

2.6 Protein Manipulation and Analysis

2.6.1 Preparation of Yeast Whole Cell Lysates

Yeast lysates were prepared by disruption with glass beads (adapted from Needleman and Tzagoloff, 1975). Cells were harvested by centrifugation at 2, 000 × *g* for 5 min, washed twice with 10 ml of water, and resuspended in an equal volume of ice-cold Disruption Buffer (Table 2-4) containing 1 × PIN (Table 2-4) and 1 mM DTT. Ice-cold glass beads were added until they reached the meniscus of the cell suspension. The mixture was vortexed for 5 min at 4°C, and glass beads were pelleted by microcentrifugation for 20 sec at 4°C. The supernatant was recovered and clarified by microcentrifugation for 20 min at 4°C.

Alternatively, yeast lysates were prepared by denaturation with alkaline and reducing agents. Cells were harvested by centrifugation at 2,000 × *g* for 5 min, transferred to a microcentrifuge tube, and resuspended in 240 to 500 µl of 1.85 M NaOH and 7.4% 2-mercaptoethanol. The cell suspension was incubated on ice for 5 min and mixed with an equal volume of 50% TCA by vortexing. The mixture was further incubated on ice for 5 min and subjected to microcentrifugation at 16,000 × *g* for 10 min at 4°C. The pellet was washed once with water, resuspended first in 50 to 150 μl of Magic A (1 M unbuffered Tris-HCl, 13% SDS) and then in an equal volume of Magic B (30% (v/v) glycerol, 200 mM DTT, 0.25% bromophenol blue). The mixture was boiled for 10 min and then subjected to microcentrifugation at 16,000 × *g* for 1 min. The supernatant was collected.

2.6.2 Precipitation of Proteins

Proteins were precipitated from solution by adding TCA to a final concentration of 10% and incubation on ice for 30 min to overnight. Precipitates were collected by microcentrifugation at 16,000 × *g* for 30 min at 4°C. The pellet was washed twice with 1 ml of ice-cold acetone, dried in a rotary vacuum dessicator and dissolved in 2 × sample buffer (Table 2-4).

2.6.3 Determination of Protein Concentration

The protein concentration of a sample was determined by the method of Bradford (1976). A standard curve was prepared by adding 1 ml of Bio-Rad Protein Assay Dye to 100 μl aliquots of water containing 2, 4, 6, 8, 10, 12, 14, 16, 18 and 20 μg of BSA. Samples were incubated for 5 min at room temperature, and absorbance was measured at 595 nm using a Beckman DU640 spectrophotometer. Absorbance values were plotted against the BSA concentrations to generate a standard curve. Absorbance of a protein sample was measured in the same way as for BSA standards, and the protein concentration was estimated by comparing the absorbance value with the standard curve.

2.6.4 Separation of Proteins by Electrophoresis

Proteins were separated by sodium dodecyl sulfate-polyacrylamide gel electrophoresis (SDS-PAGE) as described by Ausubel et al. (1989). Protein samples were mixed with an equal volume of 2 × sample buffer containing 10 mM DTT, denatured by boiling for 5 min, and separated by electrophoresis on discontinuous slab gels. Stacking gels contained 3% acrylamide (30:0.8 acylamide:*N*,*N'*-methylene-bis-acrylamide), 60 mM Tris-HCl, pH 6.8, 0.1% SDS, 0.1% (v/v) TEMED, and 0.1% ammonium persulfate. Resolving gels contained 10% acrylamide (30:0.8 acylamide:*N*,*N'*-methylene-bis-acrylamide), 370 mM Tris-HCl, pH 8.8, 0.1% SDS, 0.1% (v/v) TEMED, and 0.043% ammonium persulfate. Electrophoresis was conducted in 1 × SDS-PAGE running buffer (Table 2-4) at 50-200 V using a Bio-Rad Mini Protean II vertical gel system.

2.6.5 Detection of Proteins by Gel Staining

Proteins in polyacrylamide gels were visualized by staining with 0.1% Coomassie Brilliant Blue R-250, 10% (v/v) acetic acid, 35% (v/v) methanol for 1 h with gentle agitation. Unbound dye was removed by multiple washes in 10% (v/v) acetic acid, 35% (v/v) methanol. Gels were dried for 1 h at 80°C on a Bio-Rad Model 583 gel drier.

2.6.6 Detection of Proteins by Immunoblotting

Proteins separated by SDS-PAGE were transferred to nitrocellulose membrane (Bio-Rad) in 1 × transfer buffer (Table 2-4) at 100 mA for 16 h at room temperature using a Trans-Blot tank transfer system with plate electrodes (Bio-Rad). Proteins transferred to nitrocellulose were visualized by staining in Ponceau stain (Table 2-4) for several min and destaining in water. The nitrocellulose was incubated in blocking solution (1% skim milk powder, 1 × TBST (Table 2-4)) with gentle agitation to prevent nonspecific binding of antibodies. Specific proteins on nitrocellulose were detected by incubation with primary antibody in blocking solution for 1 h at room temperature with gentle agitation. The nitrocellulose was then incubated with appropriate HRP-labeled secondary antibody in blocking solution for 1 h. After each antibody incubation, unbound antibodies were removed by washing the nitrocellulose three times with 1 × TBST for 10 min each. Antigen-antibody complexes were detected using an ECL Western Blotting Detection Kit according to the manufacturer's instructions (Amersham Biosciences) and exposing the nitrocellulose to X-Omat BT film (Kodak).

Used nitrocellulose could be reblotted using a Re-Blot Western Blot Recycling Kit according to the manufacturer's instructions (Chemicon). The nitrocellulose was incubated with 1 × Antibody Stripping Solution at room temperature for 15 to 30 min with gentle agitation, rinsed with 1 × TBST, and blotted as described above.

2.7 Subcellular Fractionation of S. *cerevisiae* Cells

2.7.1 Peroxisome Isolation from *S. cerevisiae*

Isolation of peroxisomes from *S. cerevisiae* cells was performed as described by Smith et al. (2002). Cells grown in oleic acid-containing medium were harvested by centrifugation at 800 × *g* in a Beckman JA10 rotor at room temperature and washed twice with water. Cells were resuspended in 10 mM DTT, 100 mM Tris-HCl, pH 9.4, at a concentration of 10 ml per g of wet cells and incubated at 30°C for 35 min with gentle agitation to loosen the outer mannoprotein layer. Cells were collected by centrifugation at 2,500 × *g* in a Beckman JS13.1 rotor for 10 min at 4°C and washed once with Zymolyase buffer (50 mM potassium phosphate, pH 7.5, 1.2 M sorbitol, 1 mM EDTA). Cells were resuspended in Zymolyase buffer containing 0.125 mg of Zymolyase 100T/ml at a concentration of 8 ml per g of wet cells and incubated at 30°C for 45 min to 1 h with gentle agitation to convert cells to spheroplasts. Spheroplasts were harvested by centrifugation at 2,200 × *g* in a Beckman JS13.1 rotor for 8 min at 4°C and washed once with 1.2 M sorbitol, 2.5 mM MES, pH 6.0, 1 mM EDTA. They were then resuspended in buffer H (0.6 M sorbitol, 2.5 mM MES, pH 6.0, 1 mM EDTA, 1 × complete protease inhibitor cocktail (Roche)) at a concentration of 2 ml per g of wet cells. Resuspended spheroplasts were transferred to a homogenization mortar and disrupted by 10 strokes of a Teflon pestle driven at 1,000 rpm by a stirrer motor (Model 4376-00, Cole-Parmer). Cell debris, unbroken cells and nuclei were pelleted by centrifugation at 1,000 × *g* in a Beckman JS13.1 rotor for 8 min at 4°C. The postnuclear supernatant (PNS) was subjected to four additional centrifugations at 1,000 × *g* in a Beckman JS13.1 rotor for 8 min at 4°C. The PNS was fractionated by centrifugation at 20,000 × *g* in a Beckman JS13.1 rotor for 30 min at 4°C into pellet (20KgP) and supernatant (20KgS) fractions.

The 20KgP was resuspended in 11% (w/v) Nycodenz in buffer H and loaded onto the top of a discontinuous Nycodenz gradient (6.6 ml of 17%, 16.5 ml of 25%, 4.5 ml of 35% and 3 ml of 50% (w/v) Nycodenz in buffer H). Organelles were separated by ultracentrifugation at 100,000 × *g* for 80 min at 4°C in a Beckman VTi50 rotor. 18 fractions of 2 ml each were collected from the bottom of the gradient.

2.7.2 Extraction and Subfractionation of Peroxisomes

Extraction and subfractionation of peroxisomes were performed according to Smith et al. (2000) with modifications. Essentially, organelles in the 20KgP fraction (containing ~50 μg of protein) were lysed by incubation in 10 volumes of ice-cold Ti8 buffer (10 mM Tris-HCl, pH 8.0) containing 2 × complete protease inhibitor cocktail (Roche) on ice for 1 h with occasional vortexing and separated by ultracentrifugation at 200,000 × *g* for 1 h at 4°C in a Beckman TLA120.2 rotor into a membrane fraction (Ti8P) and a soluble fraction (Ti8S). The Ti8P fraction was resuspended in ice-cold Ti8 to a final protein concentration of 0.5 mg/ml and mixed with 10 volumes of ice-cold 0.1 M Na_2CO_3, pH 11.3. The mixture was incubated on ice for 45 min with occasional vortexing and subjected to ultracentrifugation at 200,000 × *g* for 1 h at 4°C in a TLA120.2 rotor to yield a fraction enriched for integral membrane proteins (CO_3P) and a fraction enriched for peripheral membrane proteins (CO_3S).

2.8 Microscopy

2.8.1 Confocal 4D Video Microscopy

Cells were grown in YEPD and then incubated in SCIM (Table 2-8) for 16 h. Slides were prepared according to Adames et al. (2001) with modifications. Essentially, 200 μl of hot 1% agarose in nonfluorescent medium (Table 2-9) was used to prepare a thin agarose pad on a slide with two 18-mm square wells (Cel-line Brand). 1 to 2 μl of culture was placed onto the slide, covered with a cover slip and sealed with Valap (1:1:1 mixture of vaseline, lanolin and paraffin). Cells were incubated at room temperature for image capture. Images were captured as described (Hammond and Glick, 2000) using a modified LSM 510 META confocal microscope equipped with a 63× 1.4 NA Plan-Apo objective (Carl Zeiss). A piezoelectric actuator was used to drive continuous objective movement, allowing for the rapid collection of *z*-stacks. The sides of each pixel represented 0.085 μm of the sample. Stacks of 14 optical sections spaced 0.4 μm apart were captured at each time point. The interval between time points is indicated for each movie. GFP was excited using a 488-nm laser, and its emission was collected using a 505-nm long-pass filter. The resulting images were filtered three times using a 3×3 hybrid median filter to reduce shot noise. Fluorescence images from each stack were projected using an average intensity algorithm that involved multiplication of each pixel value by an appropriate enhancement factor for better contrast. Correction for exponential photobleaching of GFP was performed by exponentially increasing the enhancement factor with each projection. The transmitted light images from each stack were projected using a maximum intensity algorithm. The resulting projections were smoothened by means of a blurring algorithm. These operations were performed using NIH Image (http://rsb.info.nih.gov/nih-image/). Adobe Photoshop (Adobe Systems) was used to merge the fluorescent and transmitted light projections. Processed projections were assembled into movies using Apple QuickTime Pro 6.5.2 at a rate of 10 frames per second. Postprocessing operations such as the tracking of peroxisomes and 3D reconstruction were performed using Imaris 4.1 (Bitplane, Zurich, Switzerland).

Deconvolution of images was achieved using algorithms provided by Huygens Professional software (Scientific Volume Imaging BV, The Netherlands). For this method, 3D data sets were processed to remove noise and reassign blur through an iterative Classic Maximum Likelihood Estimation algorithm and an experimentally derived point spread function. The transmission image was treated differently. In

Huygens, a Gaussian filter was applied to the transmission image, and blue colour was applied to the transmission image using Imaris 6.1 software. The level of the transmission image was modified, and the image was processed until only the circumference of the cell was visible. Imaris 6.1 was subsequently used to display the deconvolved 3D data set with the processed transmission image and to prepare the image files before final figure assembly in Adobe Photoshop and Adobe InDesign (Adobe Systems).

Peroxisome velocity was measured as the frame-to-frame displacement of peroxisomes over the time interval between each two consecutive frames using MetaMorph software (Universal Imaging). Only movements within mother cells were measured. For each peroxisome, maximal velocity achieved is presented. Velocities may be underestimates, since movements perpendicular to the focal plane were not considered.

2.8.2 Quantification of Rates of Peroxisome Inheritance

Rates of peroxisome inheritance were quantified as described (Rossanese et al., 2001; Fagarasanu et al., 2005). Cells synthesizing a genomically encoded chimera between GFP and the peroxisomal matrix enzyme 3-ketoacyl-CoA thiolase (Pot1p-GFP) were grown in YEPD medium for 16 h, transferred to SCIM and incubated in SCIM for 16 h to achieve an OD_{600} of 0.5. Peroxisomes were visualized by direct fluorescence confocal microscopy. For each randomly chosen field, three optical sections of 5-μm thickness were collected at a *z*-axis spacing of 1.6 μm using a high detector gain to ensure the capture of weak fluorescent signals. Optical sections were then projected to a single image. All visibly budded cells were considered for analysis, and buds were assigned to four categories of bud volume, expressed as a percentage of mother cell volume (Category I, 0-12%; Category II, 12-

24%; Category III, 24-36%; Category IV, 36-48%). For the analysis of peroxisome inheritance efficiency in *myo2* point mutants, budded cells were assigned to only two size categories: "small budded cells" representing the merger of Categories I and II above, and "large budded cells" representing the merger of Categories III and IV above. Since cell volume is not directly accessible, bud area was first measured using Zeiss LSM 5 Image Browser software and grouped into four "area" categories (that superimpose on the aforementioned "volume" categories if a spherical geometry is assumed for all cells) according to bud cross-sectional area expressed as a percentage of mother cell cross-sectional area: Category I, 0-24%; Category II, 24-39%; Category III, 39-50%; Category IV, 50-61%. Buds were then scored using an all-or-none criterion for the presence or absence of peroxisomal fluorescence. In the case of cells overproducing Inp2p, mother cells were scored in the same manner. Quantification was always performed on at least 25 budded cells from each category of bud size.

2.8.3 Immunofluorescence Microscopy

Indirect immunofluorescence microscopy of yeast cells was performed according to Pringle et al. (1991) with modifications. Cells grown in oleic acid-containing medium were fixed in 3.7% (v/v) formaldehyde for 30 min at room temperature with occasional agitation. Cells were then collected by centrifugation at 2,000 × *g* for 5 min, washed with 4 ml of solution B (Table 2-4), and resuspended in solution B at a concentration of 1 ml per 100 µl of wet cells. The cell suspension was mixed with 40 µg of Zymolyase 100T/ml and 38 mM 2-mercaptoethanol and incubated for 15 to 60 min at 30°C with gentle rotation. Spheroplasts were spotted onto slides precoated with poly *L*-lysine and allowed to dry at room temperature. Spheroplasts were permeabilized by immersion of the slides in -20°C methanol for 6 min and -20°C acetone for 30 s and allowed to dry. Slides were put in a dark humid box at room temperature for the following procedures. Spheroplasts were covered with 50 µl of blocking solution (Section 2.6.6) for 1 h. They were incubated with primary antibody to Myo2p diluted in blocking solution for 1 h, washed 10 to 20 times with 1 × TBST, and then incubated with secondary antibody conjugated to rhodamine diluted in blocking solution for 1 h. Spheroplasts were washed again 10 to 20 times with 1 × TBST and covered with 1 drop of mounting medium (0.4% *N*-propyl gallate, 74.8% (w/v) glycerol in 1 × PBS, pH 7.4). Coverslips were placed on top of slides, and the edges were sealed with nail polish. Images were captured on a LSM510 META (Carl Zeiss) laser scanning microscope.

2.9 Yeast Two-hybrid Analysis

Yeast two-hybrid analysis was performed using the Matchmaker Two-Hybrid System according to the manufacturer's instructions (Clontech) with modifications.

2.9.1 Construction of Chimeric Genes

Chimeric genes were made by amplifying the open reading frames (ORFs) of *INP2*, *INP1*, *PEX19* and the region of *MYO2* gene encoding the Myo2p cargo-binding domain (amino acids 1113-1574) by PCR and ligating them in-frame and downstream of sequences encoding the activation domain (AD) and DNA-binding domain (DB) of the GAL4 transcriptional activator in plasmids pGAD424 and pGBT9, respectively. To construct pGAD424-*INP2* and pGBT9-*INP2*, the *INP2* ORF was amplified by PCR using primers 0041SG and 0042SG (for a list of all primers, see Table 2-3). To construct pGAD424-*INP1* and pGBT9-*INP1*, the *INP1* ORF was amplified by PCR using primers 0043SG and 0044SG. To construct pGAD424-*PEX19* and pGBT9-*PEX19*, the *PEX19* ORF was amplified by PCR using primers 0045SG and 0046SG. To construct pGAD424-*MYO2* and pGBT9-*MYO2*, the region of the *MYO2* gene that encodes the Myo2p cargo-binding domain was amplified by PCR using primers 0043SG and 0044SG. All primers contained the EcoRI recognition sequence. All PCR products were digested with EcoRI and ligated into pGAD424 and pGBT9.

2.9.2 Assays for Two-hybrid Interactions

Plasmid pairs encoding AD and DB fusion proteins were transformed into *S. cerevisiae* strain *SFY526* as described in Section 2.3.3. Transformants were grown in SM. Possible interaction between AD and DB fusion proteins were detected by testing for activation of the integrated *LacZ* construct using the β-galactosidase filter assay according to the instructions of Clontech. For filter assays, cells were streaked directly onto filter paper placed on solid media and broken by 4 freeze-thaw cycles at -80°C.

2.10 Assay for Direct Protein Interaction

Glutathione-S-transferase (GST) fusion proteins of the cargo-binding domain (amino acids 1113-1574) of either wild-type Myo2p (GST-Myo2p) or various mutant variants of Myo2p were constructed using pGEX4T-1 (Amersham Biosciences). Recombinant expression and isolation of GST and GST-Myo2p were done according to the manufacturer's instructions. Maltose-binding protein (MBP) fusions to Inp1p, Inp2p (amino acids 241-705) and Vam2p were made using pMAL-c2 (NEB) and expressed in the *E. coli* BL21-DE3 strain (Novagen).

250 μg of purified GST-Myo2p or GST protein immobilized on glutathione resin were incubated with 250 μg of *E. coli* lysate containing an MBP fusion or MBP alone in H-buffer (20 mM HEPES, pH 7.5, 60 mM NaCl, 1 mM DTT, 0.5% Triton X-100, 1 μg leupeptin/ml, 1 μg pepstatin/ml, 1 μg aprotinin/ml, 1 mM phenanthroline, 1 mM PMSF) for 2 h at 4°C on a rocking platform. The immobilized fractions were allowed to settle and then washed three times with H-buffer prior to protein elution in sample buffer (50 mM Tris-HCl, pH 6.8, 2% SDS, 5% glycerol, 0.001% bromophenol blue, 5% 2-mercaptoethanol). The eluted proteins were subjected to SDS-PAGE. Immunoblotting with rabbit antibodies to MBP (NEB) and mouse monoclonal antibodies to GST (Sigma-Aldrich) combined with AlexaFluor 680/750-conjugated goat anti-mouse/anti-rabbit antibodies (Invitrogen) was used to detect protein interactions in the assay for direct protein binding. Immunoblots were processed using an Odyssey digital imaging system (Li-Cor) with resolution set to 84 μm and highest quality.

2.11 Cell Cycle Arrest

α-factor-induced G1 arrest was performed as described previously (Makhnevych et al., 2003). Cells grown in YEPD to early log phase were synchronized by treatment with 1 μg α-factor (Sigma-Aldrich)/ml for 2 h. Cell cycle arrest was monitored by microscopic examination of cells. Arrested cells were washed with fresh medium twice to remove α-factor and incubated in fresh medium at 24°C. Equal amounts of cells were then collected at each time point as indicated.

CHAPTER THREE: INP2P IS THE PEROXISOME-SPECIFIC RECEPTOR FOR THE MYOSIN V MOTOR MYO2P OF *SACCHAROMYCES CEREVISIAE*

A version of this chapter has been published.
Fagarasanu, A., M. Fagarasanu, G. A. Eitzen, J. D. Aitchison, and R. A. Rachubinski. 2006. The peroxisomal membrane protein Inp2p is the peroxisome-specific receptor for the myosin V motor Myo2p of *Saccharomyces cerevisiae*. *Dev. Cell* 10:587-600.

Overview

We used three-dimensional time-lapse (4D) confocal video microscopy (Hammond and Glick, 2000) of *S. cerevisiae* cells expressing a genomically integrated chimeric gene, *POT1-GFP*, encoding peroxisomal thiolase tagged at its carboxyl terminus with GFP (Pot1p-GFP) (Fagarasanu et al., 2005) to examine the dynamics of peroxisomes. As reported in the Introduction, most peroxisomes are immobile at the cell periphery in wild-type cells (Figures 3-1A and 3-1B; Movies S1 and S2). During bud growth, peroxisomes are recruited one by one from these static positions and transported toward the bud (Figure 3-1C; Movie S3). The velocities of these mobile peroxisomes vary, with a maximal observed velocity of approximately 0.45μm/s (Figure 3-1D). Interestingly, peroxisomes in the bud concentrate at sites of polarized cell growth, initially clustering at the bud tip. During cytokinesis, subsets of peroxisomes in the bud and in the mother cell relocate to the bud-neck region, while the remaining peroxisomes remain immobile at the bud and mother cell cortices (Figure 3-1A; Movie S1).

The partitioning of peroxisomes to buds has been shown to be dependent on Myo2p (Hoepfner et al., 2001). As mentioned in the Introduction, in addition to peroxisomes, Myo2p is responsible for the bud-directed movement of many other *S. cerevisiae* organelles. Interstingly, Myo2p associates with various organelles over distinct periods of the cell cycle, which are both different and specific for each organelle type. This explains the establishment of characteristic patterns of movement for each organelle, even though the same molecular motor carries different organelles. For example, at cytokinesis, both late-Golgi elements and peroxisomes relocate to the mother bud-neck region, where Myo2p accumulates. In contrast, vacuoles do not display Myo2p-

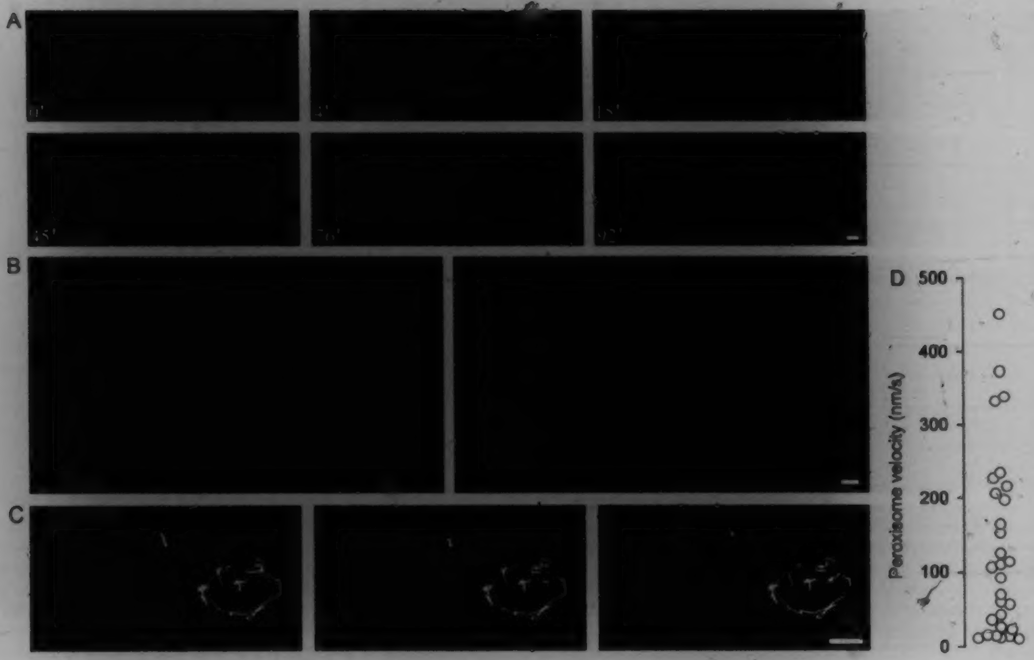

Figure 3-1. Peroxisome dynamics in wild-type *S. cerevisiae* cells. (A) Arrowheads point to peroxisomes labeled with Pot1p-GFP that clustered at sites of polarized growth. At 4 min, the cell at left underwent cytokinesis, and subsets of peroxisomes from both mother cell and bud relocated to the mother-bud neck region (red arrowheads). As soon as a new bud was visible (15′), peroxisomes within the mother cell lost their fixed positions and were inserted into the bud, where they clustered at the growing bud tip (yellow arrowhead). A cluster of peroxisomes localized to the bud tip is also visible in the bud at right (orange arrowhead). Asterisks mark some immobile peroxisomes in mother cells (Movie S1). Bar, 1 μm. (B) Immobile peroxisomes are cortically localized. Three-dimensional reconstruction of a frame taken from Movie S1 (60′), when all peroxisomes in mother cells were immobile. Peroxisomes were marked by red spheres using Imaris 4.1. In three dimensions (right), all peroxisomes within mother cells clearly localize to the cell periphery. Asterisks mark cortical peroxisomes that appear in the middle of cells in 2-dimensional images (Movie S2). Bar, 1 μm. (C) Peroxisome insertion into buds. Tracked peroxisomes were marked by blue spheres and other peroxisomes by green spheres using Imaris 4.1. A peroxisome detaches from the cortex and initially moves to the bud neck. Shortly after, it travels to the bud tip where it joins other inherited peroxisomes. The peroxisome shown here also divided following inheritance (Movie S3). Bar, 1 μm. (D) Scatter plot of velocities of peroxisomes observed in Movie S1. Maximal velocity achieved by individual peroxisomes is presented.

dependent movements at this stage of the cell cycle, and no vacuolar structures are found at the bud neck. Also, late compartments of the Golgi follow Myo2p to the shmoo tips in G1-arrested cells, in contrast to what is observed for peroxisomes and vacuoles (Rossanese et al., 2001; Tang et al., 2003; Fagarasanu et al., 2006a).

How is the Myo2p tail able to discriminate among its different cargoes in such a cell-cycle-regulated manner? Importantly, distinct Myo2p functions are genetically dissectible within the Myo2p tail. For example, mutations in the Myo2p cargo binding domain were found that disrupt specifically either vacuole inheritance or polarized secretion (Schott et al., 1999; Catlett et al., 2000). Moreover, the coexpression of two different copies of *MYO2*, one bearing a mutation preventing vacuole segregation and the other a deletion abolishing polarized secretion, resulted in normal vacuole inheritance and cell growth (Catlett et al., 2000). It has therefore been proposed that each organelle has its own Myo2p-specific receptor that binds to different regions in the Myo2p tail. Reasonably, the control of cargo movement could be achieved by regulating these organelle-specific factors or/and by conformational changes in Myo2p that could influence the exposure of different attachment sites on the Myo2p surface. The discovery of Vac17p, the vacuole-specific receptor for Myo2p, as a cell-cycle-regulated protein (Ishikawa et al., 2003; Tang et al., 2003) strongly suggested that organelle-specific receptors are the main target for regulation of organelle motility. Recently, the 2.2-Å resolution crystal structure of the globular tail of Myo2p has been determined (Pashkova et al., 2006). One important finding was that the binding sites on Myo2p for vacuoles and secretory vesicles are very distant from one another and simultaneously exposed on the

Myo2p surface. This finding again suggested that cargo-specific receptors, rather than Myo2p itself, dictate the timing of Myo2p attachment to organelles.

3.1 The Identification of Inp2p

We initially set out to identify the peroxisome-specific receptor for Myo2p by screening haploid yeast strains deleted for nonessential genes and that could exhibit compromised peroxisome inheritance. To reduce the overall number of strains to be screened, we stipulated that the peroxisome-specific receptor for Myo2p should satisfy two criteria. First, such a receptor must be localized to peroxisomes. In addition to the known peroxisomal proteins, we were interested in proteins exhibiting a "punctate composite" distribution as defined in the study reporting a global analysis of protein localization in *S. cerevisiae* (Huh et al., 2003). We also focused on proteins predicted to contain coiled-coil domains, since these domains have been found in other proteins that directly interact with the globular tail of class V myosins (Nagashima et al., 2002; Estrada et al., 2003; Ishikawa et al., 2003; Itoh et al., 2004).

To identify strains defective in peroxisome inheritance, cells of individual deletion strains expressing *POT1-GFP* were scored using a stringent all-or-none criterion for the presence of peroxisomal fluorescence within buds. Analysis of deletion mutant strains yielded one strain that was dramatically affected in peroxisome inheritance. This strain was deleted for the open reading frame *YMR163c*, encoding a protein of previously unknown function, Ymr163p (Saccharomyces Genome Database, http://www.yeastgenome.org/). Ymr163p satisfies both of our a priori selection criteria for a peroxisomal receptor for Myo2p. Its GFP chimera yields a "punctate composite" fluorescence pattern (Huh et al., 2003). Ymr163p is predicted to be 705 amino acids in length and to have two coiled-coiled domains (amino acids 477-504 and 618-646). Because of its role in peroxisome inheritance (see below), we have designated *YMR163c* as *INP2* for inheritance of peroxisomes gene 2 and its encoded protein as Inp2p.

3.2 Cells Lacking Inp2p Exhibit a Specific Impairment in Peroxisome Inheritance

Budded cells of the *inp2Δ* strain displayed an increase in the percentage of buds devoid of peroxisomes as compared to wild-type cells (Figure 3-2A). Quantification showed that when the bud volume reached 0%-12% of the mother cell volume (Category I), only 3.7% of the buds of the *inp2Δ* strain contained at least one peroxisome. In contrast, 90% of Category I buds of wild-type cells had peroxisomes. Overall, *inp2Δ* cells exhibited less buds containing at least one peroxisome than wild-type cells at all bud sizes. For *inp2Δ* cells, only 21%, 26%, and 30% of buds of Categories II, III, and IV, respectively, displayed peroxisomal fluorescence, while essentially 100% of wild-type buds in each of these categories contained peroxisomes (Figure 3-2A). In addition, we observed that whereas wild-type cells contained a fairly equal number of peroxisomes per cell, *inp2Δ* cells displayed heterogeneity in their number of peroxisomes. Some *inp2Δ* cells exhibited increased numbers of peroxisomes, while others exhibited few or even no peroxisomes.

The impairment in peroxisome segregation observed in cells lacking Inp2p could be due theoretically to generalized defects in cell polarity or actomyosin function. To test if Inp2p is required specifically for peroxisome inheritance, we examined the partitioning of other organelles in wild-type and *inp2Δ* cells. The distribution of vacuoles was

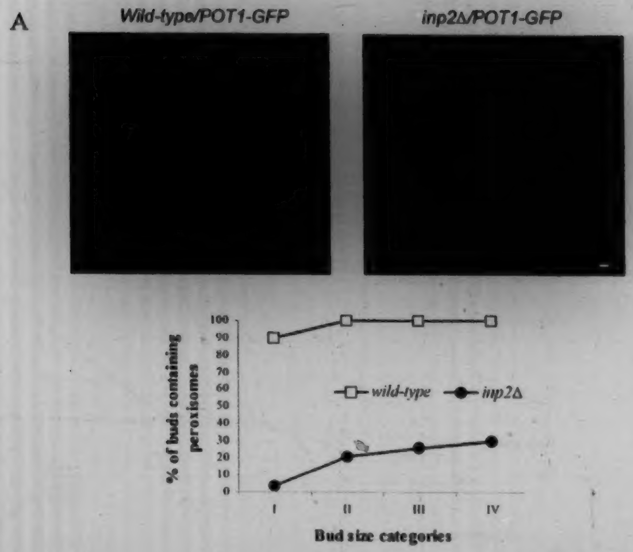

Figure 3-2. Deletion of the *INP2* gene affects specifically peroxisome inheritance. (A) Wild-type and *inp2Δ* cells expressing *POT1-GFP* were incubated in SCIM for 16 hr. Fluorescent images of randomly chosen fields of cells were acquired as a stack by confocal microscopy. Buds were sized according to four categories relative to the volume of the mother cell. The percentages of buds containing peroxisomes at each size category were plotted. Quantification was performed on at least 25 budded cells from each category. Bar, 1 µm. (B) Vacuole inheritance is unaffected in *inp2Δ* cells. Vacuoles of wild-type and *inp2Δ* cells grown in YPD medium were labeled with the fluorophore FM4-64, and confocal images were captured. Quantification was performed as in (A). Bar, 1 µm. (C) Mitochondrial segregation is unaffected in *inp2Δ* cells. Wild-type and *inp2Δ* cells expressing *SDH2-GFP* were grown in YPD medium, and confocal images were captured. Quantification was performed as in (A). Bar, 1 µm. (D) *inp2Δ* cells have properly oriented mitotic spindles. Wild-type, *inp2Δ* and *kar9Δ* cells genomically encoding a fluorescent chimera of α-tubulin, GFP-Tub1p, were grown as described (Adames et al., 2001) and visualized by confocal microscopy. The orientation of the mitotic spindle was analyzed in pre-anaphase cells as described. Quantification was performed on at least 100 pre-anaphase budded cells of each strain. Bar, 1 µm. (E) *inp2Δ* cells display a normal polarized actin cytoskeleton. Wild-type and *inp2Δ* cells were grown in YPD medium, and actin was detected with rhodamine-phalloidin and visualized by epifluorescence microscopy. Bar, 1 µm. (F) Wild-type and *inp2Δ* cells show similar growth on glucose-containing medium. Strains were grown to mid-log phase in liquid YPD medium, and equal amounts of cells were serially diluted ten-fold onto YPD agar and incubated at 30°C.

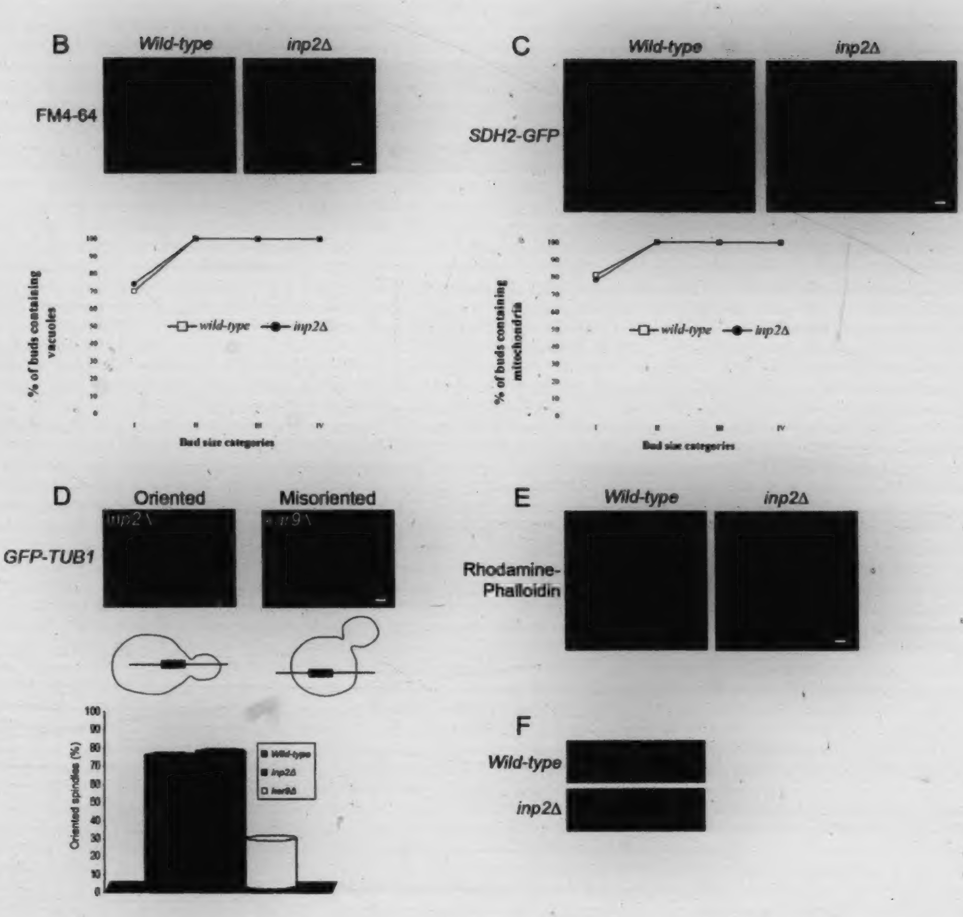
B
Wild-type
inp2Δ
FM4-64
% of buds containing vacuoles
wild-type
inp2Δ
Bud size categories
I
II
III
IV
C
Wild-type
inp2Δ
SDH2-GFP
% of buds containing mitochondria
wild-type
inp2Δ
Bud size categories
D
Oriented
Misoriented
inp2Δ
kar9Δ
GFP-TUB1
Oriented spindles (%)
0
10
20
30
40
50
60
70
80
90
100
Wild-type
inp2Δ
kar9Δ
E
Wild-type
inp2Δ
Rhodamine-Phalloidin
F
Wild-type
inp2Δ

studied using the vacuole-specific fluorophore, FM4-64. The rates of vacuole inheritance in *inp2Δ* cells were essentially the same as those observed in wild-type cells (Figure 3-2B). The rates of inheritance of mitochondria, labeled by Sdh2p-GFP, were also unchanged in *inp2Δ* cells (Figure 3-2C). The orientation of mitotic spindles, labeled by GFP-Tub1p, was unimpaired in cells lacking Inp2p (Figure 3-2D).

We also analyzed the organization of the actin cytoskeleton in wild-type cells and cells lacking Inp2p. Actin was detected by staining with rhodamine-phalloidin. In wild-type and *inp2Δ* cells, actin showed normal polarized structures, with patches at sites of growth and distinct cables within mother cells (Figure 3-2E). Moreover, since *inp2Δ* cells displayed no growth defects on rich YPD medium (Figure 3-2F), Inp2p is not required for the polarized distribution of secretory vesicles. These findings collectively indicate that Inp2p is required specifically for peroxisome inheritance.

3.3 Inp2p Is a Peroxisomal Integral Membrane Protein Whose Levels Vary with the Cell Cycle

We used confocal fluorescence microscopy to determine the subcellular localization of a genomically encoded fluorescent chimera of Inp2p and GFP (Inp2p-GFP). Peroxisomes were visualized with a plasmid-encoded fluorescent chimera (mRFP-SKL) of monomeric red fluorescent protein (mRFP) and the peroxisome targeting signal 1, Ser-Lys-Leu. Inp2p-GFP colocalized with mRFP-SKL to punctate structures characteristic of peroxisomes (Figure 3-3A). Interestingly, the levels of Inp2p in individual peroxisomes varied dramatically, with peroxisomes in daughter cells having a

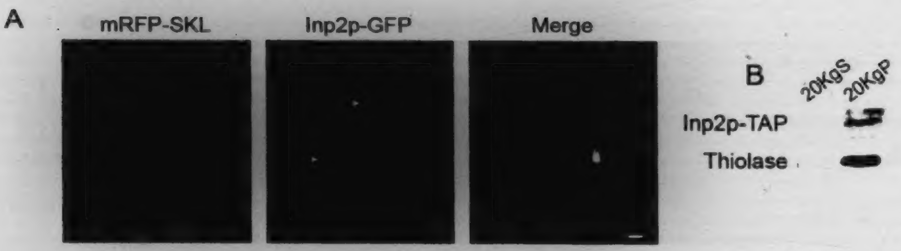

Figure 3-3. Inp2p is a peroxisomal integral membrane protein whose levels vary with the cell cycle. (A) Inp2p-GFP colocalizes with mRFP-SKL to punctate structures characteristic of peroxisomes by confocal microscopy. The panel at right presents the merged image of the left and middle panels. The weak Inp2p-GFP fluorescent signal in mother cells is indicated by arrowheads. Bar, 1 μm. (B) Inp2p-TAP localizes to the peroxisome-enriched 20KgP subcellular fraction. Immunoblot analysis of equivalent portions of the 20KgS and 20KgP subcellular fractions from cells expressing Inp2p-TAP was performed with antibodies to the peroxisomal matrix enzyme, thiolase. (C) Inp2p-TAP cofractionates with peroxisomes. Organelles in the 20KgP fraction were separated by isopycnic centrifugation on a discontinuous Nycodenz gradient. Fractions were collected from the bottom of the gradient, and equal portions of each fraction were analyzed by immunoblotting. Fractions enriched for peroxisomes and mitochondria were identified by immunodetection of thiolase and Sdh2p, respectively. (D) Peroxisomes in a postnuclear supernatant fraction were ruptured by treatment with Ti8 buffer and subjected to ultracentrifugation to obtain a supernatant fraction (Ti8S) enriched for matrix proteins and a pellet fraction (Ti8P) enriched for membrane proteins. The Ti8P fraction was treated further with alkali Na_2CO_3 and separated by ultracentrifugation into a supernatant fraction (CO_3S) enriched for peripheral membrane proteins and a pellet fraction (CO_3P) enriched for integral membrane proteins. Equivalent portions of each fraction were analyzed by immunoblotting. Immunodetection of thiolase, Pex3p, and Pex27p marked the fractionation profiles of a peroxisomal matrix, integral membrane, and peripheral membrane protein, respectively. (E) Cells expressing TAP-tagged Inp2p were grown for 16 hr in YPD medium and synchronized in G1 by addition of α factor. After removal of *factor, cells were incubated at 23°C in YPD medium. Samples were collected at the times indicated, and total cell lysates were analyzed by immunoblotting with antibodies directed against the TAP tag, the cyclin Clb2p, or Gsp1p (Ran). Clb2p levels monitor the progression of synchronized cells through the cell cycle. Gsp1p serves as a control for protein loading. (F) Cells synthesizing mRFP-SKL and Inp2p-GFP were treated as in (E). Fluorescent images of cells at different times after removal of α factor were captured with a spinning disk confocal microscope. The images represent projections of *z*-stacks of 14 optical sections spaced 0.4 μm apart. Arrowheads point to colocalization of Inp2p-GFP with peroxisomes at sites of growth. After removal of α factor (0 min), cells display mating projections (shmoos). At later time points, cells that formed buds at shmoo tips are shown. Bar, 1 μm.

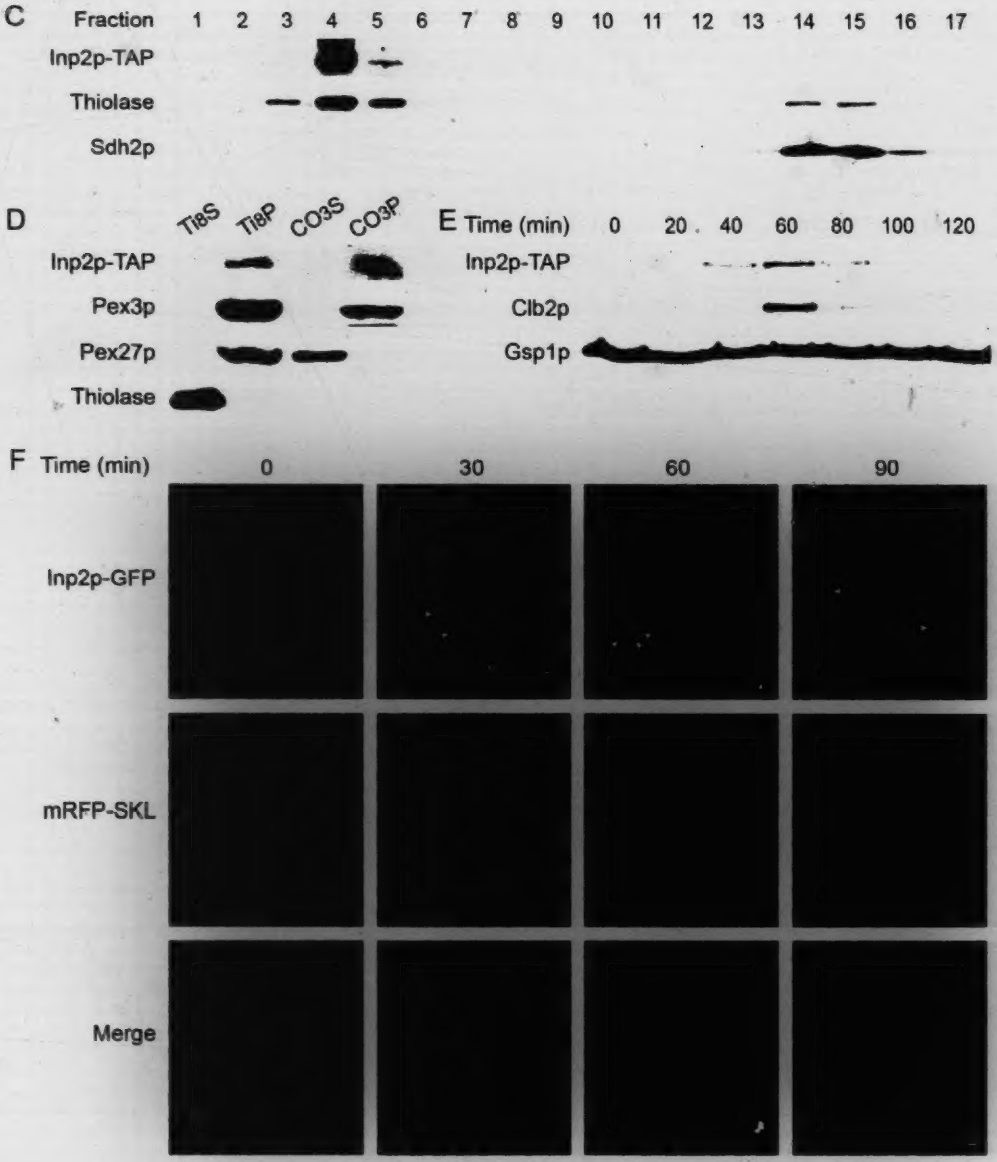
C
Fraction
1 2 3 4 5 6 7 8 9 10 11 12 13 14 15 16 17
Inp2p-TAP
Thiolase
Sdh2p
D
Ti8S
Ti8P
CO3S
CO3P
Inp2p-TAP
Pex3p
Pex27p
Thiolase
E
Time (min)
0 20 40 60 80 100 120
Inp2p-TAP
Clb2p
Gsp1p
F
Time (min)
0 30 60 90
Inp2p-GFP
mRFP-SKL
Merge

much stronger Inp2p-GFP signal than peroxisomes in mother cells. Therefore, Inp2p seems to be preferentially enriched in peroxisomes that are delivered to the bud.

Subcellular fractionation also showed Inp2p to be peroxisomal. Similar to the peroxisomal matrix protein thiolase, a genomically encoded TAP chimera of Inp2p, Inp2p-TAP, localized preferentially to the organellar pellet fraction (20KgP) enriched for peroxisomes and mitochondria (Figure 3-3B). Isopycnic density gradient centrifugation of the 20KgP fraction showed that Inp2p-TAP coenriched with thiolase but not with the mitochondrial protein Sdh2p (Figure 3-3C).

Organelle extraction showed Inp2p to be an integral membrane protein of peroxisomes. Similar to the integral PMP Pex3p and peripheral PMP Pex27p, Inp2p-TAP localized preferentially to the Ti8P fraction enriched for membrane proteins (Figure 3-3D). Upon extraction of the Ti8P fraction with alkali Na_2CO_3, Inp2p-TAP cofractionated with Pex3p to the CO_3P fraction enriched for integral membrane proteins.

The levels of mRNA coding for Inp2p have been reported to fluctuate with the cell cycle (Spellman et al., 1998). The observed enrichment of Inp2p in peroxisomes found in the bud raised the possibility that the levels of Inp2p itself might fluctuate with the cell cycle. To test this, we analyzed the levels of Inp2p-TAP in cells subjected to and released from α factor-induced G1 arrest. Inp2p-TAP levels did vary with the cell cycle, increasing 40 min after and decreasing 80 min after α factor release (Figure 3-3E).

We investigated further the dynamics of Inp2p during the cell cycle by analyzing the levels and localization of Inp2p-GFP in cells released from α-factor-induced G1 arrest (Figure 3-3F). The Inp2p-GFP signal is below the threshold of detection immediately after removal of α factor (Figure 3-3F, 0 min), and only cytoplasmic autofluorescence is seen. In small budded cells (Figure 3-3F, 30 min), Inp2p-GFP fluorescence becomes detectable and colocalizes with peroxisomes delivered to the buds, which, at this stage, are concentrated at bud tips. Inp2p-GFP fluorescence is significantly increased in large budded cells and is present on those peroxisomes that congregate at bud tips (Figure 3-3F, 60 min). Some peroxisomes in mother cells also contain detectable levels of Inp2p-GFP. The Inp2p-GFP signal is weak at cytokinesis and concentrated in those peroxisomes from the bud and mother cell that relocate to the mother-bud neck region (Figure 3-3F, 90 min).

3.4 Inp2p Interacts Directly with the Globular Tail of Myo2p

We performed yeast two-hybrid analysis to test the ability of Inp2p to interact with the carboxyl-terminal globular domain of Myo2p (amino acids 1113-1574). A strong interaction was detected between Inp2p and the Myo2p globular domain (Figure 3-4A). We also confirmed an already known interaction between Inp2p and Pex19p (Ito et al., 2001). Pex19p has been shown to be involved in the targeting/stabilization of proteins to/in the peroxisomal membrane (Schliebs and Kunau, 2004). No interaction was detected between Inp2p and Inp1p.

To define regions of Inp2p involved in binding the Myo2p tail, we generated Inp2p deletion mutants and tested them in the two-hybrid system (Figure 3-4B). The region between the two coiled-coil domains of Inp2p (amino acids 504-618) interacted weakly with the Myo2p tail. In contrast, the entire portion of Inp2p carboxyl-terminal to the predicted transmembrane domain (amino acids 240-705) bound Myo2p as strongly as

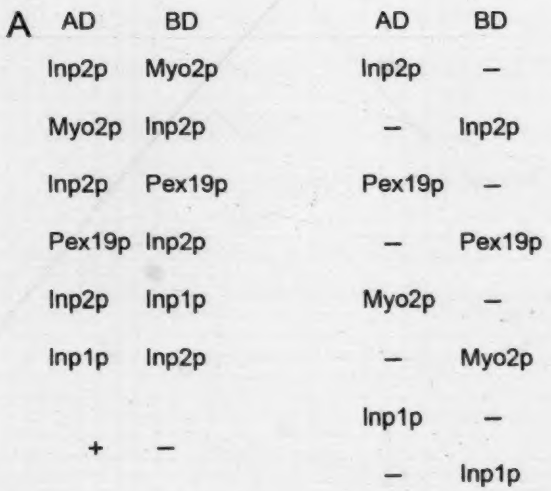

Figure 3-4. Inp2p interacts directly with the globular tail of Myo2p. (A) *S. cerevisiae SFY526* cells synthesizing both Gal4-AD and Gal4-BD protein fusions to Inp2p, the tail of Myo2p (amino acids 1113-1574), Pex19p, and Inp1p were tested for their ability to interact with each other by a β-galactosidase filter detection assay. A positive interaction is detected by the production of blue color. The color intensities of controls for the presence (+) or absence (−) of a protein interaction are presented at bottom, left. No construct is auto-activating, since no β-galactosidase activity is detected for cells synthesizing only one fusion protein (right). (B) Two hybrid analysis was performed as in (A) to test the ability of the indicated regions of Inp2p to interact with the globular tail of Myo2p. TM = predicted transmembrane region. CC = predicted coiled-coil region. No construct is auto-activating (AD). A strong interaction is denoted by two plus signs (++), while a weak interaction is denoted by one plus sign (+). The absence of an interaction is denoted by a minus sign (−). (C) Glutathione sepharose beads containing either GST fused to the cargo binding tail of Myo2p (GST-Myo2p) or GST alone were incubated with extracts of *E. coli* synthesizing MBP, MBP-Inp1p, MBP-Inp2p, or MBP-Vam2p. Bound proteins, as well as 10% of input proteins, were analyzed by immunoblotting with anti-MBP antibodies (upper panel). Arrowheads highlight full-length MBP or MBP fusion proteins. Total GST-Myo2p or GST protein levels were visualized by immunoblotting with anti-GST antibodies (lower panel).

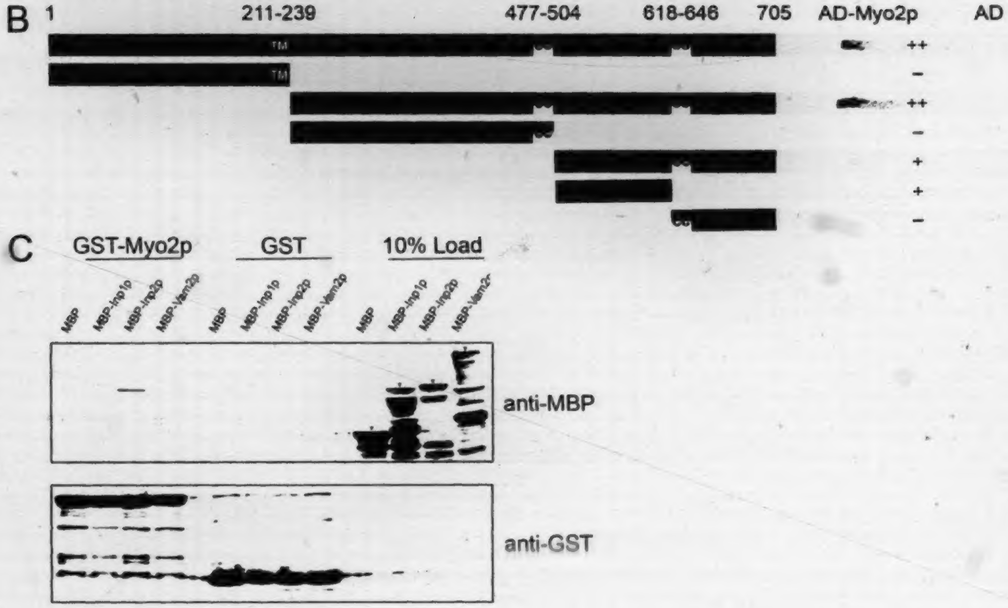
B
1
211-239
477-504
618-646
705
AD-Myo2p
AD
TM
TM
++
−
++
−
+
+
−
C
GST-Myo2p
GST
10% Load
MBP
MBP-Inp1p
MBP-Inp2p
MBP-Vam2p
MBP
MBP-Inp1p
MBP-Inp2p
MBP-Vam2p
MBP
MBP-Inp1p
MBP-Inp2p
MBP-Vam2
anti-MBP
anti-GST

full-length Inp2p, suggesting that other regions within this fragment are important for the interaction between Inp2p and the Myo2p tail.

If Inp2p is the bona fide peroxisomal receptor for Myo2p, we expect it to interact directly with Myo2p. Since yeast two-hybrid analysis does not differentiate between direct and bridged protein interactions, we performed a GST pull-down assay using recombinant Inp2p and Myo2p tail made in *E. coli* (Figure 3-4C). To improve the solubility of the maltose binding protein (MBP) fusion with Inp2p (MBP-Inp2p), only amino acids 241-705 of Inp2p were fused to MBP, thereby excluding the hydrophobic region of Inp2p (amino acids 211-239) but still preserving the region between amino acids 240 and 705 capable of interacting with Myo2p (Figure 3-4B). MBP-Inp2p was pulled down by GST-Myo2p but not GST alone (Figure 3-4C). Also, MBP alone or MBP fused to either Inp1p or Vam2p, proteins whose functions are unrelated to Myo2p, did not show an interaction with GST-Myo2p or GST alone. These results show that Inp2p binds directly that part of Myo2p specialized in binding to cargo.

3.5 Peroxisome Inheritance Is Abolished or Delayed in Cells Lacking Inp2p

4D video microscopy showed that peroxisome inheritance in cells lacking Inp2p was either abolished or significantly delayed (Figure 3-5; Movies S4-S7). During bud growth, peroxisomes appeared immobile at cortical locations within the mother cell and generally failed to be transferred to the bud (Figure 3-5A; Movie S4). In other cases, a subset of peroxisomes within the mother cell exhibited random movement but still failed to be efficiently localized to the bud (Figures 3-5B and 3-5C; Movies S5 and S6). Overall, peroxisomes in cells lacking Inp2p moved more slowly and in a less directed

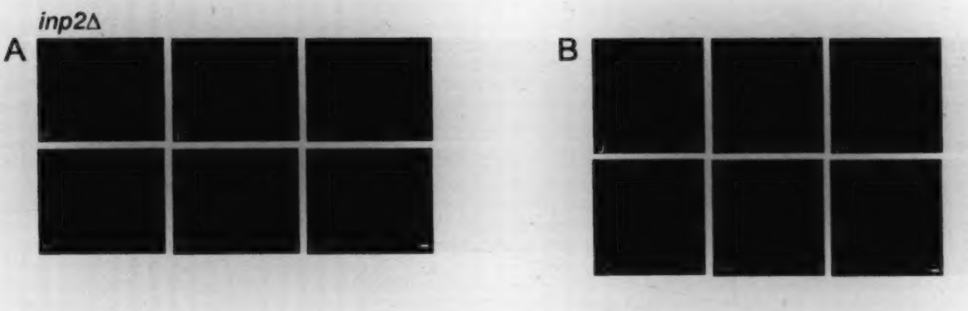

Figure 3-5. Peroxisome dynamics in *inp2Δ*, *bni1Δ*, and *myo2-66* cells. (A and B) Abolished peroxisome inheritance in *inp2Δ* cells. (A) In this movie, the bud does not receive peroxisomes before cytokinesis. The next bud shares the same fate as the first and does not receive peroxisomes (67' -102'). All peroxisomes in the mother cell retain fixed positions. (Movie S4). (B) At the beginning of this movie (0'), the bud at top is devoid of peroxisomes, while there is a single peroxisome in the bud at bottom. This peroxisome will return to the mother cell (9'). During bud growth, no peroxisome is inserted into either bud. Some peroxisomes in the mother cells perform chaotic movements (Movie S5). (C and D) Delayed peroxisome inheritance in *inp2Δ* cells. A few peroxisomes are delivered to the buds with significant delay. These peroxisomes do not show a preference for bud tips (Movies S6 and S7). Arrowheads point to bud tips devoid of peroxisomes. (E) Quantification of peroxisomes at bud tips. Wild-type and *inp2Δ* cells expressing *POT1-GFP* were incubated for 16 hr in SCIM. Only buds containing peroxisomes were analyzed. The percentages of buds containing peroxisomes at the bud tips were calculated. (F–H) Peroxisome movements within buds are dependent on the acto-myosin system. (F) Peroxisome dynamics in *bni1Δ* cells. Peroxisomes tend to accumulate at the bud neck, as seen in the cell and its associated bud at top, right (32'-92'). Peroxisomes can also sometimes enter the bud and associate along the bud cortex, as seen in the cell and its associated bud at bottom, right (19'-92'). Arrowheads indicate bud tips devoid of peroxisomes (Movie S8). (G) Peroxisome dynamics in *myo2-66* cells. Peroxisomes remain anchored at the cortex of the mother cell. After significant delay (48'), one peroxisome is transported to the bud. This peroxisome is initially correctly localized to the bud tip (arrowhead) but subsequently leaves the bud (53') (Movie S9). (H) Quantification of the presence of peroxisomes at bud tips was performed as described in the legend to panel (E).

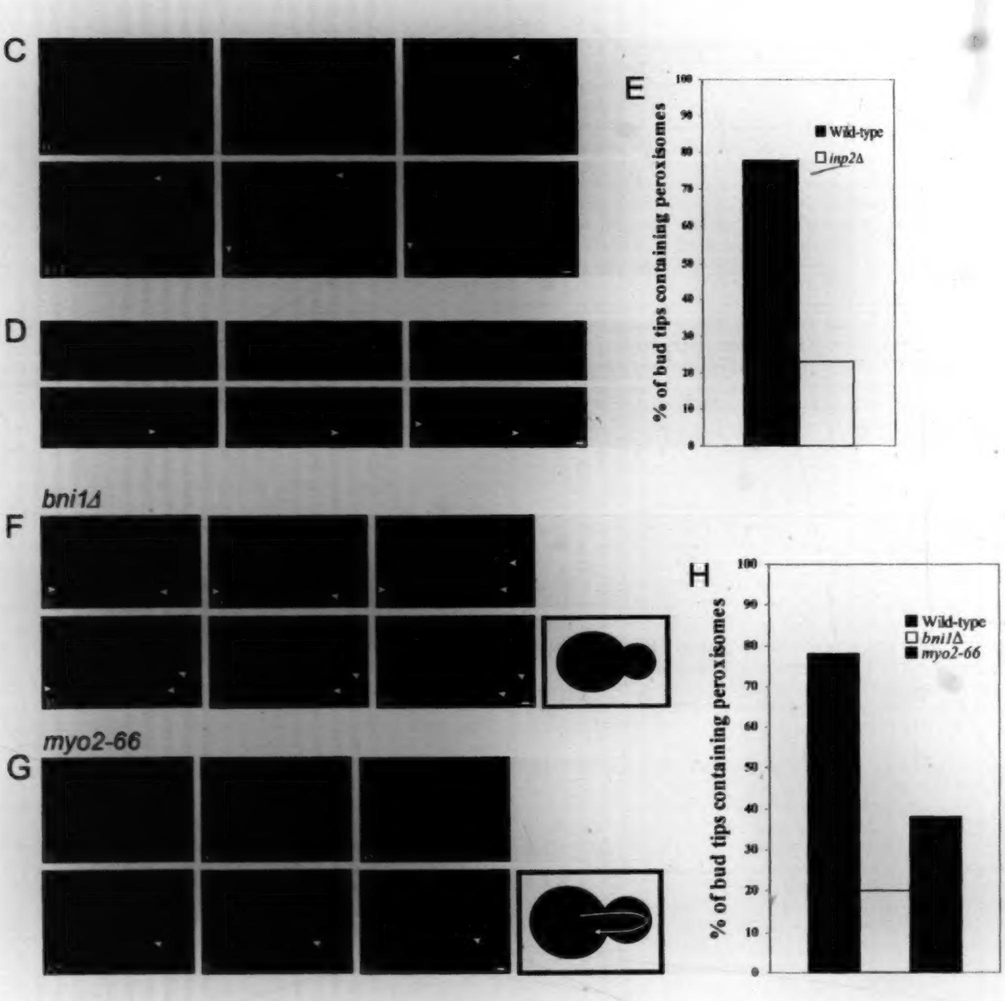
C
D
E
% of bud tips containing peroxisomes
100
90
80
70
60
50
40
30
20
10
0
■ Wild-type
☐ inp2Δ
bni1Δ
F
myo2-66
G
H
% of bud tips containing peroxisomes
100
90
80
70
60
50
40
30
20
10
0
■ Wild-type
☐ bni1Δ
■ myo2-66

manner compared to peroxisomes in wild-type cells (Figure 3-6). Consistent with our quantification of peroxisome inheritance (see Figure 3-2), we also observed peroxisomes being transferred to buds. Interestingly, in most cases, only one peroxisome would be delivered to the bud, and this event would take place with significant delay after emergence of the bud (Figures 3-5C and 3-5D; Movies S6 and S7). Notably, upon cytokinesis, we never observed relocation of peroxisomes from mother cells or buds to the mother-bud neck region (Figures 3-5A-3-5C; Movies S4-S6). Moreover, after peroxisomes reached the buds of *inp2Δ* cells, they did not show a preference for sites of polarized growth (Figures 3-5B-3-5D; Movies S5-S7). Quantification showed that only 23% of *inp2Δ* buds containing peroxisomes displayed peroxisomal fluorescence at bud tips compared to 78% of buds of wild-type cells (Figure 3-5E).

3.6 Peroxisome Movements within Buds of *inp2Δ* Cells Are Not Dependent on the Actomyosin System

The inability of peroxisomes to localize to bud tips in *inp2Δ* cells might result from their failure to associate with the actomyosin system. Many yeast organelles are translocated to the bud by Myo2p along actin cables that extend to the bud tip (Rossanese et al., 2001; Ishikawa et al., 2003). Moreover, the congregation of organelles at the bud tip is also dependent on Myo2p (Rossanese et al., 2001; Boldogh et al., 2004), which presumably tethers them to apical actin structures.

We investigated whether the actomyosin system plays a similar role in peroxisome movement within buds. We first analyzed the movements of peroxisomes in *bni1Δ* cells, which have significantly less actin cables inside buds (Pruyne et al., 2004b). 4D video

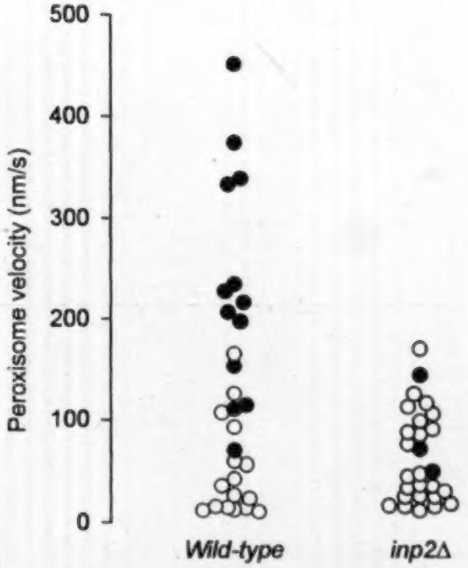

Figure 3-6. Peroxisome velocity in wild-type and *inp2Δ* cells. Scatter plot of velocities displayed by peroxisomes in wild-type cells (from Movie S1) and *inp2Δ* cells (from Movie S6). For each peroxisome, the maximal velocity achieved is shown. Filled circles indicate peroxisomes that displayed vectorial movement toward buds.

microscopy showed that peroxisomes in *bni1Δ* cells were recruited from the mother cell but tended to accumulate at the mother-bud neck (Figure 3-5F; Movie S8). On occasion, peroxisomes associated with the bud cortex but never clustered at bud tips. In fact, bud tips were frequently devoid of peroxisomes. Only 20% of *bni1Δ* cells displayed peroxisomes at bud tips as compared to 78% of wild-type cells (Figure 3-5H). Actin cables are therefore required for targeting peroxisomes to bud tips.

myo2-66 cells carry a conditional mutation in the Myo2p motor domain. These cells exhibit severe defects in the inheritance of vacuoles (Hill et al., 1996), late Golgi (Rossanese et al., 2001), and peroxisomes even at room temperature. Video microscopy of *myo2-66* cells at 24°C (Figure 3-5G; Movie S9) showed a significant delay in the insertion of peroxisomes into buds, consistent with the role for Myo2p in the movement of peroxisomes (Hoepfner et al., 2001). After peroxisomes reached the bud tips, they usually did not remain there and sometimes returned to mother cells. Quantification showed that only 38% of *myo2-66* buds containing peroxisomes displayed peroxisomes at bud tips (Figure 3-5H). Irrespective of mechanism, these data collectively suggest that the actomyosin system functions in both targeting peroxisomes to sites of growth and maintaining them at these sites. Therefore, the observed chaotic movements of peroxisomes within the buds of cells lacking Inp2p most likely reflect their lack of attachment to the actomyosin system, which is unaltered in this mutant.

3.7 Overexpression of *INP2* Leads to the Depletion of Peroxisomes from Mother Cells

We showed that peroxisomes in buds have more Inp2p than peroxisomes in mother cells (Figure 3-3A). This asymmetric distribution of Inp2p could reflect a relationship between the quantity of Inp2p on an individual peroxisome and its ability to be transferred to the bud by Myo2p. Such a scenario leads to the prediction that overproducing Inp2p should enable an increased number of peroxisomes to be transported to the bud. We determined whether this was the case by overexpressing *INP2* from the multicopy plasmid YEp13 in wild-type cells synthesizing Pot1p-GFP.

As predicted, budded cells of the strain overproducing Inp2p had most of their peroxisomes localized to the buds (Figure 3-7A). Moreover, a significant percentage of mother cells were devoid of peroxisomes. This asymmetric distribution of peroxisomes, with the entire peroxisomal population present in the bud, was never observed in wild-type cells containing the parental plasmid YEp13 alone (Figure 3-7A). Quantification showed that cells overproducing Inp2p exhibited an increased percentage of mother cells without peroxisomes with increasing bud size, with 9% of mother cells with the smallest buds (Category I) and 32% of mother cells with the largest bud (Category IV) lacking peroxisomes (Figure 3-7A).

4D video microscopy showed that in a cell overproducing Inp2p, the entire population of peroxisomes was found concentrated at the site of polarized growth. As soon as the bud was visible, most of the peroxisomes accumulated at the site of bud emergence and were then inserted into the bud (Figure 3-7B; Movie S10). The few cortically anchored peroxisomes in the mother cell were also recruited and transferred to the bud, thereby depleting the mother cell of peroxisomes. Once in the bud, all peroxisomes clustered at the bud tip. In contrast to wild-type cells, all peroxisomes relocated en masse from the bud tip to the bud neck region upon cytokinesis.

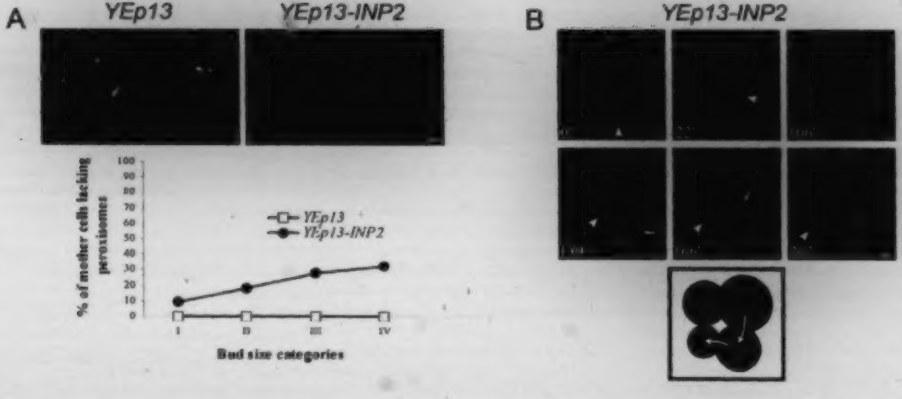

Figure 3-7. Overproduction of Inp2p alters the partitioning of peroxisomes without affecting the segregation of other organelles. (A) Wild-type and *INP2*-overexpressing cells synthesizing Pot1p-GFP were incubated in SCIM and examined by confocal microscopy. Scoring for the presence or absence of peroxisomes in buds of different sizes and in mother cells was performed on at least 25 budded cells from each category of bud size. Bar, 1 µm. (B) Peroxisome dynamics in cells overproducing Inp2p. Arrowheads point to peroxisomes clustered at sites of polarized growth. Imaging was initiated after all peroxisomes had been delivered to the bud. The peroxisomes in the bud form a cluster at the bud tip (0'). At cytokinesis (22'), all peroxisomes move *en masse* to the mother-bud neck region (arrowhead). Later, peroxisomes detach from one another and are found scattered in the former bud (106'). As soon as the cell containing peroxisomes forms a new bud (139'), peroxisomes relocate to the presumptive bud site (arrowhead) and are then inserted into the bud (166'), where they localize to the bud tip (arrowhead). One small peroxisome (arrow) remains anchored at the mother cell cortex for about 20 min. This peroxisome will be recruited from its fixed position (166') and move into the bud (Movie S10). (C) Overproduction of Inp2p leads to enhanced recruitment of peroxisomes to sites of polarized growth. Wild-type cells overexpressing *INP2* (*YEp13-INP2*) or containing the parental plasmid (*YEp13*) and synthesizing Pot1p-GFP were incubated in SCIM. Cells were processed for immunofluorescence microscopy with antibody to Myo2p. Primary anti-Myo2p antibody was detected with rhodamine-conjugated secondary antibody. Panels at right show the merge of signals from GFP and rhodamine. Bar, 1 µm. (D) Vacuole segregation is unaffected by overproduction of Inp2p. Wild-type and *INP2*-overexpressing cells synthesizing Pot1p-GFP were incubated in SCIM. Vacuoles were labeled with FM4-64, and cells were analyzed by confocal microscopy. Bar, 1 µm. (E) Mitochondria segregation is unaffected by overproduction of Inp2p. Wild-type and *INP2*-overexpressing cells synthesizing Pot1p-mRFP and Sdh2p-GFP were incubated in SCIM and analyzed by confocal microscopy. Quantification was performed on at least 25 budded cells from each category of bud size. Bar, 1 µm. (F) Orientation of the mitotic spindle is unaffected by overproduction of Inp2p. Pre-anaphase wild-type, *INP2* overexpressing, and *kar9Δ* cells synthesizing GFP-Tub1p were analyzed for orientation of the mitotic spindle. Quantification was performed on at least 100 pre-anaphase budded cells of each strain. Bar, 1 µm.

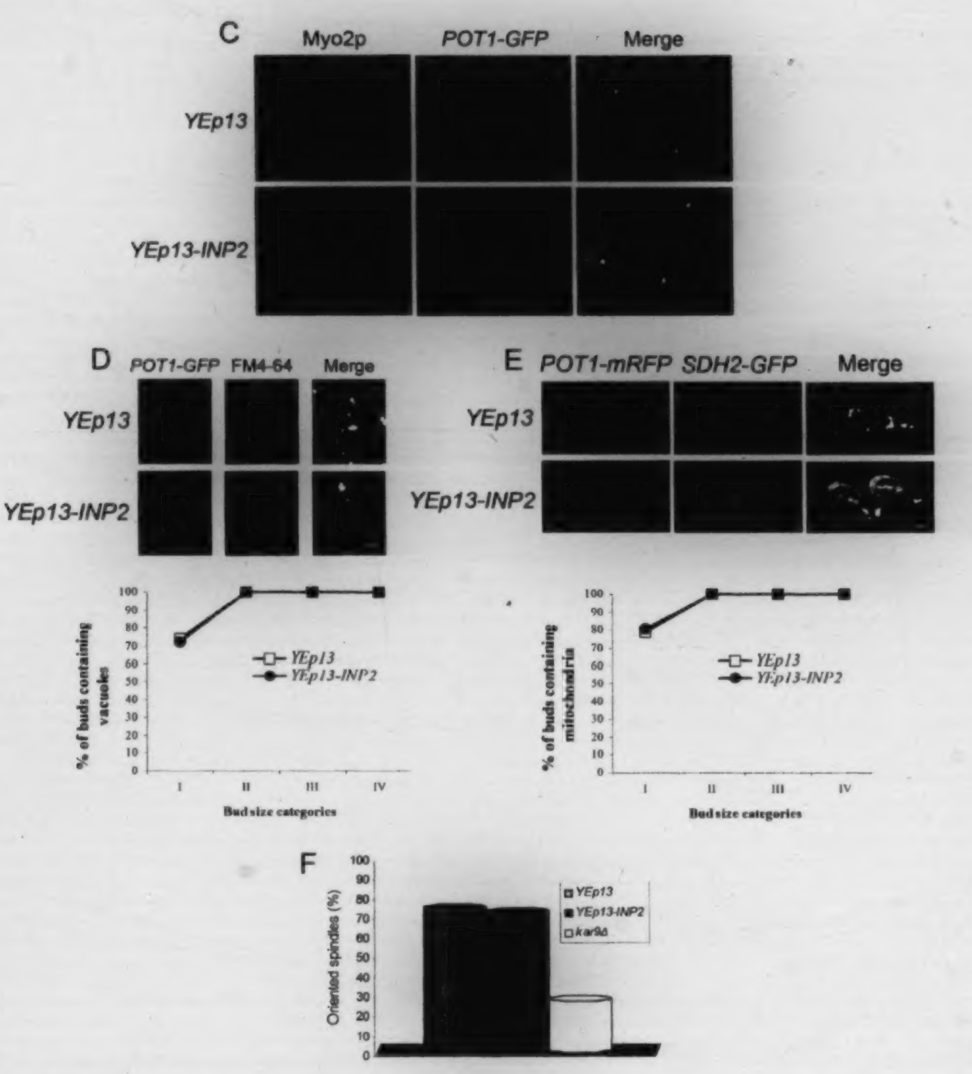
C
Myo2p
POT1-GFP
Merge
YEp13
YEp13-INP2
D
POT1-GFP
FM4-64
Merge
YEp13
YEp13-INP2
E
POT1-mRFP
SDH2-GFP
Merge
YEp13
YEp13-INP2
% of buds containing vacuoles
YEp13
YEp13-INP2
Bud size categories
I
II
III
IV
0
10
20
30
40
50
60
70
80
90
100
% of buds containing mitochondria
YEp13
YEp13-INP2
Bud size categories
I
II
III
IV
F
Oriented spindles (%)
YEp13
YEp13-INP2
kar9Δ
0
10
20
30
40
50
60
70
80
90
100

Colocalization studies between peroxisomes and Myo2p showed that in wild-type cells, only a small number of peroxisomes colocalized with Myo2p at sites of polarized growth, while the majority of peroxisomes were found within the mother cell (Figure 3-7C, upper panels). In contrast, in cells overproducing Inp2p, the entire population of peroxisomes associated with Myo2p at sites of polarized growth, sometimes as soon as bud formation was apparent (Figure 3-7C, lower panels).

The segregation of vacuoles and mitochondria was unaffected in cells overproducing Inp2p (Figures 10D and 10E). Mitotic spindles were also oriented properly in cells overproducing Inp2p (Figure 3-7F).

3.8 The Interplay between Inp2p and Inp1p

The transfer of all peroxisomes from mother cell to bud has also been observed in cells lacking Inp1p, a protein that anchors peroxisomes to the mother cell cortex (Fagarasanu et al., 2005). Overproducing Inp2p in cells lacking Inp1p led to the more rapid appearance of peroxisomes in buds than in *inp1Δ* cells or wild-type cells overproducing Inp2p (Figure 3-8A). The opposite was observed in *inp2Δ* cells overexpressing *INP1*, as the percentage of buds lacking peroxisomes was greater at all bud size categories in these cells than in either *inp2Δ* cells or wild-type cells overexpressing *INP1* (Figure 3-8B). Therefore, the effect of overproducing either of these two apparently counteracting proteins is enhanced by the absence of the other protein. To gain further insight into the interplay between Inp1p and Inp2p, we constructed cells deleted for both *INP1* and *INP2*. We observed a large number of buds of *inp1Δ/inp2Δ* cells that lacked peroxisomes. However, the percentages of budded cells lacking

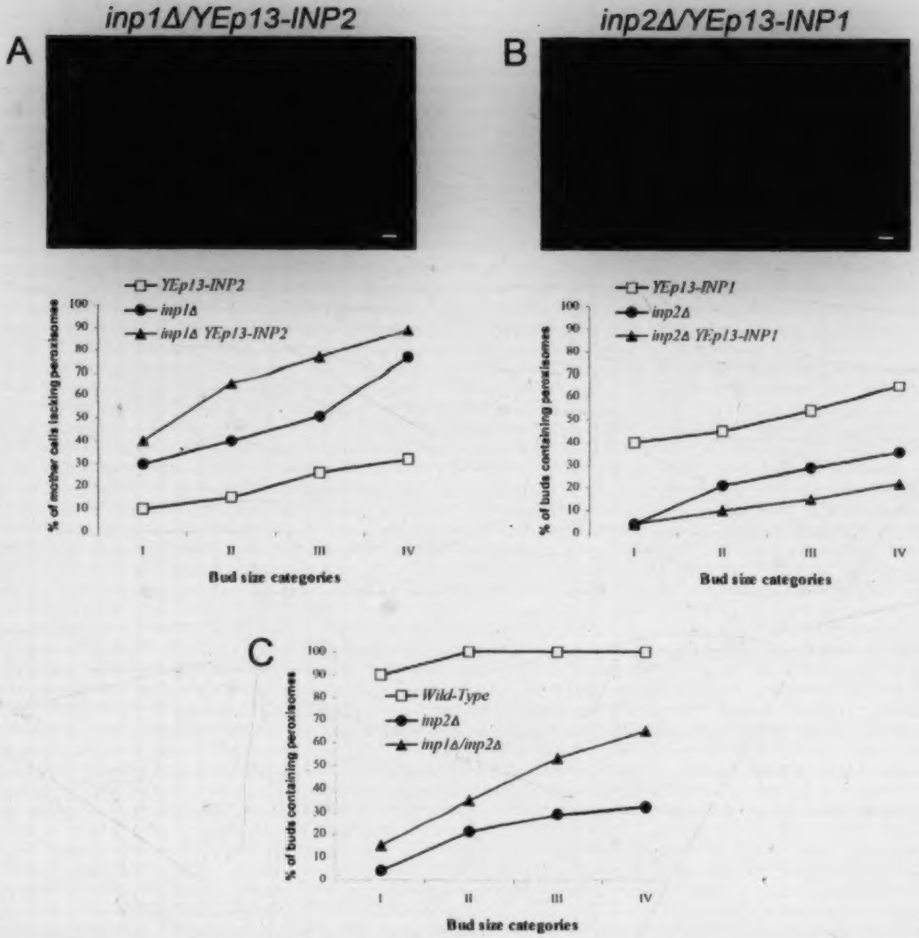

Figure 3-8. Interplay between Inp1p and Inp2p. (A–C) The indicated strains were incubated and subjected to quantification of peroxisome inheritance as described in the legend to Figure 2A. Bar, 1 µm. (D) A model for Inp2p function in peroxisome inheritance. At a point in the cell cycle, Inp2p is synthesized and loaded onto peroxisomes. The increased levels of Inp2p on some peroxisomes result in the formation of Inp2p-Myo2p transport complexes that can dislodge these peroxisomes from their fixed cortical positions. The Inp2p-Myo2p complexes move the attached peroxisomes along polarized actin cables. Once in the bud, the Inp2p-Myo2p complexes are long-lived and responsible for localizing peroxisomes to sites of active growth, where Myo2p is concentrated. The regulated turnover of Inp2p later in the cell cycle results in detachment of peroxisomes from the Myo2p motor. As a result, only a subset of peroxisomes follows Myo2p to the mother-bud neck at cytokinesis. To prepare the bud for the ensuing cell cycle, peroxisomes become anchored at the bud cortex, a process dependent on Inp1p (not depicted).

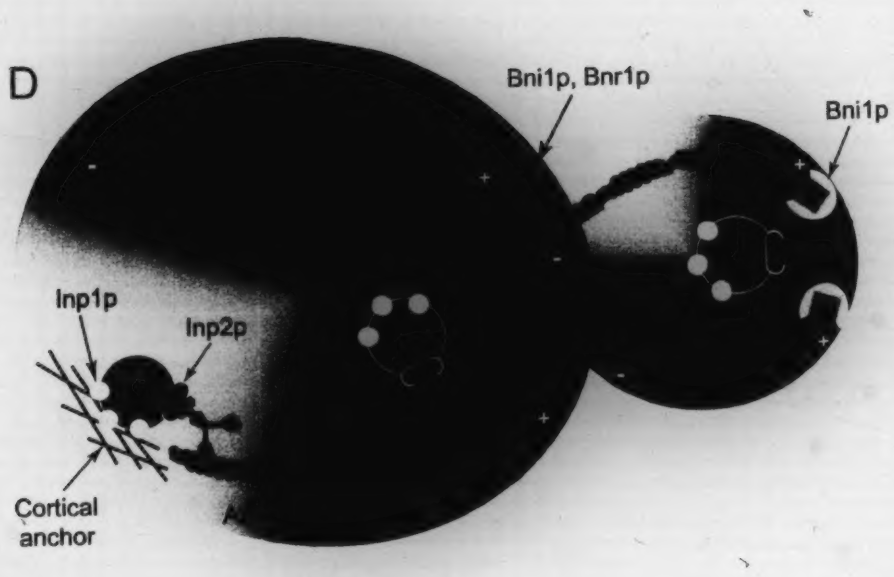
D
Bni1p, Bnr1p
Bni1p
Inp1p
Inp2p
Cortical anchor

peroxisomes within buds were lower than those observed for cells lacking Inp2p alone but still greater than those observed for wild-type cells (Figure 3-8C). Notably, no *inp1Δ/inp2Δ* budded cell was observed that had its entire complement of peroxisomes within its bud, a feature characteristic of *inp1Δ* cells.

3.9 Discussion

3.9.1 Inp2p is the Peroxisome-specific Receptor for Myo2p

Given the many different types of membrane-bounded organelles in a typical eukaryotic cell, ensuring their correct delivery to a specific destination at a specific time requires a tightly regulated transport system. The intracellular transport of organelles is supported by either microtubule or actin networks and powered by motor proteins that associate with these networks. How motor proteins recognize their target organelles and what is the molecular basis for the temporal and spatial regulation of this recognition represent important questions in cell biology.

In *S. cerevisiae*, the movement of each organelle during the cell cycle has specific temporal and spatial characteristics, despite the fact that most of these organelles are carried by the same motor protein, the class V myosin Myo2p. This promiscuity in organelle movement by Myo2p has been explained by the existence of organelle-specific receptors for Myo2p that are regulated according to cell cycle cues. Vac17p was the first such receptor identified, functioning as the vacuole-specific receptor for Myo2p (Ishikawa et al., 2003). We identified Inp2p, a novel protein that possesses all the attributes expected for a peroxisome-specific receptor for Myo2p: (*a*) Inp2p is an integral PMP that interacts directly with the globular tail of Myo2p. (*b*) Peroxisomes in cells lacking Inp2p display decreased velocities and fail to be delivered to buds. As a result, mother cells retain the entire peroxisome population. (*c*) As is the case for Vac17p and vacuole inheritance, Inp2p levels oscillate with the cell cycle in a pattern that correlates with peroxisome dynamics. (*d*) The overproduction of Inp2p drives the entire complement of peroxisomes out of mother cells into buds, an event never observed in wild-type cells. (*e*) Inp2p is unequally distributed on different peroxisomes; it is preferentially enriched in those peroxisomes delivered to the bud. (*f*) Inp2p specifically affects peroxisome motility since the segregation of other organelles is unimpaired in cells lacking or overproducing Inp2p. All these findings strongly support Inp2p as the link between peroxisomes and Myo2p. The discovery of Inp2p as the peroxisome-specific receptor for Myo2p supports the proposition that different organelles have different specific Myo2p receptors.

Inp2p appears to be devoted solely to linking Myo2p to peroxisomes. Inp2p is not involved in the metabolic functions of peroxisomes, since *inp2Δ* cells are able to grow in oleic acid-containing medium with essentially the same kinetics as wild-type cells (Smith et al., 2006). Peroxisomes in cells lacking Inp2p are also able to efficiently import proteins targeted by either PTS1 or PTS2. Probably, the fluctuating levels of Inp2p on peroxisomes, which ensure their delivery to correct intracellular locations at the right time, makes Inp2p unsuitable for performing any metabolic or biogenic functions that have to be coordinated with different environmental conditions rather than the timing of the cell cycle and peroxisome positioning. Similarly, Vac17p does not seem to perform any other function apart from being the adaptor molecule for Myo2p on the vacuolar membrane (Weisman, 2006).

3.9.2 Inp2p Dynamics during the Cell Cycle

The levels of both Inp2p and its corresponding mRNA fluctuate during the cell cycle in a pattern that correlates with the dynamics of peroxisomes observed in wild-type cells. Inp2p becomes detectable during early budding, when peroxisome inheritance begins, and its levels peak in medium-sized budded cells, when most insertions of peroxisomes into daughter cells occur. Given that Inp2p functions as the peroxisome-specific receptor for Myo2p, these observations suggest that the regulated synthesis and turnover of Inp2p coordinate peroxisome motility with cell cycle events.

There are several peculiarities in the dynamics of Inp2p. Inp2p-GFP levels in individual peroxisomes vary significantly, being greatest in those peroxisomes delivered to the bud. This results in a highly polarized Inp2p-GFP signal along the cell division axis. Since Inp2p is crucial for the delivery of peroxisomes to daughter cells, as judged by the phenotype of cells lacking Inp2p, it is tempting to propose that Myo2p selectively carries those peroxisomes having increased amounts of Inp2p to the growing bud. Intriguingly, analysis of Inp2p-GFP dynamics during the cell cycle showed that Inp2p-GFP is first detected in peroxisomes localized to the bud. One explanation for this observation is that initially the amount of Inp2p-GFP in peroxisomes is below the threshold of detection, but upon the clustering of several Inp2p-containing peroxisomes at the bud tip, the Inp2p-GFP fluorescent signal becomes discernable. However, later in the cell cycle, individual peroxisomes in daughter cells can be observed that have a much stronger Inp2p-GFP signal than any peroxisome in mother cells. This suggests that those peroxisomes that were initially capable of recruiting Inp2p to their membranes continue to recruit more Inp2p, further contributing to the polarization of the Inp2p-GFP signal along the division axis. Therefore, the Inp2p gradient along the division axis is established by the competency of a subset of peroxisomes to recruit Inp2p continuously, coupled with the selectivity of Myo2p in carrying and then retaining only these Inp2p-containing peroxisomes in the bud.

Why is it beneficial for peroxisomes to accumulate more Inp2p once they have been delivered to the bud? The continuous accumulation of Inp2p on transferred peroxisomes increases their probability of remaining attached to the Myo2p motor. This could contribute to the retention of peroxisomes in daughter cells. Indeed, video microscopy of *myo2-66* mutant cells, which carry a single amino acid substitution in the Myo2p motor domain (Johnston et al., 1991; Govindan et al., 1995), showed that Myo2p motor activity is important not only for the vectorial transport of peroxisomes from mother cell to bud but also for their retention at bud tips. Moreover, peroxisomes in *inp2Δ* budded cells that are localized to buds do not exhibit any preference for sites of polarized growth at which Myo2p accumulates. Myo2p is known to play a similar role in the retention of other organelles at the bud tip (Hill et al., 1996; Rossanese et al., 2001; Boldogh et al., 2004). Class V myosins in general participate in the retention of organelles at different intracellular locations (Wu et al., 1998; Rogers and Gelfand, 1998; Mermall et al., 1998). It has been proposed that the processivity of class V myosins, and hence their prolonged contact with actin tracks, might underlie their role as organelle tethers (Mehta et al., 1999).

Inp2p is degraded later in the cell cycle, resulting in the detachment of Myo2p from transferred peroxisomes. As a result, at cytokinesis, only a few peroxisomes accompany

Myo2p to the bud neck region (Fagarasanu et al., 2006a, 2006b). These peroxisomes are the only ones that still contain detectable levels of Inp2p at this stage of the cell cycle. Importantly, the remaining peroxisomes within the bud have already assumed static positions at the bud periphery. This observation points to the existence of a tight coordination between the factors promoting the movement of peroxisomes and those regulating peroxisome retention.

If we assume that the Inp2p degradation machinery is present in both the mother cell and bud, its activation not only would cause the release of bud-residing peroxisomes from the grip of Myo2p but also would prevent new recruitments of additional peroxisomes from the mother cell. This would explain why the degradation of Inp2p is triggered somewhat later in the cell cycle, when sufficient peroxisomes have been transmitted to the bud (Fagarasanu et al., 2006a, 2006b). It would be important to know whether the regulated degradation of Inp2p, which terminates peroxisome inheritance, is inherently initiated at a specific point of the cell cycle or if it is triggered by cellular surveillance mechanisms that monitor peroxisome partitioning (see next chapter).

3.9.3 Coordination between Peroxisome Retention and Transport: Interplay between Inp1p and Inp2p

Inp1p and Inp2p are two key regulators of peroxisome inheritance with apparently antagonistic functions. Interestingly, the overproduction of one of the two proteins negates the function of the other (Fagarasanu et al., 2006b, 2007). The Inp1p function of retaining peroxisomes can be overcome by the overproduction of Inp2p, a condition that drives all peroxisomes into the bud (Fagarasanu et al., 2006a). Conversely, Inp2p's function in promoting the Myo2p-driven transport of peroxisomes to daughter cells is abolished by the overexpression of *INP1*, which causes all peroxisomes to remain immobile in the mother cell (Fagarasanu et al. 2005). Furthermore, the effects caused by the overexpression of either *INP1* or *INP2* are enhanced if the other gene is absent (Fagarasanu et al., 2006a, 2006b). Inp1p and Inp2p are unlikely to influence directly each other's activities because no interaction between these two proteins has been detected (Fagarasanu et al., 2006a). We propose that a tug-of-war for peroxisomes between the Inp1p-interacting anchoring machinery and the Inp2p-Myo2p transport complex may determine which peroxisomes are recruited for transportation to the bud (Fagarasanu et al., 2006a, 2006b). In this scenario, Inp2p is synthesized at a specific time in the cell cycle and is then loaded onto peroxisomes. The increased levels of Inp2p on a subset of peroxisomes result in the formation of Inp2p-Myo2p transport complexes that can dislodge these peroxisomes from their fixed cortical positions (Figure 3-8D). Cells have to balance these molecular "contests of strength" to allow for approximately only half of the peroxisomes to dissociate from the mother cell cortex to be transported to the bud, ultimately resulting in a harmonious distribution of their peroxisomes at cytokinesis.

A lack of Inp1p results in the complete transfer of peroxisomes to the daughter cell (Fagarasanu et al., 2005, 2006b). This suggests that all peroxisomes contain Inp2p in sufficient amounts to promote their Myo2p-driven movement in the absence of an opposing force. However, in wild-type cells, for approximately half the peroxisomes, the regulation of Inp1p function counteracts the tendency of peroxisomes to become mobile (Fagarasanu et al., 2006b).

Coordination between the functions of Inp1p and Inp2p is likely to occur in the bud as well as in the mother cell. As soon as peroxisomes are delivered to the bud, they congregate at the bud tip through the interaction of Inp2p and Myo2p. Later in the cell cycle, peroxisomes gradually start to relocate to the bud cell cortex, where they gain fixed positions. Only a few peroxisomes follow Myo2p back to the bud neck at cytokinesis. Most peroxisomes are therefore transferred from the grip of the Myo2p motor to the Inp1p-interacting cortical anchors. This process mirrors the one that originally dislodged peroxisomes from the mother cell cortex. We can speculate that a tug-of-war between Inp1p and Inp2p, similar to the one predicted for the mother cell, determines whether a peroxisome becomes cortically anchored or remains attached to Myo2p within the bud (Fagarasanu et al., 2006b). The regulated turnover of Inp2p, which results in the disassembly of Inp2p-Myo2p transport complexes, probably swings the balance of such molecular contests of strength toward the establishment of Inp1p-cortex connections. Two observations are consistent with this model. First, only those peroxisomes that are carried by Myo2p back to the bud neck at cytokinesis contain detectable amounts of Inp2p. Second, bud-localized peroxisomes in both cells overproducing Inp2p and cells lacking Inp1p often move en masse to the mother bud neck region at cytokinesis, eluding the anchoring machinery altogether (Fagarasanu et al., 2005, 2006a) (Figure 3-8D).

In *inp1Δ/inp2Δ* cells, peroxisomes are left without any means of anchoring to the cell cortex and also without any possibility of attaching to the translocation machinery, which probably leads to a random distribution of peroxisomes. The presence, under these conditions, of buds devoid of peroxisomes most likely reflects the inefficiency of stochastic segregation of peroxisomes in a cell that divides by budding.

CHAPTER FOUR: IDENTIFICATION OF THE SURFACE AREA OF THE PEROXISOME-BINDING REGION OF MYO2P

4.1 Overview

Peroxisome partitioning and cell cycle progression are linked in wild-type cells, with about half of the peroxisome population being delivered to the bud at approximately the same stage of the cell cycle. Thus, the observed regulated degradation of Inp2p could be inherently initiated at a specific point of the cell cycle. An alternative possibility is that sensors exist that respond to the proportion of the peroxisomal population that has been delivered to the bud (or left the mother cell), irrespective of the cell cycle. When about half of the peroxisomes have reached the bud, signals would be sent to trigger the degradation of Inp2p. These two possibilities can be distinguished by following the dynamics of Inp2p when peroxisome inheritance is artificially uncoupled from the cell cycle. This can be achieved by isolating mutants of Myo2p that are specifically defective in transporting peroxisomes. Cells harboring such a Myo2p mutant as the sole copy of Myo2p should produce buds devoid of peroxisomes but which are able to progress normally through the cell cycle, thereby resulting in the dissociation of the two processes of peroxisome segregation and cell-cycle progression. Two alternative scenarios can be envisaged if, under these conditions, Inp2p is observed to aberrantly accumulate instead of cycling: 1) cellular surveillance mechanisms that monitor peroxisome partitioning underlie the downregulation of Inp2p observed in wild-type cells, so Inp2p degradation is not linked to cell cycle progression and 2) the machinery responsible for Inp2p turnover is confined to the daughter cell. As a consequence, Inp2p is not exposed to the degradation machinery when peroxisome transport is defective. Conversely, if Inp2p continues to cycle normally in cells harboring peroxisome-specific Myo2p mutants, then degradation of Inp2p is cell-cycle-dependent and independent of completion of peroxisome segregation. Moreover, in this case, the Inp2p degradation machinery would not be confined to buds, as is the case for Vac17p (see Introduction).

A prerequisite to studies investigating the regulation of Inp2p degradation is a mapping of the peroxisome-binding region of the Myo2p tail. Mild proteolysis experiments (Pashkova et al., 2005) and X-ray crystallographic studies (Pashkova et al., 2006) showed the globular tail of Myo2p to be composed of subdomains I (residues 1131-1309 and 1528-1574) and II (residues 1310-1527) (Figure 4-1). The vacuole-binding site on Myo2p occupies a small region in subdomain I, while the residues required for Myo2p attachment to secretory vesicles reside within subdomain II (Catlett and Weisman, 1998; Schott et al, 1999; Catlett et al, 2000; Pashkova et al, 2005, 2006) (Figure 4-1). The spatial segregation of various organelle-binding regions was believed to be an important feature of Myo2p, allowing it to function as a scaffold that exposes all its cargo-binding sites simultaneously, thereby avoiding competition for the transport of different cargoes (Weisman, 2006). However, this view has recently changed, since two surface residues that participate in vacuole-binding were found also to function in the association of Myo2p with mitochondria (Altmann et al., 2008).

Importantly, Pashkova et al. (2006) analyzed the surface residues of the Myo2p tail to identify areas of high sequence conservation among class V myosins from phylogenetically distant organisms, including *S. cerevisiae*, *Caenorhabditis elegans*, *Drosophila melanogaster*, *Ustilago maydis*, *Strongylocentrotus purpuratus* and *Mus musculus.* They showed that Myo2p contains several patches of conserved surface residues in both subdomains I and II. Conserved surface residues generally indicate sites of protein-protein interaction, and therefore the conserved patches on the surface of the

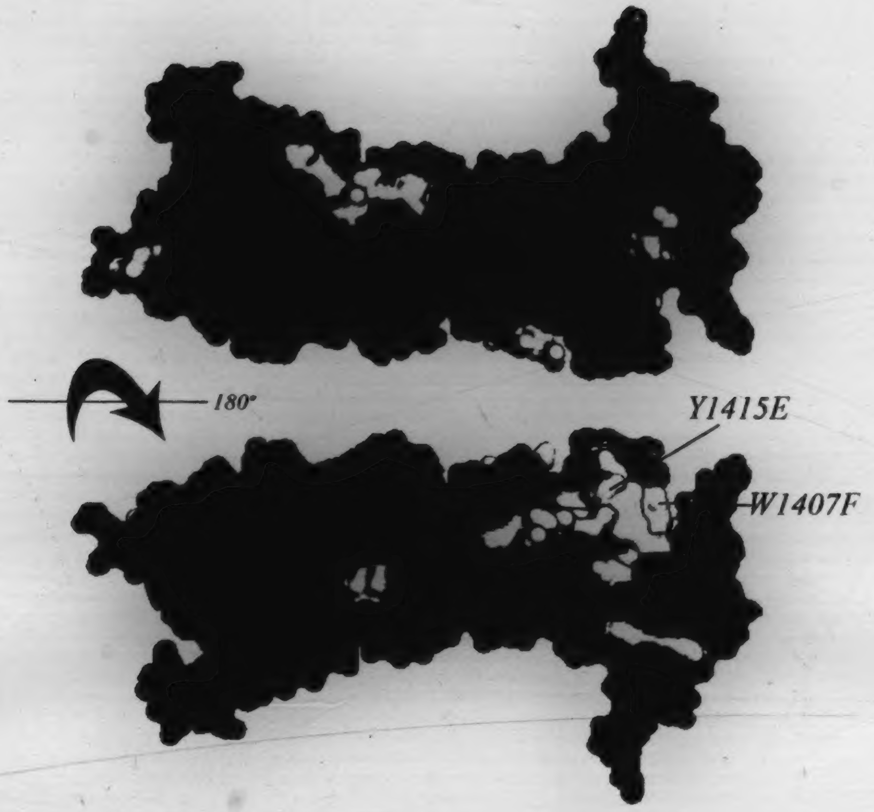

Figure 4-1. Surface representation of the Myo2p globular tail indicating the initial point mutants tested for defects in peroxisome inheritance. Subdomains I and II are shown in blue and red, respectively. The mutated conserved surface residues initially screened for defects in peroxisome inheritance are shown in white. The black outline demarcates the vacuole binding site. The teal outline demarcates the secretory vesicle binding site.

Myo2p cargo-binding domain are likely to be regions that attach to specific cargoes. Indeed, the exposed residues that make up vacuole and secretory vesicle binding sites were found to be highly conserved (Pashkova et al., 2006).

4.2 Isolation of Mutants of the Myo2p Globular Tail Defective in Peroxisome Distribution

Following the same reasoning, we set out to identify the peroxisome-binding domain on the Myo2p surface by initially screening cells harboring single point mutations in the conserved exposed regions of the Myo2p tail for defects in peroxisome inheritance (Figure 4-1). Since the attachment sites of organelles could potentially overlap in space (see Section 4-1), we also included in our analysis point mutations in the vacuole and secretory vesicle binding regions. To screen the Myo2p point mutations, we systematically made haploid strains harboring the various *myo2* alleles previously made by Pashkova et al. (Table 2-9) as sole copies of the *MYO2* gene (see Materials and Methods). Cells of individual mutant strains expressing *POT1-GFP* to label peroxisomes were scored using a stringent all-or-none criterion for the presence of peroxisomes within buds (see Materials and Methods). Two point mutations, Y1415E and W1407F, in subdomain II of the globular tail were observed to induce severe defects in peroxisome distribution (Figures 4-1 and 4-2). Quantification showed that when the bud volume reached 0%-24% of the mother cell volume (small budded cells), only 21% and 38% of the buds of the *myo2-Y1415E* and *myo2-W1407F* mutants, respectively, contained at least one peroxisome. In contrast, 85% of small buds of cells harboring the wild-type *MYO2* gene had peroxisomes (Figure 4-2B). When the bud volume reached 24%-48% of the

A

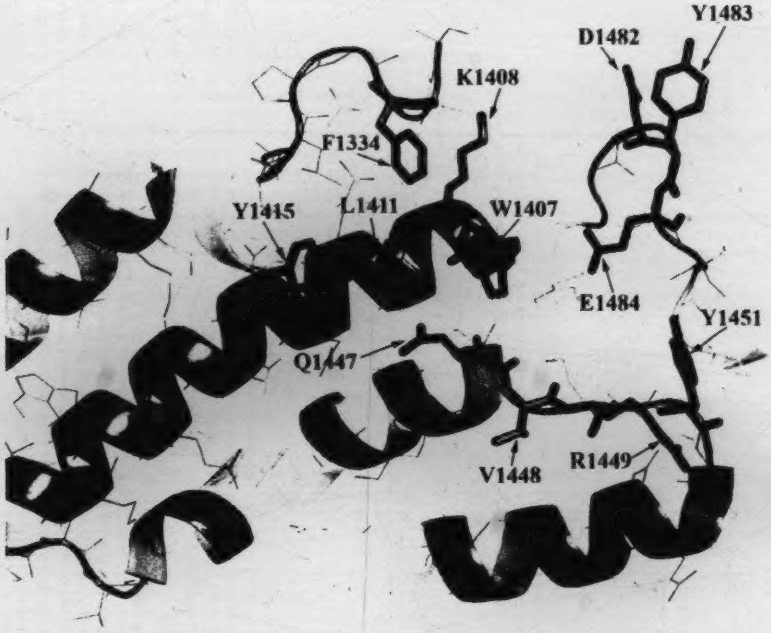

Figure 4-2. Screening of point mutations in subdomain II of Myo2p for defects in peroxisome inheritace. (A) Ribbon representation of a portion of subdomain II of Myo2p highlighting the amino acids that were mutated. (B) Quantification of peroxisome inheritance in cells expressing the indicated *myo2* point mutants. Cells harboring either wild-type *MYO2* or *myo2* mutants and expressing *POT1-GFP* were incubated in SCIM for 16 h. Fluorescent images of randomly chosen fields of cells were acquired as a stack by confocal microscopy and then deconvolved. Buds were sized according to two categories relative to the volume of the mother cell (see Materials and Methods). The percentages of buds containing peroxisomes at each size category were plotted. Quantification was performed on at least 50 budded cells from each category. Bar, 5 µm.

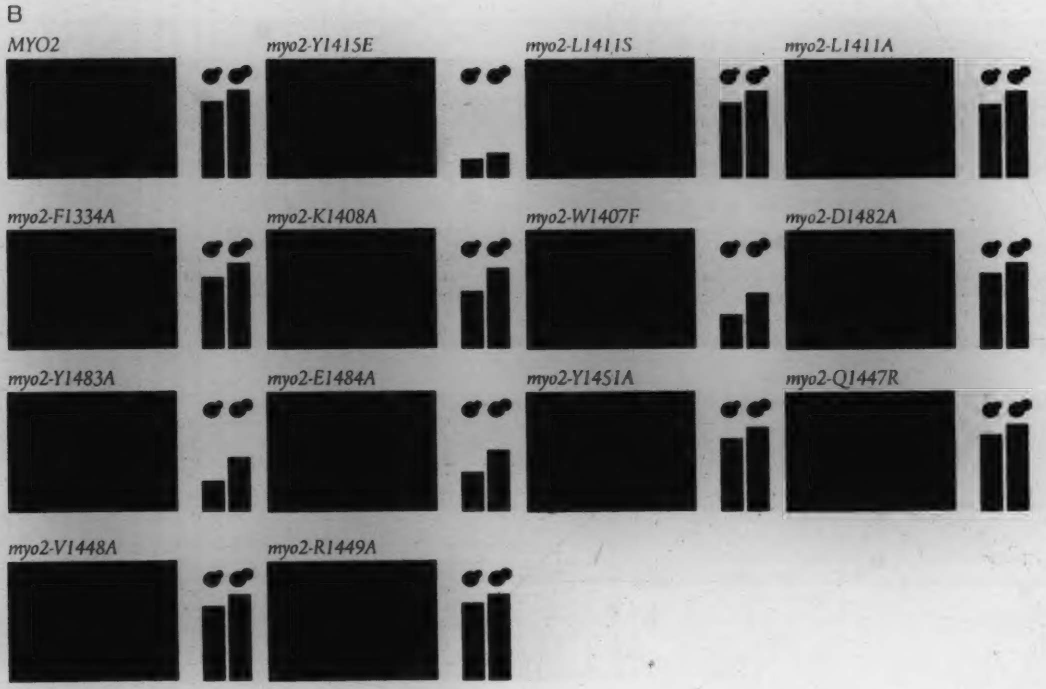
B
MYO2
myo2-Y1415E
myo2-L1411S
myo2-L1411A
myo2-F1334A
myo2-K1408A
myo2-W1407F
myo2-D1482A
myo2-Y1483A
myo2-E1484A
myo2-Y1451A
myo2-Q1447R
myo2-V1448A
myo2-R1449A

mother cell volume (large budded cells), only 28% and 62% of the buds of the *myo2-Y1415E* and *myo2-W1407F* mutants, respectively, displayed peroxisomal fluorescence, as compared to 98% for cells with the wild-type *MYO2* allele at the same bud sizes (Figure 4-2B).

To delineate the peroxisome-binding domain on Myo2p, we systematically replaced surface residues in the region neighboring Y1415 and W1407 with alanine (see Materials and Methods) and assessed the ability of the resultant mutants to sustain peroxisome transport to buds (Table 2-9 and Figure 4-2). Two additional substitutions, Y1483A and E1484A, were observed to disrupt the transport of peroxisomes to daughter cells (Figure 4-2B). Quantification of rates of peroxisome inheritance showed that only 34% and 45% of small budded cells and 61% and 68% of large budded cells of the *myo2-Y1483A* and *myo2-E1484A* strains, respectively, displayed peroxisomal fluorescence within buds. In contrast, 85% of small buds and 98% of large buds of cells having the wild-type *MYO2* gene contained peroxisomes (Figure 4-2B). Another mutation, *myo2-K1408A,* displayed a slight defect in peroxisome distribution, with 64% of small buds and 90% of large buds containing peroxisomes. This might indicate that K1408 is part of the peroxisome-binding region of Myo2p. However, care should be taken in the interpretation of these results, since the ε-ammonium of the K1408 side chain is predicted to form a hydrogen bond with the backbone carbonyl oxygen of F1334 (Figure 4-2A). Therefore, the effect of the K1408A substitution on peroxisome partitioning could be due to a destabilization of the local architecture of subdomain II of the Myo2p tail.

4.3 Mutants of Myo2p Defective in Peroxisome Inheritance Display Decreased Affinity for Inp2p

If Y1415, W1407, Y1483 and E1484, whose mutation affects peroxisome transport to the bud, form a region on the surface of Myo2p specialized in binding peroxisomes, we expect mutations in these amino acids to decrease the affinity of Myo2p for peroxisomes. We assessed the ability of various Myo2p point mutants to interact with the peroxisome by in vitro binding assays between the wild-type or a mutated Myo2p tail and Inp2p, the peroxisomal receptor for Myo2p. We had previously demonstrated a direct interaction between GST-Myo2p tail and MBP-Inp2p fusion proteins made in *E. coli* (see Chapter Three). We used a similar approach to quantify the interaction between Inp2p and the various Myo2p point mutants initially tested by microscopy for defects in peroxisome inheritance (Figure 4-3). To improve the solubility of the MBP-Inp2p fusion protein, only amino acids 241-705 of Inp2p were used so as to exclude its predicted membrane-spanning region (amino acids 211-239) while retaining the region between amino acids 241 and 705 capable of interacting with Myo2p (Fagarasanu et al., 2006a). Myo2p-Y1415E, Myo2p-W1407F, Myo2p-Y1483A and Myo2p-E1484A displayed decreased affinity for Inp2p as compared to wild-type Myo2p tail (Figure 4-3). Also, Myo2p-K1408A was slightly impaired in its ability to interact with Inp2p. Interestingly, some Myo2p point mutants displayed an increased interaction with Inp2p as compared to the wild-type Myo2p tail, indicating that regions outside of the Inp2p binding domain of Myo2p function to negatively regulate the Inp2p-Myo2p interaction.

These in vitro binding results correlate well with the results of our microscopy analysis, wherein *myo2-Y1415E*, *myo2-W1407F*, *myo2-Y1483A*, *myo2-E1484A* and, only

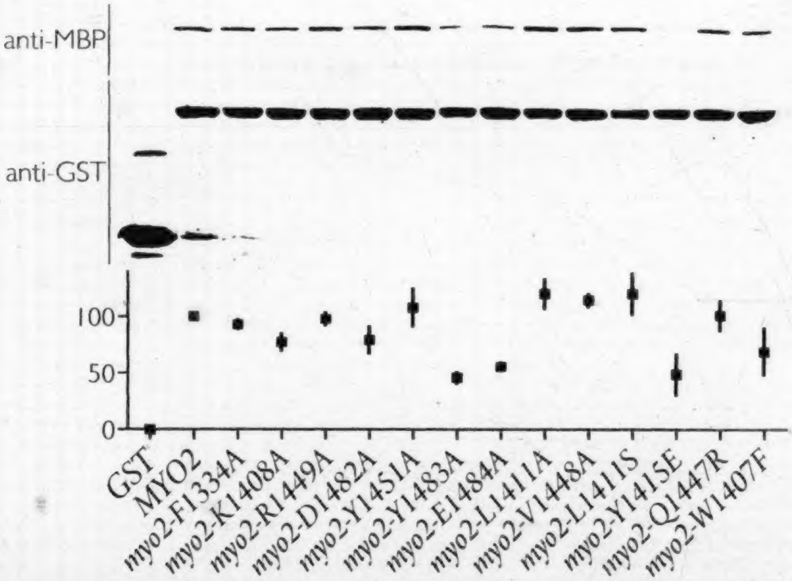

Figure 4-3. Mutants of Myo2p defective in peroxisome inheritance display decreased affinity for Inp2. Glutathione sepharose beads containing either GST fused to the cargo binding tail of wild-type or mutant Myo2p, or GST alone, were incubated with extracts of *E. coli*-synthesized MBP-Inp2p. Bound MBP-Inp2p was analyzed by immunoblotting with anti-MBP antibodies (upper panel). Total GST-Myo2p or GST protein levels were visualized by immunoblotting with anti-GST antibodies (middle panel). The amount of bound MBP-Inp2p was quantified by band densitometry (lower graph) using an Odyssey Imaging system in which background signal from the GST-only lane was first subtracted and band density then normalized to wild-type Myo2p. Graphic results are the means of three independent experiments. Bars represent Standard Error of the Mean (SEM).

partially, *myo2-K1408A* exhibited a defect in peroxisome localization to buds. This strong correlation demonstrates a clear relationship between the strength of Myo2p-Inp2p interactions and the efficiency of peroxisome inheritance displayed by the various Myo2p point mutants.

To conclude, we have identified four surface residues in subdomain II of the Myo2p cargo-binding domain, namely Y1415, W1407, Y1483 and E1484, that are crucial for the interaction of Myo2p with Inp2p and consequently for the transport of peroxisomes to daughter cells.

4.4 Myo2p Point Mutants Defective in Peroxisome Inheritance Are Not Defective in Vacuolar or Mitochondrial Inheritance

There is a valid concern that the identified Myo2p point mutants defective in peroxisome distribution do not impair specifically the process of peroxisome inheritance but in fact alter the overall structure of the Myo2p tail. However, in this case, one would expect that other functions of the Myo2p globular tail would also be affected when these Myo2p mutants are expressed as the sole copy of Myo2p. To test the specificity for peroxisome inheritance of the amino acyl residues identified as important for binding Myo2p to peroxisomes, we examined whether Myo2p with point mutations in these residues still retained the ability to segregate other organelles. The distribution of mitochondria was followed with the fluorescent label, MitoTracker Red. The rates of mitochondrial inheritance in cells harboring one of the four *myo2* alleles, *myo2-Y1415E*, *myo2-W1407F*, *myo2-Y1483A* or *myo2-E1484A*, identified as being compromised in peroxisome inheritance, were essentially the same as those observed in cells expressing

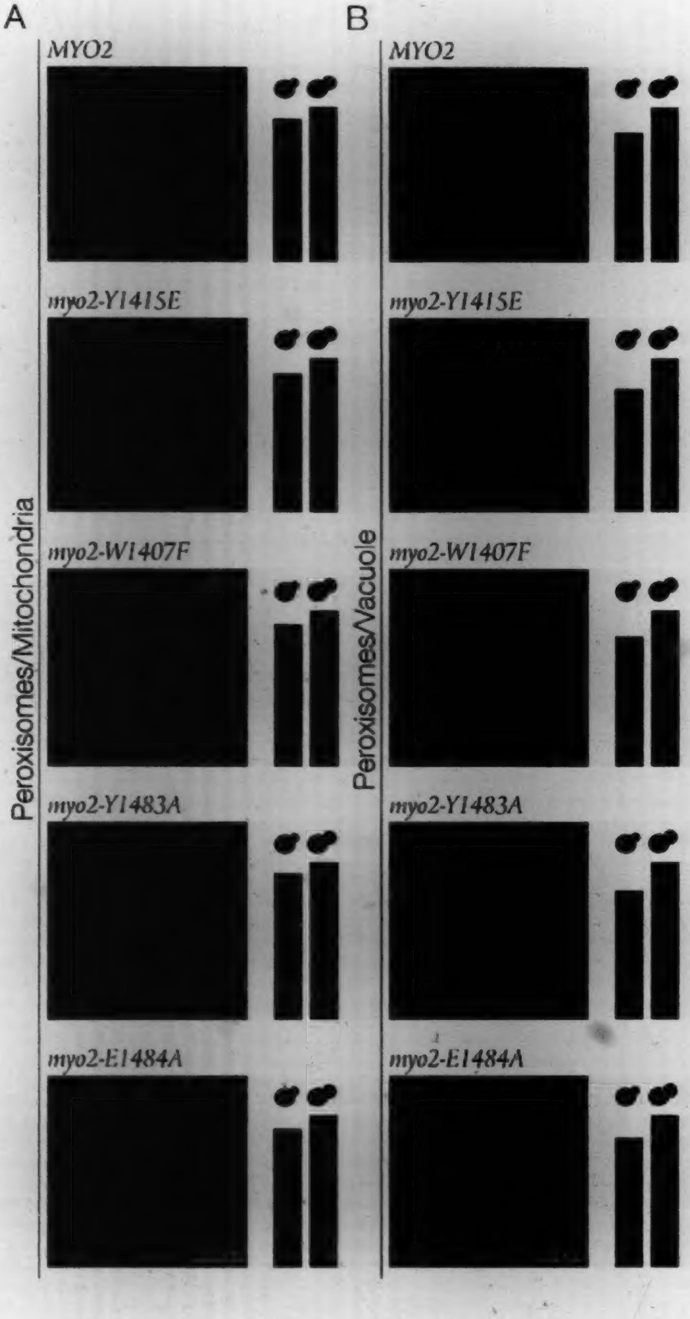

Figure 4-4. Myo2p point mutants defective in peroxisome inheritance are not defective in vacuolar or mitochondrial inheritance. (A) Mitochondrial segregation is unaffected in cells harboring Myo2p point mutants defective in peroxisome distribution. Cells expressing wild-type *MYO2* or mutant *myo2* were grown in SCIM, and confocal images were captured. Mitochondria were labeled with the fluorescent dye, MitoTracker Red. Peroxisomes were labeled with *POT1-GFP*. Quantification was performed as in Figure 4-2B. (B) Vacuole inheritance is unaffected in cells harboring Myo2p point mutants defective in peroxisome distribution. Cells expressing wild-type *MYO2* or mutant *myo2* were grown in SCIM, and confocal images were captured. Vacuoles were labeled with the fluorophore, FM4-64. Peroxisomes were labeled with *POT1-GFP*. Quantification was performed as in Figure 4-2B.

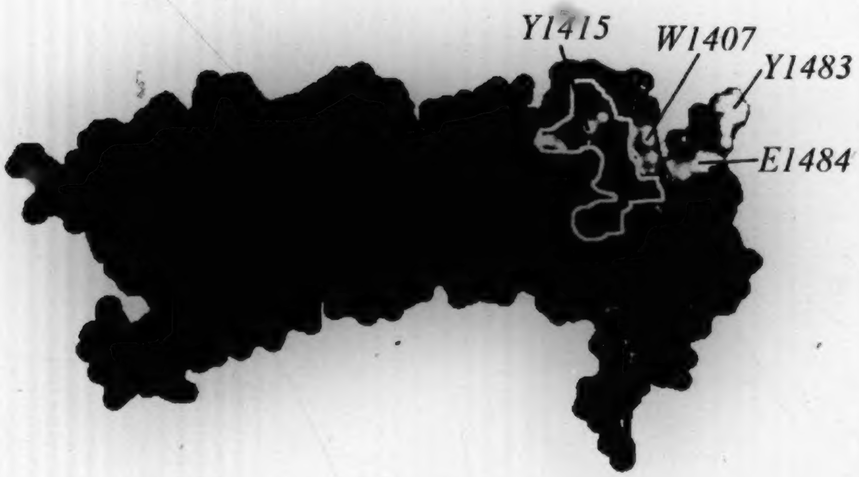

Figure 4-5. Surface representation of the Myo2p globular tail indicating the regions that bind peroxisomes and secretory vesicles. The peroxisome binding region is highlighted in yellow. The secretory vesicle binding region is outlined in teal.

wild-type *MYO2* (Figure 4-4A). The rates of inheritance of vacuoles, labeled by the vacuole-specific fluorophore FM4-64, were also unchanged in these point mutants (Figure 4-4B).

Collectively, our findings demonstrate that residues Y1415, W1407, Y1483 and E1484 define the surface area of the Myo2p tail devoted to binding peroxisomes. This peroxisome binding region resides in subdomain II of the Myo2 globular tail and partially overlaps with the region that binds secretory vesicles (Figure 4-5). Since single point mutations in the peroxisome binding region are sufficient to cause a significant defect in peroxisome inheritance, all four residues must cooperate to securely anchor Myo2p to the peroxisomal membrane during bud-directed movement.

CHAPTER FIVE: PERSPECTIVES

5.1 Synopsis

In conclusion, this thesis reports the identification and characterization of Inp2p as the peroxisome-specific receptor for Myo2p in *S. cerevisiae*. Inp2p is implicated in the motility of peroxisomes by linking them to the Myo2p motor, which then propels their movement along actin cables. We have also gained insight into the regulated interplay between retention and mobilization of peroxisomes that ultimately results in an equitable distribution of peroxisomes during cell division. We went further and uncovered structural details of the Inp2p-Myo2p interaction, which will form the basis of studies aimed to unravel the different levels of regulation of Inp2p activity during the cell cycle.

5.2 Future directions for studies on Inp2p

However, apart from the regulation of Inp2p turnover during the cell cycle, there are several important questions regarding Inp2p that remain to be answered:

How does Inp2p get loaded preferentially on only a subset of peroxisomes? Studies on the mechanism of mitotic spindle alignment may provide some insight into this question. Budding yeast has to align its intranuclear mitotic spindle along a polarity axis pre-established by the site of bud emergence. Myo2p is directly involved in orienting the spindle by carrying the plus ends of cytoplasmic microtubules into the bud. The adaptor/receptor protein that links Myo2p to the microtubule ends is Kar9p (Yin et al., 2000; Lee et al., 2000), which associates with microtubules in a Bim1p-dependent manner. Kar9p is loaded only onto the older, i.e. inherited from the previous cell division, spindle pole body (SPB) and then translocates down the cytoplasmic microtubules that emanate from this SPB (Kusch et al., 2002; Liakopoulos et al., 2003) (Figure 1-3). Kar9p is prevented from associating with the new SPB through its phosphorylation by Clb4p/Cdc28p, which inactivates it. Clb4p specifically binds the new SPB, which is destined for the mother cell, inactivating Kar9p only at this location (Liakopoulos et al., 2003). The microtubules associated with the new SPB will not be decorated with Kar9p and therefore will not be directed to the daughter cell. The asymmetric loading of Kar9p thus ensures that only one spindle pole is transmitted to the bud, resulting in the proper alignment of the mitotic spindle with the cell division axis (Pruyne et al., 2004a). Similarly, Inp2p is enriched in a subset of peroxisomes, and only these Inp2p-containing peroxisomes are destined for the daughter cell. It would be interesting to see if inhibitory factors are present on the remaining peroxisomes that prevent their recruitment of Inp2p. Also, as in the case of spindle poles, there might be a correlation between the age of different peroxisomes and their ability to recruit Inp2p. During the constitutive division of peroxisomes, a process required for maintenance of the peroxisomal population during cell division, new peroxisomes arise from older, parental peroxisomes. Various membrane constituents might segregate asymmetrically during peroxisome division, conferring different affinities for Inp2p on daughter and parental peroxisomes.

Inp2p is an integral membrane protein of peroxisomes and contains a putative membrane-spanning region between amino acids 211–239. However, the vacuolar Myo2p-specific receptor, Vac17p, is a peripheral membrane protein that associates with the vacuole membrane through interaction with Vac8p, producing a Vac8p-Vac17p-Myo2p transport complex (Tang et al., 2003). A similar tripartite complex, Rab27a-melanophilin-MyoVa, is required for the myosin Va-driven transport of melanosomes in mammalian melanocytes (Wu et al., 2002). Since Inp2p is a membrane-spanning protein, it would be interesting to investigate whether Inp2p functions alone as the receptor linking Myo2p to peroxisomes or is part of a protein receptor/adaptor complex in the peroxisomal membrane. Moreover, it would be interesting to determine if Inp2p is confined to a particular lipid environment suited to withstand the pulling force of Myo2p on the peroxisomal membrane, as has been proposed for the Vac8p-associated lipid domain present in the vacuolar membrane (Weisman, 2003).

5.3 Future directions for studies on peroxisome inheritance in general

Several important questions regarding the overall process of peroxisome inheritance and dynamics in *S. cerevisiae* remain to be answered:

1. What is the nature of the cortical anchor to which peroxisomes attach? 2. Are the division and retention of peroxisomes intrinsically related? Does Inp1p associate with different protein complexes to function in these two processes? 3. Organelle inheritance and cell cycle events need to be coordinated. How is this coordination established and maintained? What is the nature of the interplay between Inp1p and Inp2p? What advantage is the oscillation of Inp1p during the cell cycle? How is the oscillation of Inp1p coordinated with fluctuations in the levels of Inp2p? What is the degradation machinery responsible for the turnover of Inp1p and Inp2p, and how is it regulated? Is Inp1p loaded evenly on different peroxisomes? Are Inp1p or/and Inp2p functions regulated by post-translational processes like phosphorylation, or do their synthesis and turnover alone regulate their activities? 4. Inp1p is a peripheral membrane protein of peroxisomes. What is the docking site for Inp1p on the peroxisomal membrane? 5.

Orthologs of the Inp proteins are present in other fungal species. Do they function similarly or differently to *S. cerevisiae* Inp1p and Inp2p?

5.4 Future directions for the field of organelle inheritance

Each cytoplasmic organelle uses specific molecular pathways to ensure its inheritance by future generations of cells. The challenge now is to identify those fundamental rules that apply to all mechanisms of organelle inheritance. By analyzing the strategies used by budding yeast to ensure correct organelle partitioning during cell division, a requirement for certain components common to the inheritance of all cytoplasmic organelles is becoming apparent. Such common components controlling the placement, and thus the inheritance, of cytoplasmic organelles include (Weisman, 2003; Fagarasanu et al., 2006b) (1) a cytoskeletal track to direct organelle movement, (2) a molecular engine to power organelle movement, (3) a mechanism to initiate and terminate organelle movement, (4) a capturing device for organelles at their destination, i.e. in the daughter cell, and (5) an anchoring system to retain a subset of the organelle population in the mother cell. All the abovementioned components must cooperate and act discriminately on different organelle subsets to ensure correct organelle partitioning at cell division. Moreover, they must be temporally coordinated with the processes of organelle growth and division, as well as with cell cycle events, to ensure the perpetuation of organelle populations during cell proliferation.

Similarities among the partitioning strategies of different organelles become even more apparent when differences in morphologies between organelles are artificially eliminated. For example, cells lacking the dynamin-like protein Vps1p often contain only one giant peroxisome because of the inability of peroxisomes in these cells to undergo fission (Hoepfner et al., 2001. During cell division, the large peroxisome present in *vps1Δ* cells emits a tubular projection that passes through the mother-bud neck into the daughter cell (Hoepfner et al., 2001). Therefore, peroxisome inheritance in cells that have the entire peroxisome population coalesced into a single-copy compartment is achieved through a mechanism that bears a striking resemblance to the process of vacuole inheritance.

Given the common molecular components used by cells to move their organelles, it would not be surprising to identify master regulators that control the distribution of all organelles and coordinate their dynamics with cell cycle events. One candidate for just such a regulator is the serine/threonine phosphatase, Ptc1p, that has been implicated to date in the distribution of mitochondria, vacuoles and cortical ER during cell division (Du et al., 2006; Roeder et al., 1998). The total inventory of proteins identified to play a role in organelle inheritance is far from complete. For example, there are several yeast organelles whose specific receptors for class V myosins, Myo2p or Myo4p, have yet to be discovered, including late Golgi elements (Rossanese et al., 2001), secretory vesicles (Schott et al., 1999), cortical ER (Estrada et al., 2003) and mitochondria (Altmann et al., 2008). The common features shared by Inp2p and Vac17p might prove useful for identifying these organelle-specific receptors. For example, both Inp2p and Vac17p contain two predicted coiled-coil domains that are each about 30 amino acid residues in length (Ishikawa et al., 2003; Fagarasanu et al., 2006a). Interestingly, mathematical models predict that an elastic coiled-coil connection between a myosin V and its bulky cargo results in a requirement for much reduced forces generated by myosin to allow cargo to follow the motor movements without delay (Schilstra and Martin, 2006). Moreover, such a pliant link is beneficial, since it transiently absorbs the abrupt mechanical transitions of the motor molecule and, at the same time, imposes a regular gait on the motion of the myosin V motor (Schilstra and Martin, 2006). Therefore, coiled-coil domains may represent a feature common to all organelle receptors for class V myosins. In support of this prediction, tandem coiled-coil domains of about the same size as the ones found in Inp2p and Vac17p were also found in melanophilin (Nagashima et al., 2002). In addition, the levels of mRNA encoding Inp2p and Vac17p (Spellman et al., 1998) and the levels of the proteins themselves oscillate during the cell cycle in patterns that parallel the segregation of peroxisomes and vacuoles, respectively. If assembly/disassembly of transport complexes is a general mechanism regulating organelle positioning, one could predict the mRNA and protein profiles of an organelle-specific class V myosin receptor by analyzing the dynamics of that organelle during the cell cycle. For example, since late compartments of the Golgi are polarized in G1-arrested cells (Rossanese et al., 2001), in contrast to what is observed for peroxisomes and vacuoles, a very different profile is expected for the late Golgi receptor for Myo2p compared to the profiles for Inp2p and Vac17p.

The identification and characterization of additional proteins involved in organelle inheritance will provide further insight into the spatial and temporal control of organelle motility and the molecular basis of membrane movement in general.

5.5 Concluding remarks

The past two decades have witnessed remarkable progress in our understanding of peroxisome biology. Notably, a large array of genes encoding proteins required for the peroxisome biogenesis has been cloned and characterized, including those whose mutations underlie Zellweger syndrome and other members of the peroxisome biogenesis disorders. Importantly, the debate on the origin of peroxisomes has finally subsided into an interesting marriage of the two seemingly contradictory concepts of peroxisome biogenesis: de novo formation of peroxisomes from the ER and the growth and division of preexisting peroxisomes.

However, the total inventory of proteins implicated in peroxisome division and inheritance is far from complete. Even less is known about the molecular players that orchestrate the vesicular flow from the ER and through the peroxisomal endomembrane system. The challenge now is to identify and characterize functionally the entire set of proteins involved in peroxisome biogenesis, division, and inheritance.

In addition, it is worthwhile to set aside the view of these different processes as being independent and self-contained. Instead, understanding how they are coordinately integrated will provide invaluable information about the strategies used by cells to maintain peroxisomes under varied and varying conditions.

A starting point to elucidate the relative contributions of peroxisome de novo formation, division, and inheritance to peroxisome homeostasis is to take advantage of new fluorescent live-cell-imaging technologies such as photo-chase assays (Kim et al. 2006), in different cell types and under different environmental conditions. Defining the panoply of peroxisome dynamics in real time will be an exciting goal for cell biologists in the years to come.

CHAPTER SIX: REFERENCES

Adames, N.R., J.R. Oberle, and J.A. Cooper. 2001. The surveillance mechanism of the spindle position checkpoint in yeast. *J. Cell Biol.* 153:159–168.

Allan, B.B. and W.E.Balch. 1999. Protein sorting by directed maturation of Golgi compartments. *Science* 285:63-66.

Altmann, K., M.Frank, D.Neumann, S.Jakobs, and B.Westermann. 2008. The class V myosin motor protein, Myo2, plays a major role in mitochondrial motility in *Saccharomyces cerevisiae*. *J. Cell Biol.* 181:119-130.

Ausubel, F.J., R.Brent, R.E.Kingston, D.D.Moore, J.G.Seidman, J.A.Smith, and K.Struhl. 1989. Current Protocols in Molecular Biology. Greene Publishing Associates, New York, NY.

Barnett, P., H.F.Tabak, and E.H.Hettema. 2000. Nuclear receptors arose from pre-existing protein modules during evolution. *Trends Biochem. Sci.* 25:227-228.

Beach, D.L., J.Thibodeaux, P.Maddox, E.Yeh, and K.Bloom. 2000. The role of the proteins Kar9 and Myo2 in orienting the mitotic spindle of budding yeast. *Curr. Biol.* 10:1497-1506.

Berger, K.H., L.F.Sogo, and M.P.Yaffe. 1997. Mdm12p, a component required for mitochondrial inheritance that is conserved between budding and fission yeast. *J. Cell Biol.* 136:545-553.

Boldogh, I.R. and L.A.Pon. 2006. Interactions of mitochondria with the actin cytoskeleton. *Biochim. Biophys. Acta* 1763:450-462.

Boldogh, I.R. and L.A.Pon. 2007. Mitochondria on the move. *Trends Cell Biol.* 17:502-510.

Boldogh, I.R., K.L.Fehrenbacher, H.C.Yang, and L.A.Pon. 2005. Mitochondrial movement and inheritance in budding yeast. *Gene* 354:28-36.

Boldogh, I.R., S.L.Ramcharan, H.C.Yang, and L.A.Pon. 2004. A type V myosin (Myo2p) and a Rab-like G-protein (Ypt11p) are required for retention of newly inherited mitochondria in yeast cells during cell division. *Mol. Biol. Cell* 15:3994-4002.

Boldogh, I.R., H.C.Yang, W.D.Nowakowski, S.L.Karmon, L.G.Hays, J.R.Yates, III, and L.A.Pon. 2001. Arp2/3 complex and actin dynamics are required for actin-based mitochondrial motility in yeast. *Proc. Natl. Acad. Sci. U. S. A.* 98:3162-3167.

Bonangelino, C.J., N.L.Catlett, and L.S.Weisman. 1997. Vac7p, a novel vacuolar protein, is required for normal vacuole inheritance and morphology. *Mol. Cell. Biol.* 17:6847-6858.

Bonifacino, J.S. and B.S.Glick. 2004. The mechanisms of vesicle budding and fusion. *Cell* 116:153-166.

Bretscher, A. 2003. Polarized growth and organelle segregation in yeast: the tracks, motors, and receptors. *J. Cell Biol.* 160:811-816.

Broach, J.R., J.N.Strathern, and J.B.Hicks. 1979. Transformation in yeast: development of a hybrid cloning vector and isolation of the *CAN1* gene. *Gene* 8:121-133.

Burgess, S.M., M.Delannoy, and R.E.Jensen. 1994. *MMM1* encodes a mitochondrial outer membrane protein essential for establishing and maintaining the structure of yeast mitochondria. *J. Cell Biol.* 126:1375-1391.

Burnette, W.N. 1981. "Western Blotting": electrophoretic transfer of proteins from sodium dodecyl sulphate-polyacrylamide gels to unmodified nitrocellulose and radiographic detection with antibody and radioiodinated protein A. *Anal. Biochem.* 112:195-203.

Buvelot, F.S., P.B.Rahl, M.Nussbaum, B.J.Briggs, M.Calero, S.Janeczko, A.D.Regan, C.Z.Chen, Y.Barral, G.R.Whittaker, and R.N.Collins. 2006. Bioinformatic and comparative localization of Rab proteins reveals functional insights into the uncharacterized GTPases Ypt10p and Ypt11p. *Mol. Cell. Biol.* 26:7299-7317.

Cajaraville, M.P., I.Cancio, A.Ibabe, and A.Orbea. 2003. Peroxisome proliferation as a biomarker in environmental pollution assessment. *Microsc. Res. Tech.* 61:191-202.

Catlett, N.L. and L.S.Weisman. 1998. The terminal tail region of a yeast myosin-V mediates its attachment to vacuole membranes and sites of polarized growth. *Proc. Natl. Acad. Sci. U. S. A.* 95:14799-14804.

Catlett, N.L. and L.S.Weisman. 2000. Divide and multiply: organelle partitioning in yeast. *Curr. Opin. Cell Biol.* 12:509-516.

Catlett, N.L., J.E.Duex, F.Tang, and L.S.Weisman. 2000. Two distinct regions in a yeast myosin-V tail domain are required for the movement of different cargoes. *J. Cell Biol.* 150:513-526.

Cerveny, K.L., S.L.Studer, R.E.Jensen, and H.Sesaki. 2007. Yeast mitochondrial division and distribution require the cortical Num1 protein. *Dev. Cell* 12:363-375.

Conradt, B., J.Shaw, T.Vida, S.Emr, and W.Wickner. 1992. In vitro reactions of vacuole inheritance in *Saccharomyces cerevisiae*. *J. Cell Biol.* 119:1469-1479.

de Duve, C. 1965. The separation and characterization of subcellular particles. *Harvey Lect.* 59:49-87.

de Duve, C. and P.Baudhuin. 1966. Peroxisomes (microbodies and related particles). *Physiol. Rev.* 46:323-357.

Dibrov, E., S.Fu, and B.D.Lemire. 1998. The *Saccharomyces cerevisiae TCM62* gene encodes a chaperone necessary for the assembly of the mitochondrial succinate dehydrogenase (complex II). *J. Biol. Chem.* 273:32042-32048.

Drubin, D.G., H.D.Jones, and K.F.Wertman. 1993. Actin structure and function: roles in mitochondrial organization and morphogenesis in budding yeast and identification of the phalloidin-binding site. *Mol. Biol. Cell* 4:1277-1294.

Du, Y., S.Ferro-Novick, and P.Novick. 2004. Dynamics and inheritance of the endoplasmic reticulum. *J. Cell Sci.* 117:2871-2878.

Du, Y., M.Pypaert, P.Novick, and S.Ferro-Novick. 2001. Aux1p/Swa2p is required for cortical endoplasmic reticulum inheritance in *Saccharomyces cerevisiae*. *Mol. Biol. Cell* 12:2614-2628.

Du, Y., L.Walker, P.Novick, and S.Ferro-Novick. 2006. Ptc1p regulates cortical ER inheritance via Slt2p. *EMBO J.* 25:4413-4422.

Efe, J.A., R.J.Botelho, and S.D.Emr. 2007. Atg18 regulates organelle morphology and Fab1 kinase activity independent of its membrane recruitment by phosphatidylinositol 3,5-bisphosphate. *Mol. Biol. Cell* 18:4232-4244.

Eitzen, G.A., R.K.Szilard, and R.A.Rachubinski. 1997. Enlarged peroxisomes are present in oleic acid-grown *Yarrowia lipolytica* overexpressing the *PEX16* gene encoding an intraperoxisomal peripheral membrane peroxin. *J. Cell Biol.* 137:1265-1278.

Eitzen, G.A., V.I.Titorenko, J.J.Smith, M.Veenhuis, R.K.Szilard, and R.A.Rachubinski. 1996. The *Yarrowia lipolytica* gene *PAY5* encodes a peroxisomal integral membrane protein homologous to the mammalian peroxisome assembly factor PAF-1. *J. Biol. Chem.* 271:20300-20306.

Erdmann, R. and G.Blobel. 1995. Giant peroxisomes in oleic acid-induced *Saccharomyces cerevisiae* lacking the peroxisomal membrane protein Pmp27p. *J. Cell Biol.* 128:509-523.

Estrada, P., J.Kim, J.Coleman, L.Walker, B.Dunn, P.Takizawa, P.Novick, and S.Ferro-Novick. 2003. Myo4p and She3p are required for cortical ER inheritance in *Saccharomyces cerevisiae*. *J. Cell Biol.* 163:1255-1266.

Estrada de Martin, P., P.Novick, and S.Ferro-Novick. 2005. The organization, structure, and inheritance of the ER in higher and lower eukaryotes. *Biochem. Cell Biol.* 83:752-761.

Faber, K.N., J.A.Heyman, and S.Subramani. 1998. Two AAA family peroxins, PpPex1p and PpPex6p, interact with each other in an ATP-dependent manner and are associated with different subcellular membranous structures distinct from peroxisomes. *Mol. Cell. Biol.* 18:936-943.

Fagarasanu, A., M.Fagarasanu, G.A.Eitzen, J.D.Aitchison, and R.A.Rachubinski. 2006a. The peroxisomal membrane protein Inp2p is the peroxisome-specific receptor for the myosin V motor Myo2p of *Saccharomyces cerevisiae*. *Dev. Cell* 10:587-600.

Fagarasanu, A., M.Fagarasanu, and R.A.Rachubinski. 2007. Maintaining peroxisome populations: a story of division and inheritance. *Annu. Rev. Cell Dev. Biol.* 23:321-344.

Fagarasanu, A. and R.A.Rachubinski. 2007. Orchestrating organelle inheritance in *Saccharomyces cerevisiae*. *Curr. Opin. Microbiol.* 10:528-538.

Fagarasanu, M., A.Fagarasanu, and R.A.Rachubinski. 2006b. Sharing the wealth: peroxisome inheritance in budding yeast. *Biochim. Biophys. Acta* 1763:1669-1677.

Fagarasanu, M., A.Fagarasanu, Y.Y.C.Tam, J.D.Aitchison, and R.A.Rachubinski. 2005. Inp1p is a peroxisomal membrane protein required for peroxisome inheritance in *Saccharomyces cerevisiae*. *J. Cell Biol.* 169:765-775.

Fahimi, H.D. 1968. Cytochemical localization of peroxidase activity in rat hepatic microbodies (peroxisomes). *J. Histochem. Cytochem.* 16:547-550.

Fehrenbacher, K.L., I.R.Boldogh, and L.A.Pon. 2005. A role for Jsn1p in recruiting the Arp2/3 complex to mitochondria in budding yeast. *Mol. Biol. Cell* 16:5094-5102.

Fehrenbacher, K.L., D.Davis, M.Wu, I.Boldogh, and L.A.Pon. 2002. Endoplasmic reticulum dynamics, inheritance, and cytoskeletal interactions in budding yeast. *Mol. Biol. Cell* 13:854-865.

Fehrenbacher, K., T.Huckaba, H.C.Yang, I.Boldogh, and L.Pon. 2003. Actin comet tails, endosomes and endosymbionts. *J. Exp. Biol.* 206:1977-1984.

Fehrenbacher, K.L., H.C.Yang, A.C.Gay, T.M.Huckaba, and L.A.Pon. 2004. Live cell imaging of mitochondrial movement along actin cables in budding yeast. *Curr. Biol.* 14:1996-2004.

Finger, F.P., T.E.Hughes, and P.Novick. 1998. Sec3p is a spatial landmark for polarized secretion in budding yeast. *Cell* 92:559-571.

Geuze, H.J., J.L.Murk, A.K.Stroobants, J.M.Griffith, M.J.Kleijmeer, A.J.Koster, A.J.Verkleij, B.Distel, and H.F.Tabak. 2003. Involvement of the endoplasmic reticulum in peroxisome formation. *Mol. Biol. Cell* 14:2900-2907.

Giaever, G., A.M.Chu, L.Ni, C.Connelly, L.Riles, S.Veronneau, S.Dow, A.Lucau-Danila, K.Anderson, B.Andre, A.P.Arkin, A.Astromoff, M.El-Bakkoury, R.Bangham, R.Benito, S.Brachat, S.Campanaro, M.Curtiss, K.Davis, A.Deutschbauer, K.D.Entian, P.Flaherty, F.Foury, D.J.Garfinkel, M.Gerstein, D.Gotte, U.Guldener, J.H.Hegemann, S.Hempel, Z.Herman, D.F.Jaramillo, D.E.Kelly, S.L.Kelly, P.Kotter, D.LaBonte, D.C.Lamb, N.Lan, H.Liang, H.Liao, L.Liu, C.Luo, M.Lussier, R.Mao, P.Menard, S.L.Ooi, J.L.Revuelta, C.J.Roberts, M.Rose, P.Ross-Macdonald, B.Scherens, G.Schimmack, B.Shafer, D.D.Shoemaker, S.Sookhai-Mahadeo, R.K.Storms, J.N.Strathern, G.Valle, M.Voet, G.Volckaert, C.Y.Wang, T.R.Ward, J.Wilhelmy, E.A.Winzeler, Y.Yang, G.Yen, E.Youngman, K.Yu, H.Bussey, J.D.Boeke, M.Snyder, P.Philippsen, R.W.Davis, and M.Johnston. 2002. Functional profiling of the *Saccharomyces cerevisiae* genome. *Nature* 418:387-391.

Gietz, R.D. and R.A.Woods. 2002. Transformation of yeast by lithium acetate/single-stranded carrier DNA/polyethylene glycol method. *Methods Enzymol.* 350:87-96.

Gomes de Mesquita, D.S., R.ten Hoopen, and C.L.Woldringh. 1991. Vacuolar segregation to the bud of *Saccharomyces cerevisiae*: an analysis of morphology and timing in the cell cycle. *J. Gen. Microbiol.* 137:2447-2454.

Govindan, B., R.Bowser, and P.Novick. 1995. The role of Myo2, a yeast class V myosin, in vesicular transport. *J. Cell Biol.* 128:1055-1068.

Guo, T., C.Gregg, T.Boukh-Viner, P.Kyryakov, A.Goldberg, S.Bourque, F.Banu, S.Haile, S.Milijevic, K.H.San, J.Solomon, V.Wong, and V.I.Titorenko. 2007. A signal from inside the peroxisome initiates its division by promoting the remodeling of the peroxisomal membrane. *J. Cell Biol.* 177:289-303.

Guo, T., Y.Y.Kit, J.M.Nicaud, M.T.Le Dall, S.K.Sears, H.Vali, H.Chan, R.A.Rachubinski, and V.I.Titorenko. 2003. Peroxisome division in the yeast *Yarrowia lipolytica* is regulated by a signal from inside the peroxisome. *J. Cell Biol.* 162:1255-1266.

Hammond, A.T. and B.S.Glick. 2000. Raising the speed limits for 4D fluorescence microscopy. *Traffic* 1:935-940.

Hill, K.L., N.L.Catlett, and L.S.Weisman. 1996. Actin and myosin function in directed vacuole movement during cell division in *Saccharomyces cerevisiae*. *J. Cell Biol.* 135:1535-1549.

Hirai, K.I. 1969. Light microscopic study of the peroxidatic activity of catalase in formaldehyde-fixed rat liver. *J. Histochem. Cytochem.* 17:585-590.

Hobbs, A.E., M.Srinivasan, J.M.McCaffery, and R.E.Jensen. 2001. Mmm1p, a mitochondrial outer membrane protein, is connected to mitochondrial DNA (mtDNA) nucleoids and required for mtDNA stability. *J. Cell Biol.* 152:401-410.

Hoepfner, D., D.Schildknegt, I.Braakman, P.Philippsen, and H.F.Tabak. 2005. Contribution of the endoplasmic reticulum to peroxisome formation. *Cell* 122:85-95.

Hoepfner, D., M.van den Berg, P.Philippsen, H.F.Tabak, and E.H.Hettema. 2001. A role for Vps1p, actin, and the Myo2p motor in peroxisome abundance and inheritance in *Saccharomyces cerevisiae*. *J. Cell Biol.* 155:979-990.

Honsho, M., S.Tamura, N.Shimozawa, Y.Suzuki, N.Kondo, and Y.Fujiki. 1998. Mutation in PEX16 is causal in the peroxisome-deficient Zellweger syndrome of complementation group D. *Am. J. Hum. Genet.* 63:1622-1630.

Hoppins, S., L.Lackner, and J.Nunnari. 2007. The machines that divide and fuse mitochondria. *Annu. Rev. Biochem.* 76:751-780.

Huh, W.K., J.V.Falvo, L.C.Gerke, A.S.Carroll, R.W.Howson, J.S.Weissman, and E.K.O'Shea. 2003. Global analysis of protein localization in budding yeast. *Nature* 425:686-691.

Huynh, T.V., R.A. Young, and R.W.Davis. 1985. DNA cloning: A Practical Approach. IRL Press, Oxford.

Ishikawa, K., N.L.Catlett, J.L.Novak, F.Tang, J.J.Nau, and L.S.Weisman. 2003. Identification of an organelle-specific myosin V receptor. *J. Cell Biol.* 160:887-897.

Ito, T., T.Chiba, R.Ozawa, M.Yoshida, M.Hattori, and Y.Sakaki. 2001. A comprehensive two-hybrid analysis to explore the yeast protein interactome. *Proc. Natl. Acad. Sci. U. S. A.* 98:4569-4574.

Itoh, T., E.Toh, and Y.Matsui. 2004. Mmr1p is a mitochondrial factor for Myo2p-dependent inheritance of mitochondria in the budding yeast. *EMBO J.* 23:2520-2530.

Itoh, T., A.Watabe, E.Toh, and Y.Matsui. 2002. Complex formation with Ypt11p, a Rab-type small GTPase, is essential to facilitate the function of Myo2p, a class V myosin, in mitochondrial distribution in *Saccharomyces cerevisiae*. *Mol. Cell. Biol.* 22:7744-7757.

Johnston, G.C., J.A.Prendergast, and R.A.Singer. 1991. The *Saccharomyces cerevisiae MYO2* gene encodes an essential myosin for vectorial transport of vesicles. *J. Cell Biol.* 113:539-551.

Kaksonen, M., C.P.Toret, and D.G.Drubin. 2006. Harnessing actin dynamics for clathrin-mediated endocytosis. *Nat. Rev. Mol. Cell Biol.* 7:404-414.

Kamiryo, T., M.Abe, K.Okazaki, S.Kato, and N.Shimamoto. 1982. Absence of DNA in peroxisomes of *Candida tropicalis*. *J. Bacteriol,* 152:269-274.

Kiel, J.A., M.Veenhuis, and I.J.van der Klei. 2006. *PEX* genes in fungal genomes: common, rare or redundant. *Traffic* 7:1291-1303.

Kim, P.K., R.T.Mullen, U.Schumann, and J.Lippincott-Schwartz. 2006. The origin and maintenance of mammalian peroxisomes involves a de novo PEX16-dependent pathway from the ER. *J. Cell Biol.* 173:521-532.

Koch, A., G.Schneider, G.H.Luers, and M.Schrader. 2004. Peroxisome elongation and constriction but not fission can occur independently of dynamin-like protein 1. *J. Cell Sci.* 117:3995-4006.

Koch, A., M.Thiemann, M.Grabenbauer, Y.Yoon, M.A.McNiven, and M.Schrader. 2003. Dynamin-like protein 1 is involved in peroxisomal fission. *J. Biol. Chem.* 278:8597-8605.

Koch, A., Y.Yoon, N.A.Bonekamp, M.A.McNiven, and M.Schrader. 2005. A role for Fis1 in both mitochondrial and peroxisomal fission in mammalian cells. *Mol. Biol. Cell* 16:5077-5086.

Kondo-Okamoto, N., J.M.Shaw, and K.Okamoto. 2003. Mmm1p spans both the outer and inner mitochondrial membranes and contains distinct domains for targeting and foci formation. *J. Biol. Chem.* 278:48997-49005.

Koning, A.J., P.Y.Lum, J.M.Williams, and R.Wright. 1993. DiOC6 staining reveals organelle structure and dynamics in living yeast cells. *Cell Motil. Cytoskel.* 25:111-128.

Kuravi, K., S.Nagotu, A.M.Krikken, K.Sjollema, M.Deckers, R.Erdmann, M.Veenhuis, and I.J.van der Klei. 2006. Dynamin-related proteins Vps1p and Dnm1p control peroxisome abundance in *Saccharomyces cerevisiae*. *J. Cell Sci.* 119:3994-4001.

Kusch, J., A.Meyer, M.P.Snyder, and Y.Barral. 2002. Microtubule capture by the cleavage apparatus is required for proper spindle positioning in yeast. *Genes Dev.* 16:1627-1639.

Lazarow, P.B. and Y.Fujiki. 1985. Biogenesis of peroxisomes. *Annu. Rev. Cell Biol.* 1:489-530.

Lazzarino, D.A., I.Boldogh, M.G.Smith, J.Rosand, and L.A.Pon. 1994. Yeast mitochondria contain ATP-sensitive, reversible actin-binding activity. *Mol. Biol. Cell* 5:807-818.

Lee, L., J.S.Tirnauer, J.Li, S.C.Schuyler, J.Y.Liu, and D.Pellman. 2000. Positioning of the mitotic spindle by a cortical-microtubule capture mechanism. *Science* 287:2260-2262.

Li, X. and S.J.Gould. 2003. The dynamin-like GTPase DLP1 is essential for peroxisome division and is recruited to peroxisomes in part by PEX11. *J. Biol. Chem.* 278:17012-17020.

Liakopoulos, D., J.Kusch, S.Grava, J.Vogel, and Y.Barral. 2003. Asymmetric loading of Kar9 onto spindle poles and microtubules ensures proper spindle alignment. *Cell* 112:561-574.

Lingard, M.J. and R.N.Trelease. 2006. Five *Arabidopsis* peroxin 11 homologs individually promote peroxisome elongation, duplication or aggregation. *J. Cell Sci.* 119:1961-1972.

Long, R.M., R.H.Singer, X.Meng, I.Gonzalez, K.Nasmyth, and R.P.Jansen. 1997. Mating type switching in yeast controlled by asymmetric localization of *ASH1* mRNA. *Science* 277:383-387.

Losev, E., C.A.Reinke, J.Jellen, D.E.Strongin, B.J.Bevis, and B.S.Glick. 2006. Golgi maturation visualized in living yeast. *Nature* 441:1002-1006.

Lowe, M. and F.A.Barr. 2007. Inheritance and biogenesis of organelles in the secretory pathway. *Nat. Rev. Mol. Cell Biol.* 8:429-439.

Makhnevych, T., C.P.Lusk, A.M.Anderson, J.D.Aitchison, and R.W.Wozniak. 2003. Cell cycle regulated transport controlled by alterations in the nuclear pore complex. *Cell* 115:813-823.

Maniatis, T., E.F.Fritsch, and J.Sambrook. 1982. Molecular Cloning: A Laboratory Manual. Cold Spring Harbor Laboratory, Cold Spring Harbor.

Mano, S., C.Nakamori, M.Kondo, M.Hayashi, and M.Nishimura. 2004. An *Arabidopsis* dynamin-related protein, DRP3A, controls both peroxisomal and mitochondrial division. *Plant J.* 38:487-498.

Marshall, P.A., J.M.Dyer, M.E.Quick, and J.M.Goodman. 1996. Redox-sensitive homodimerization of Pex11p: a proposed mechanism to regulate peroxisomal division. *J. Cell Biol.* 135:123-137.

Marshall, P.A., Y.I.Krimkevich, R.H.Lark, J.M.Dyer, M.Veenhuis, and J.M.Goodman. 1995. Pmp27 promotes peroxisomal proliferation. *J. Cell Biol.* 129:345-355.

Masters, C. and D.Crane. 1996. Recent developments in peroxisome biology. *Endeavour* 20:68-73.

McCartney, A.W., J.S.Greenwood, M.R.Fabian, K.A.White, and R.T.Mullen. 2005. Localization of the tomato bushy stunt virus replication protein p33 reveals a peroxisome-to-endoplasmic reticulum sorting pathway. *Plant Cell* 17:3513-3531.

McMahon, H.T. and J.L.Gallop. 2005. Membrane curvature and mechanisms of dynamic cell membrane remodelling. *Nature* 438:590-596.

Mehta, A.D., R.S.Rock, M.Rief, J.A.Spudich, M.S.Mooseker, and R.E.Cheney. 1999. Myosin-V is a processive actin-based motor. *Nature* 400:590-593.

Mermall, V., P.L.Post, and M.S.Mooseker. 1998. Unconventional myosins in cell movement, membrane traffic, and signal transduction. *Science* 279:527-533.

Motley, A.M. and E.H.Hettema. 2007. Yeast peroxisomes multiply by growth and division. *J. Cell Biol.* 178:399-410.

Mullen, R.T. and R.N.Trelease. 2006. The ER-peroxisome connection in plants: development of the "ER semi-autonomous peroxisome maturation and replication" model for plant peroxisome biogenesis. *Biochim. Biophys. Acta* 1763:1655-1668.

Mullen, R.T., C.S.Lisenbee, J.A.Miernyk, and R.N.Trelease. 1999. Peroxisomal membrane ascorbate peroxidase is sorted to a membranous network that resembles a subdomain of the endoplasmic reticulum. *Plant Cell* 11:2167-2185.

Nagashima, K., S.Torii, Z.Yi, M.Igarashi, K.Okamoto, T.Takeuchi, and T.Izumi. 2002. Melanophilin directly links Rab27a and myosin Va through its distinct coiled-coil regions. *FEBS Lett.* 517:233-238.

Novikoff, A.B. and S.Goldfischer. 1969. Visualization of peroxisomes (microbodies) and mitochondria with diaminobenzidine. *J. Histochem. Cytochem.* 17:675-680.

Osteryoung, K.W. and J.Nunnari. 2003. The division of endosymbiotic organelles. *Science* 302:1698-1704.

Pashkova, N., N.L.Catlett, J.L.Novak, G.Wu, R.Lu, R.E.Cohen, and L.S.Weisman. 2005. Myosin V attachment to cargo requires the tight association of two functional subdomains. *J. Cell Biol.* 168:359-364.

Pashkova, N., Y.Jin, S.Ramaswamy, and L.S.Weisman. 2006. Structural basis for myosin V discrimination between distinct cargoes. *EMBO J.* 25:693-700.

Praefcke, G.J. and H.T.McMahon. 2004. The dynamin superfamily: universal membrane tubulation and fission molecules? *Nat. Rev. Mol. Cell Biol.* 5:133-147.

Preuss, D., J.Mulholland, A.Franzusoff, N.Segev, and D.Botstein. 1992. Characterization of the *Saccharomyces* Golgi complex through the cell cycle by immunoelectron microscopy. *Mol. Biol. Cell* 3:789-803.

Preuss, D., J.Mulholland, C.A.Kaiser, P.Orlean, C.Albright, M.D.Rose, P.W.Robbins, and D.Botstein. 1991. Structure of the yeast endoplasmic reticulum: localization of ER proteins using immunofluorescence and immunoelectron microscopy. *Yeast* 7:891-911.

Pringle, J.R., A.E.Adams, D.G.Drubin, and B.K.Haarer. 1991. Immunofluorescence methods for yeast. *Methods Enzymol.* 194:565-602.

Provance, D.W., T.L.James, and J.A.Mercer. 2002. Melanophilin, the product of the leaden locus, is required for targeting of myosin-Va to melanosomes. *Traffic* 3:124-132.

Pruyne, D., L.Gao, E.Bi, and A.Bretscher. 2004a. Stable and dynamic axes of polarity use distinct formin isoforms in budding yeast. *Mol. Biol. Cell* 15:4971-4989.

Pruyne, D., A.Legesse-Miller, L.Gao, Y.Dong, and A.Bretscher. 2004b. Mechanisms of polarized growth and organelle segregation in yeast. *Annu. Rev. Cell Dev. Biol.* 20:559-591.

Purdue, P.E. and P.B.Lazarow. 2001. Peroxisome biogenesis. *Annu. Rev. Cell Dev. Biol.* 17:701-752.

Raymond, C.K., P.J.O'Hara, G.Eichinger, J.H.Rothman, and T.H.Stevens. 1990. Molecular analysis of the yeast VPS3 gene and the role of its product in vacuolar protein sorting and vacuolar segregation during the cell cycle. *J. Cell Biol.* 111:877-892.

Raymond, C.K., C.J.Roberts, K.E.Moore, I.Howald, and T.H.Stevens. 1992. Biogenesis of the vacuole in *Saccharomyces cerevisiae*. *Int. Rev. Cytol.* 139:59-120.

Reinke, C.A., P.Kozik, and B.S.Glick. 2004. Golgi inheritance in small buds of *Saccharomyces cerevisiae* is linked to endoplasmic reticulum inheritance. *Proc. Natl. Acad. Sci. U. S. A.* 101:18018-18023.

Resh, M.D. 1999. Fatty acylation of proteins: new insights into membrane targeting of myristoylated and palmitoylated proteins. *Biochim. Biophys. Acta* 1451:1-16.

Rogers, S.L. and V.I.Gelfand. 1998. Myosin cooperates with microtubule motors during organelle transport in melanophores. *Curr. Biol.* 8:161-164.

Rose, M.D., F.Winston, and P.Hieter. 1988. Laboratory Course Manual for Methods in Yeast Genetics. Cold Spring Harbor Laboratory, Cold Spring Harbor.

Rossanese, O.W. and B.S.Glick. 2001. Deconstructing Golgi inheritance. *Traffic* 2:589-596.

Rossanese, O.W., C.A.Reinke, B.J.Bevis, A.T.Hammond, I.B.Sears, J.O'Connor, and B.S.Glick. 2001. A role for actin, Cdc1p, and Myo2p in the inheritance of late Golgi elements in *Saccharomyces cerevisiae*. *J. Cell Biol.* 153:47-62.

Rottensteiner, H., K.Stein, E.Sonnenhol, and R.Erdmann. 2003. Conserved function of Pex11p and the novel Pex25p and Pex27p in peroxisome biogenesis. *Mol. Biol. Cell* 14:4316-4328.

Salina, D., K.Bodoor, P.Enarson, W.H.Raharjo, and B.Burke. 2001. Nuclear envelope dynamics. *Biochem. Cell Biol.* 79:533-542.

Schekman, R. 2005. Peroxisomes: another branch of the secretory pathway? *Cell* 122:1-2.

Schilstra, M.J. and S.R.Martin. 2006. An elastically tethered viscous load imposes a regular gait on the motion of myosin-V. Simulation of the effect of transient force relaxation on a stochastic process. *J. R. Soc. Interface* 3:153-165.

Schliebs, W. and W.H.Kunau. 2004. Peroxisome membrane biogenesis: the stage is set. *Curr. Biol.* 14:R397-R399.

Schmid, M., A.Jaedicke, T.G.Du, and R.P.Jansen. 2006. Coordination of endoplasmic reticulum and mRNA localization to the yeast bud. *Curr. Biol.* 16:1538-1543.

Scholz, O., A.Thiel, W.Hillen, and M.Niederweis. 2000. Quantitative analysis of gene expression with an improved green fluorescent protein. *Eur. J. Biochem.* 267:1565–1570.

Schott, D., J.Ho, D.Pruyne, and A.Bretscher. 1999. The COOH-terminal domain of Myo2p, a yeast myosin V, has a direct role in secretory vesicle targeting. *J. Cell Biol.* 147:791-808.

Schott, D.H., R.N.Collins, and A.Bretscher. 2002. Secretory vesicle transport velocity in living cells depends on the myosin-V lever arm length. *J. Cell Biol.* 156:35-39.

Schrader, M. 2006. Shared components of mitochondrial and peroxisomal division. *Biochim. Biophys. Acta* 1763:531-541.

Schrader, M. and H.D.Fahimi. 2006. Growth and division of peroxisomes. *Int. Rev. Cytol.* 255:237-290.

Schrader, M. and H.D.Fahimi. 2008. The peroxisome: still a mysterious organelle. *Histochem. Cell Biol.* 129:421-440.

Schrader, M., B.E.Reuber, J.C.Morrell, G.Jimenez-Sanchez, C.Obie, T.A.Stroh, D.Valle, T.A.Schroer, and S.J.Gould. 1998. Expression of PEX11β mediates peroxisome proliferation in the absence of extracellular stimuli. *J. Biol. Chem.* 273:29607-29614.

Seabra, M.C. and E.Coudrier. 2004. Rab GTPases and myosin motors in organelle motility. *Traffic* 5:393-399.

Sellers, J.R. and C.Veigel. 2006. Walking with myosin V. *Curr. Opin. Cell Biol.* 18:68-73.

Shepard, K.A., A.P.Gerber, A.Jambhekar, P.A.Takizawa, P.O.Brown, D.Herschlag, J.L.DeRisi, and R.D.Vale. 2003. Widespread cytoplasmic mRNA transport in yeast: identification of 22 bud-localized transcripts using DNA microarray analysis. *Proc. Natl. Acad. Sci. U. S. A.* 100:11429-11434.

Smith, J.J., T.W.Brown, G.A.Eitzen, and R.A.Rachubinski. 2000. Regulation of peroxisome size and number by fatty acid β-oxidation in the yeast *Yarrowia lipolytica*. *J. Biol. Chem.* 275:20168-20178.

Smith, J.J., M.Marelli, R.H.Christmas, F.J.Vizeacoumar, D.J.Dilworth, T.Ideker, T.Galitski, K.Dimitrov, R.A.Rachubinski, and J.D.Aitchison. 2002. Transcriptome profiling to identify genes involved in peroxisome assembly and function. *J. Cell Biol.* 158:259-271.

Smith, J.J., Y.Sydorskyy, M.Marelli, D.Hwang, H.Bolouri, R.A.Rachubinski, and J.D.Aitchison. 2006. Expression and functional profiling reveal distinct gene classes involved in fatty acid metabolism. *Mol. Syst. Biol.* 2:0009.

Sogo, L.F. and M.P.Yaffe. 1994. Regulation of mitochondrial morphology and inheritance by Mdm10p, a protein of the mitochondrial outer membrane. *J. Cell Biol.* 126:1361-1373.

Spellman, P.T., G.Sherlock, M.Q.Zhang, V.R.Iyer, K.Anders, M.B.Eisen, P.O.Brown, D.Botstein, and B.Futcher. 1998. Comprehensive identification of cell cycle-regulated genes of the yeast *Saccharomyces cerevisiae* by microarray hybridization. *Mol. Biol. Cell* 9:3273-3297.

Takizawa, P.A. and R.D.Vale. 2000. The myosin motor, Myo4p, binds Ash1 mRNA via the adapter protein, She3p. *Proc. Natl. Acad. Sci. U. S. A.* 97:5273-5278.

Tam, Y.Y.C., A.Fagarasanu, M.Fagarasanu, and R.A.Rachubinski. 2005. Pex3p initiates the formation of a preperoxisomal compartment from a subdomain of the endoplasmic reticulum in *Saccharomyces cerevisiae*. *J. Biol. Chem.* 280:34933-34939.

Tam, Y.Y.C., J.C.Torres-Guzman, F.J.Vizeacoumar, J.J.Smith, M.Marelli, J.D.Aitchison, and R.A.Rachubinski. 2003. Pex11-related proteins in peroxisome dynamics: a role for the novel peroxin Pex27p in controlling peroxisome size and number in *Saccharomyces cerevisiae*. *Mol. Biol. Cell* 14:4089-4102.

Tanaka, A., S.Kobayashi, and Y.Fujiki. 2006. Peroxisome division is impaired in a CHO cell mutant with an inactivating point-mutation in dynamin-like protein 1 gene. *Exp. Cell Res.* 312:1671-1684.

Tang, F., E.J.Kauffman, J.L.Novak, J.J.Nau, N.L.Catlett, and L.S.Weisman. 2003. Regulated degradation of a class V myosin receptor directs movement of the yeast vacuole. *Nature* 422:87-92.

Thoms, S. and R.Erdmann. 2005. Dynamin-related proteins and Pex11 proteins in peroxisome division and proliferation. *FEBS J.* 272:5169-5181.

Titorenko, V.I. and R.T.Mullen. 2006. Peroxisome biogenesis: the peroxisomal endomembrane system and the role of the ER. *J. Cell Biol.* 174:11-17.

Titorenko, V.I. and R.A.Rachubinski. 1998a. Mutants of the yeast *Yarrowia lipolytica* defective in protein exit from the endoplasmic reticulum are also defective in peroxisome biogenesis. *Mol. Cell. Biol.* 18:2789-2803.

Titorenko, V.I. and R.A.Rachubinski. 1998b. The endoplasmic reticulum plays an essential role in peroxisome biogenesis. *Trends Biochem. Sci.* 23:231-233.

Titorenko, V.I. and R.A.Rachubinski. 2004. The peroxisome: orchestrating important developmental decisions from inside the cell. *J. Cell Biol.* 164:641-645.

Titorenko, V.I., D.M.Ogrydziak, and R.A.Rachubinski. 1997. Four distinct secretory pathways serve protein secretion, cell surface growth, and peroxisome biogenesis in the yeast *Yarrowia lipolytica*. *Mol. Cell. Biol.* 17:5210-5226.

Towbin, H., T.Staehelin, and J.Gordon.1979. Electrophoretic transfer of proteins from polyacrylamide gels to nitrocellulose sheets: procedure and some applications. *Proc. Natl. Acad. Sci. U. S. A.* 76:4350-4354.

Valiathan, R.R. and L.S.Weisman. 2008. Pushing for answers: is myosin V directly involved in moving mitochondria? *J. Cell Biol.* 181:15-18.

van der Zand, A., I.Braakman, H.J.Geuze, and H.F.Tabak. 2006. The return of the peroxisome. *J. Cell Sci.* 119:989-994.

van Roermund, C.W.T., H.F.Tabak, M.van den Berg, R.J.A.Wanders, and E.H.Hettema. 2000. Pex11p plays a primary role in medium-chain fatty acid oxidation, a process that affects peroxisome number and size in *Saccharomyces cerevisiae*. *J. Cell Biol.* 150:489-498.

Vizeacoumar, F.J., J.C.Torres-Guzman, D.Bouard, J.D.Aitchison, and R.A.Rachubinski. 2004. Pex30p, Pex31p, and Pex32p form a family of peroxisomal integral membrane proteins regulating peroxisome size and number in *Saccharomyces cerevisiae*. *Mol. Biol. Cell* 15:665-677.

Vizeacoumar, F.J., J.C.Torres-Guzman, Y.Y.C.Tam, J.D.Aitchison, and R.A.Rachubinski. 2003. *YHR150w* and *YDR479c* encode peroxisomal integral membrane proteins involved in the regulation of peroxisome number, size, and distribution in *Saccharomyces cerevisiae*. *J. Cell Biol.* 161:321-332.

Wang, Y.X., N.L.Catlett, and L.S.Weisman. 1998. Vac8p, a vacuolar protein with armadillo repeats, functions in both vacuole inheritance and protein targeting from the cytoplasm to vacuole. *J. Cell Biol.* 140:1063-1074.

Warren, G. and W.Wickner. 1996. Organelle inheritance. *Cell* 84:395-400.

Weisman, L.S. 2003. Yeast vacuole inheritance and dynamics. *Annu. Rev. Genet.* 37:435-460.

Weisman, L.S. 2006. Organelles on the move: insights from yeast vacuole inheritance. *Nat. Rev. Mol. Cell Biol.* 7:243-252.

Weisman, L.S. and W.Wickner. 1988. Intervacuole exchange in the yeast zygote: a new pathway in organelle communication. *Science* 241:589-591.

Wickner, W. and A.Haas. 2000. Yeast homotypic vacuole fusion: a window on organelle trafficking mechanisms. *Annu. Rev. Biochem.* 69:247-275.

Wiederkehr, A., Y.Du, M.Pypaert, S.Ferro-Novick, and P.Novick. 2003. Sec3p is needed for the spatial regulation of secretion and for the inheritance of the cortical endoplasmic reticulum. *Mol. Biol. Cell* 14:4770-4782.

Wu, X., B.Bowers, K.Rao, Q.Wei, and J.A.Hammer, III. 1998. Visualization of melanosome dynamics within wild-type and dilute melanocytes suggests a paradigm for myosin V function in vivo. *J. Cell Biol.* 143:1899-1918.

Wu, X.S., K.Rao, H.Zhang, F.Wang, J.R.Sellers, L.E.Matesic, N.G.Copeland, N.A.Jenkins, and J.A.Hammer, III. 2002. Identification of an organelle receptor for myosin-Va. *Nat. Cell Biol.* 4:271-278.

Yan, M., N.Rayapuram, and S.Subramani. 2005. The control of peroxisome number and size during division and proliferation. *Curr. Opin. Cell Biol.* 17:376-383.

Yang, H.C. and L.A.Pon. 2002. Actin cable dynamics in budding yeast. *Proc. Natl. Acad. Sci. U. S. A.* 99:751-756.

Yang, H.C., A.Palazzo, T.C.Swayne, and L.A.Pon. 1999. A retention mechanism for distribution of mitochondria during cell division in budding yeast. *Curr. Biol.* 9:1111-1114.

Yildiz, A., J.N.Forkey, S.A.McKinney, T.Ha, Y.E.Goldman, and P.R.Selvin. 2003. Myosin V walks hand-over-hand: single fluorophore imaging with 1.5-nm localization. *Science* 300:2061-2065.

Yin, H., D.Pruyne, T.C.Huffaker, and A.Bretscher. 2000. Myosin V orientates the mitotic spindle in yeast. *Nature* 406:1013-1015.